INCREASING TRANSPARENCY AND PRESENCE IN TELEOPERATION THROUGH HUMAN-CENTERED DESIGN

Rebecca M. Pierce

A DISSERTATION

in

Mechanical Engineering and Applied Mechanics

Presented to the Faculties of the University of Pennsylvania in Partial Fulfillment of the Requirements for the Degree of Doctor of Philosophy

2015

Katherine J. Kuchenbecker, Supervisor of Dissertation
Associate Professor, Department of Mechanical Engineering and Applied Mechanics

Prashant Purohit, Graduate Group Chairperson
Associate Professor, Department of Mechanical Engineering and Applied Mechanics

Dissertation Committee:
Michelle Johnson
Assistant Professor of Physical Medicine and Rehabilitation
Katherine J. Kuchenbecker
Associate Professor of Mechanical Engineering and Applied Mechanics
Mark Yim
Professor of Mechanical Engineering and Applied Mechanics

ACKNOWLEDGMENTS

I will forever be grateful for the many people who have supported me during my PhD studies. First, and foremost, I would like to thank my husband, Shaan, for always being there for me. Both his serious, driven side and his lighthearted, carefree, Frisbee-loving side provided continual support over the past five years.

I also need to thank my advisor, Dr. Katherine Kuchenbecker, who has shown me what it means to be a truly great academic leader. Her excellence in research is matched only by her excellence in mentorship. Her commitment to always producing her best work, supporting her students, and creating the best learning environment possible is inspiring.

I thank my sisters, Cassie and Laura, for being my biggest cheerleaders and best friends. My dad for fostering curiosity by answering any and all questions before bedtime and encouraging me to keep asking more. My mom, for loving me as much as any mother has ever loved her daughter. She provided enough wisdom, love, and guidance in the 19 years I had with her to last a lifetime, even if 19 years with her was not nearly be enough. My grandmom for being the toughest person I will ever meet. My grandpop for recognizing my mechanical bent early on and always asking me to be his assistant in household projects and for always being a source of pure joy in my life.

Finally, I need to thank my friends and colleagues in the Haptics Group and the GRASP laboratory. Especially, Heather Culbertson, whose drive and grit produces

amazing research. I am so happy that we traversed the PhD together. Our many hours of talking about everything from our ambitions and goals, to our most frustrating problems, to our dreams for women in STEM, to our favorite movies and TV shows are invaluable and formed the basis for what I am certain will be a lifelong friendship. Denise Wong, whose sunny, optimistic personality has never failed to boost my mood and energy. I love laughing uncontrollably over silly jokes, training for triathlons, and eating copious amounts of food with you. 3pm visits to your desk to see your experiments, hear about your amazing research, and plan workouts were always a better pick-me-up than coffee. Vivienne Clayton, whose ability to see the good in all people is unmatched and who cares more deeply about her friends than anyone I know. Her professional savvy, design skills, and mechanical intuition make her a great engineer, whom I can always rely on for insightful professional advice. I'm so lucky to have the three of you as friends.

ABSTRACT

INCREASING TRANSPARENCY AND PRESENCE IN TELEOPERATION THROUGH HUMAN-CENTERED DESIGN

Rebecca M. Pierce

Katherine J. Kuchenbecker

Teleoperation allows a human to control a robot to perform dexterous tasks in remote, dangerous, or unreachable environments. A perfect teleoperation system would enable the operator to complete such tasks at least as easily as if he or she was to complete them by hand. This ideal teleoperator must be perceptually transparent, meaning that the interface appears to be nearly nonexistent to the operator, allowing him or her to focus solely on the task environment, rather than on the teleoperation system itself. Furthermore, the ideal teleoperation system must give the operator a high sense of presence, meaning that the operator feels as though he or she is physically immersed in the remote task environment. This dissertation seeks to improve the transparency and presence of robot-arm-based teleoperation systems through a human-centered design approach, specifically by leveraging scientific knowledge about the human motor and sensory systems.

First, this dissertation aims to improve the forward (efferent) teleoperation control channel, which carries information from the human operator to the robot. The traditional method of calculating the desired position of the robot's hand simply scales the measured position of the human's hand. This commonly used motion mapping erroneously assumes that the human's produced motion identically matches his or

her intended movement. Given that humans make systematic directional errors when moving the hand under conditions similar to those imposed by teleoperation, I propose a new paradigm of data-driven human-robot motion mappings for teleoperation. The mappings are determined by having the human operator mimic the target robot as it autonomously moves its arm through a variety of trajectories in the horizontal plane. Three data-driven motion mapping models are described and evaluated for their ability to correct for the systematic motion errors made in the mimicking task. Individually-fit and population-fit versions of the most promising motion mapping model are then tested in a teleoperation system that allows the operator to control a virtual robot. Results of a user study involving nine subjects indicate that the newly developed motion mapping model significantly increases the transparency of the teleoperation system.

Second, this dissertation seeks to improve the feedback (afferent) teleoperation control channel, which carries information from the robot to the human operator. We aim to improve a teleoperation system a teleoperation system by providing the operator with multiple novel modalities of haptic (touch-based) feedback. We describe the design and control of a wearable haptic device that provides kinesthetic grip-force feedback through a geared DC motor and tactile fingertip-contact-and-pressure and high-frequency acceleration feedback through a pair of voice-coil actuators mounted at the tips of the thumb and index finger. Each included haptic feedback modality is known to be fundamental to direct task completion and can be implemented without

great cost or complexity. A user study involving thirty subjects investigated how these three modalities of haptic feedback affect an operator's ability to control a real remote robot in a teleoperated pick-and-place task. This study's results strongly support the utility of grip-force and high-frequency acceleration feedback in teleoperation systems and show more mixed effects of fingertip-contact-and-pressure feedback.

Contents

List of Tables

List of Figures

Chapter 1

Introduction

Teleoperation allows an operator to complete tasks that require human-level intelligence in environments where a human's physical presence is not possible or is highly undesirable. For example, traditional open surgery requires a large incision through healthy tissue to let the surgeon to see the operation site and manipulate it with his or her hands. Alternatively, the surgeon can complete the operation with a teleoperated robotic minimally invasive surgical system that requires only tiny incisions and gives the surgeon a high level of dexterity [33]. In another example, a search-and-rescue worker can use a teleoperated robot to look for survivors in the wake of a natural or man-made disaster, such as a nuclear power plant meltdown [8, 15]. The rescue worker can drive robots over the disaster field from a safe location to look for survivors. Once a survivor is located, the rescue worker can teleoperate a manipulator on the rescue robot to help free the survivor without being exposed to the disaster's hazards. Teleoperation is useful not only in these and other high-stakes applications, but also in everyday tasks such as allowing a telecommuter to control a robotic agent at the office.

Although the uses of teleoperation vary widely, the basic components of all teleoperators are the same [69]. The *human operator* interacts with a *master interface* to send motion commands to the robot over the forward communication channel, akin to the efferent channel of the human nervous system. The *slave robot*, located in the remote environment, executes the received motion commands, while simultaneously measuring information about its environment. The robot sends this information back to the operator via the feedback communication channel, akin to the afferent channel of the human nervous system. The master interface relays information back to the operator via visual, auditory, and/or haptic cues. The *control system* calculates the desired behavior of the slave robot based on input from the human operator. Depending on the control architecture, the slave robot can have varying levels of autonomy. In *direct control*, which is the focus of this dissertation, the human operator fully controls the movement of the slave robot, without any autonomous actions performed by the slave robot. The control system also regulates the flow of information back to the human operator based on data measured by sensors attached to the slave robot.

The utility of teleoperation has led to vibrant research on improving the usability of teleoperators to facilitate task completion in the remote environment. Research in this domain can be categorized either as improving the efferent filter, which maps information from the human operator to the remote robot, or as improving the afferent filter, which sends information from the remote robot back to the human operator [90]. Research on improving the efferent (forward) filter has been focused either on creating devices that can more effectively gather motion data from the human operator, such as [4,52,74,98], or on creating better control laws to enable the remote robot to follow the operator's motion commands more closely, as reviewed by [40,73]. Improvements to the afferent (feedback) filter are often made by the creation of new teleoperation interfaces that are meant to immerse the human operator in the remote environment. A rich field of study aimed at understanding human perception via visual, auditory, and haptic sensory channels has allowed engineers to create better two-dimensional and three-dimensional visual displays, auditory displays, and haptic interfaces. Systems created to immerse users in remote environments, as well as virtual environments, are reviewed extensively in [3,35,63,93,94].

Sections 2.1 and 4.1 give a more complete review of prior work in teleoperation as it relates to this dissertation. However, even given the significant body of work seeking to improve teleoperators, many control interfaces are still difficult and nonintuitive to use [9].

1.1 Motivation

The field of teleoperation began in 1947 when Raymond C. Goertz created a system that allowed scientists to conduct experiments on nuclear materials while remaining behind the safety of a nuclear shield [24]. The master interface of this first teleoperation system consisted of on-off switches that controlled the individual degrees of freedom of the slave manipulator. Although this control interface was functional, Goertz and colleagues found that this teleoperation system was too hard to operate to be of practical use in the laboratory setting. Although this teleoperation system was developed before the formal adaptations of the terms, Goertz describes his original system as unusable due to its low *transparency* and low *presence*. Goertz states that the on-off switches were clumsy and awkward to use, indicating that the original system had low transparency. A teleoperation system with high transparency appears to be nearly nonexistent to the operator, meaning that he or she needs to invest little or no cognitive effort to control the slave robot [58, 82]. Goertz states that the operator needed to use extreme care when handling the dangerous nuclear materials because he or she was not able to feel the remote object, indicating that the original system also offered low levels of presence. A teleoperation system provides a high sense of presence to the operator if he or she feels physically immersed in the remote environment [5, 42, 90, 91, 110].

To address the shortcomings of the original design, Goertz created a new system in which the master interface was physically connected to a kinematically identical slave manipulator [25]. When the operator moved the master interface, his or her motion was almost identically reproduced by the slave robot. The physical linkage between the master and slave also allowed the operator to feel forces acting on the slave manipulator. The new system was easy to use, and videos of operators using the device show that it had high levels of transparency and presence. Similar systems are still in use today for hazardous material handling.

The advantages of higher levels of transparency and presence achieved by physically connecting the master and the slave are usually outweighed by the limitations imposed on the maximum possible separation between the master and the slave. Therefore, many current teleoperation master interfaces consist of buttons, switches, and knobs, e.g. [78,109]. However, starting with Goertz himself [26], many researchers have designed master interfaces that measure natural human motion. These systems often consist of large, heavy, expensive, force-reflecting exoskeletons that must be customized to the user and the remote robot and are thus not appropriate for the majority of telerobotic applications, e.g., [59, 74]. Although many of my findings translate to force-reflecting master interfaces, this dissertation specifically focuses on lightweight wearable control interfaces that do not provide grounded force feedback.

The decision to focus on lightweight, wearable master interfaces is supported by the recommendations of Casper and Murphy, who tested teleoperated rescue robotic platforms in the aftermath of the terrorist attacks on September 11, 2001, assisting with search and rescue at Ground Zero in New York City. Casper and Murphy reported these experiences and recommended a variety of improvements for rescue robotics technology, including significant changes to the human-machine interfaces [8]. First, they state that rescue robots must be transportable and controllable by one person to minimize the number of people at risk during a mission. Furthermore, the danger of carrying large objects across hazardous environments requires all equipment to be transportable via wearable containers. Second, rescue workers usually do not sleep during the first forty-eight hours on the scene, and they sleep for no more than a few hours per day thereafter. Therefore, Casper and Murphy suggest that the control interfaces for rescue workers need to be made as intuitive as possible to account for the lower cognitive capacities that arise under extreme sleep deprivation. These guidelines strongly support investigation of wearable control interfaces that measure natural human motion and provide sensory cues to facilitate teleoperation.

1.2 Thesis Overview and Contributions

The main hypothesis of this dissertation is that taking a human-centered design approach by leveraging previous scientific discoveries about the human motor and sensory systems will improve the usability of teleoperation systems that measure natural human motion to control a remote robot. A high-level overview of the work completed in this dissertation is shown in Figure 1.1. In Chapter 2, I propose implementing data-driven motion mappings to calculate the desired robot position from the measured human position. Chapter 3 shows that such data-driven motion mappings improve the operator's ability to control the motion of the remote robot. Then I switch the focus from the efferent (forward) channel to the afferent (feedback) channel. Chapter 4 describes the design of a wearable haptic device that provides tactile fingertip-contact,

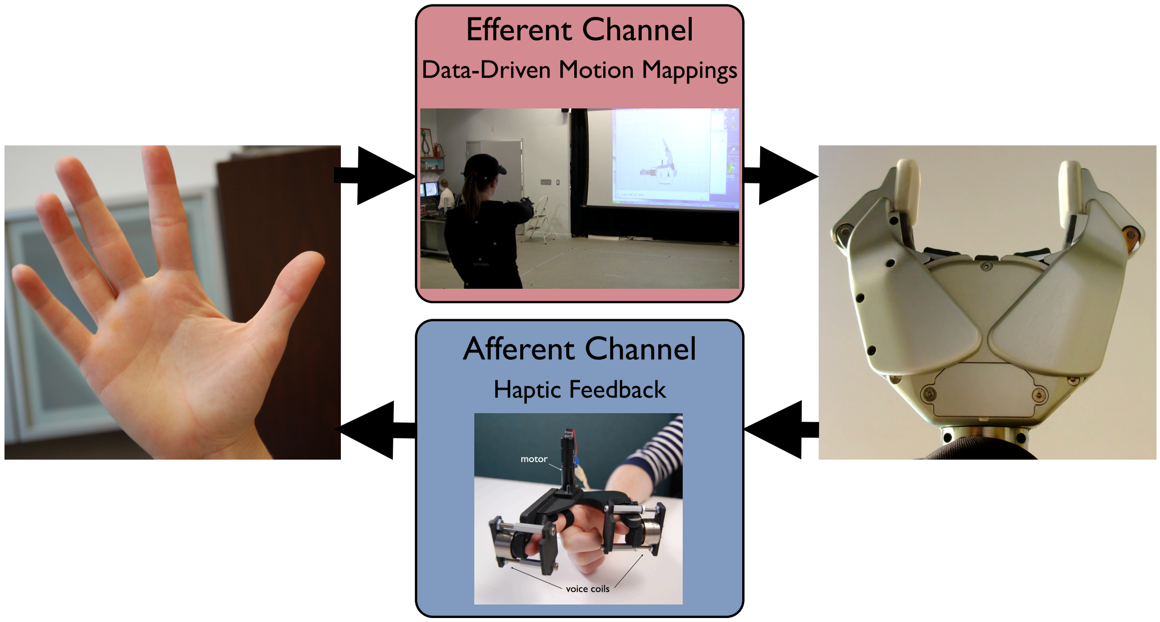

Figure 1.1: An overview of the work presented in this dissertation. I first sought to improve teleoperation by designing and implementing data-driven motion mappings on the efferent (forward) channel. I then turned my focus to the afferent (feedback) channel. I created a wearable device that provides multiple modalities of haptic (touch-based) feedback to the operator.

fingertip-pressure, and high-frequency acceleration feedback in addition to kinesthetic grip-force feedback. I investigate the effects of these distinct haptic feedback modalities in Chapter 5.

The contributions of this thesis are as follows:

- Chapter 2: Determining Natural Human-Robot Motion Mappings in Teleoperation
  - A new paradigm for deriving data-driven motion mappings to calculate the desired robot hand position from the position of the human operator's hand. A person mimics the robot moving through preprogrammed trajec-

tories. The human's motion is recorded and compared to the motion of the robot to fit the mapping parameters.

  - The proposal of three novel motion mapping models. The traditional Cartesian scaling simply multiplies the human's motion by a scalar to obtain the robot's motion. The three new motion mappings (similarity, affine, and variable similarity) are fit to data to capture distortions in how the human moves relative to the robot.
  - Evaluation of the proposed motion mapping models for nine users. The most promising model, the variable-similarity motion mapping, distorts the human's motion to correct for systematic directional errors made by the human when completing the mimicking task. Notably, the way in which the human's motion needs to warp to best fit the robot's motion generalizes across subjects and matches prior findings in the neuroscience literature.

- Chapter 3: Evaluation of Data-Driven Motion Mappings
  - A teleoperation system created to investigate the value of the variable-similarity motion mapping. It consists of a Vicon motion capture system that measures the pose of the operator's hand and a virtual PR2 humanoid robot.
  - A user study involving twelve subjects investigating how well operators are

able to control the motion of the virtual robot when their measured motion is transformed via the data-driven variable-similarity motion mapping, as compared to a Cartesian scaling. Two forms of the variable-similarity motion mapping are tested. The parameters of the first variable-similarity motion mapping are fit to the aggregate data of the subjects who participated in the experiment in Chapter 2, so it corrects for errors made by the general population. The parameters of the second variable-similarity motion mapping are fit to data collected when each subject completed the mimicking calibration task.

  - Evidence proving that subjects were able to complete a targeted reaching task with higher accuracy in initial direction of robot motion, at higher speeds, and with more natural and efficient reaching movements under the variable-similarity motion mappings. These results indicate that subjects experienced a higher level of transparency when using the virtual teleoperator with the variable-similarity motion mappings than with the standard Cartesian mapping. Subjects also preferred the variable-similarity motion mappings.

- Chapter 4: A Wearable Device for Controlling a Robot Gripper with Ungrounded Haptic Feedback
  - Design and construction of a haptic device thats controls the opening of a remote robot's gripper. The device provides kinesthetic grip-force feedback

and tactile fingertip-contact-and-pressure and high-frequency acceleration feedback via a DC motor and a pair of voice-coil actuators.

  - Development of a control scheme that converts haptic information measured by sensors on the remote robotic gripper to haptic feedback delivered by the actuators on the device.
  - Preliminary evaluation of the device through teleoperated interactions with a variety of objects.

- Chapter 5: Effects of Ungrounded Haptic Feedback on a Teleoperated Pick-and-Place Task
  - Development of an experimental system for investigating the effects of grip-force feedback, fingertip-contact feedback, and high-frequency acceleration feedback on the user's performance of a teleoperated pick-and-place task. The teleoperation system consisted of a Vicon motion capture system and a real remote PR2 robot.
  - Execution of a human-subject experiment that enrolled thirty subjects to test the developed teleoperation system under different types of haptic feedback.
  - Evidence supporting the utility of grip-force feedback with gain switching. Grip-force feedback enabled subjects to handle objects more delicately, hold objects more stably, and better control the motion of the remote

robot's hand.

- Confirmation that fingertip contact-and-pressure feedback allowed subject to better sense when the object is in the remote robot's hand. However, this dissertation makes no recommendations about the use of fingertip contact feedback in teleoperation because the current implementation generally led subjects to handle the object more roughly.
- Results indicating that high-frequency acceleration feedback slightly improved the subject's performance when setting the object down, as originally hypothesized. However, more interestingly, high-frequency acceleration feedback also allowed subjects to feel vibrations produced by the robot's motion, causing them to be more careful when completing the task.

Chapter 2

Determining Natural Human-Robot Motion Mappings in Teleoperation

Many aspects of teleoperation systems have been fine-tuned through research. However, the robot's commanded movement is almost always calculated by scaling and applying an offset to the operator's measured movement. While this mapping has proven to be usable, it may not be the human operator's preferred motion mapping. Furthermore, the traditional Cartesian-scaling motion mapping assumes that the human's executed movement matches his or her intended movement. This assumption is known to be false when a person moves his or her hand while relying upon proprioception, rather than direct vision.

I propose that implementing nontraditional data-driven motion mappings has the potential to improve the usability of teleoperation platforms, making it easier for a human to remotely complete challenging tasks. This chapter presents a new paradigm for determining data-driven human-robot motion mappings for teleoperation: the human operator mimics the target robot as it autonomously moves its arm through a variety of trajectories. The resulting human motion reveals the human's chosen mapping, skewed by systematic motion errors the human made when relying on proprioception to execute these arm movements.

I begin this chapter by discussing relevant background material in Section 2.1. I discuss the experimental setup and the procedures implemented to test the proposed paradigm with nine human subject in Sections 2.2 and 2.3, respectively. Section 2.4 gives further details about the traditional Cartesian scaling motion mapping and proposes three data-driven motion mapping models. In Section 2.5, I use data recorded in the described study to analyze each mapping's ability to transform human motion data to corresponding robot motion. Finally, I leave the reader with the main conclusions drawn from this work in Section 2.7. This work was originally published in the proceedings of the 2012 IEEE RAS & EMBS International Conference on Biomedical Robotics and Biomechatronics [76].

2.1 Background

Developed by Goertz and colleagues in the 1940's, the first successful teleoperators consisted of kinematically identical master interfaces and slave manipulators that were mechanically coupled [24–26]. Consequently, the measured motion of the human operator was reproduced almost exactly by the slave in the remote environment. Since that time, roboticists have believed that a perfect isomorphism would enable the best execution of remote tasks [90]. Therefore, most of today's teleoperators still attempt to identically reproduce the human's motion with the slave manipulator. When a perfect reproduction is not possible, the shape of the human's input motion is preserved by applying a uniform Cartesian scaling and an offset [69].

While this method of calculating desired position has proven successful, it is important to remember that it represents just one of a wide variety of possible motion mappings between the human and the robot. Romano et al. compared the standard position mapping scheme to a rate controller, which maps the master's position to the slave's velocity, and to a mouse ballistics-inspired hybrid controller, which nonlinearly maps the master's velocity to the slave's velocity [85]. A user study showed that subjects were able to complete a targeting task using teleoperated steerable needles most accurately using the hybrid control law. This work provides evidence that humans may find nontraditional motion mappings to be more intuitive than the standard approach, depending on the needs of the task.

Many other researchers have created operator-adapted controllers to improve the fidelity, transparency, and robustness of teleoperation systems [73]. These researchers often look to mathematical models of human motion to create higher quality control schemes. One of the most commonly implemented models is Flash and Hogan's minimum jerk criterion, which describes voluntary human arm motion as following the smoothest possible path [17]. For example, Maeda et al. [60] and Corteville et al. [12] successfully used the minimum jerk criterion to predict human motion for improved cooperative object transportation and manipulation. These methods could easily be adapted to teleoperative applications.

The minimum jerk criterion, however, does not describe errors made by humans when executing voluntary arm motions. To complete the seemingly simple task of accurately moving one's hand to a desired location, one must have a model of the external space represented in a hand-centered coordinate frame, an estimate of the hand's initial position, and a dynamic model of the limb to be moved [21]. Ghez et al. proposed this theory using their prior work and the work of several other researchers who showed that subjects make large systematic errors if either the model of external space [22, 30, 108], estimate of initial hand position [20, 27, 103], or dynamic model of the limb [29, 87, 89] become degraded. In particular, many of these studies used a targeted reaching task to show that humans make directional motion errors that depend on hand position when any of the three representations is inaccurate. When the hand is laterally displaced to the left of the shoulder, the subject makes large errors in the counter-clockwise direction, so that if a person were to try to move his or her hand directly forward, the final position of the hand would be to the left of the target location. When the hand is laterally displaced to the right of the shoulder, the subject makes large clockwise reaching errors, so that if the person again tries to move his or her hand directly forward, the hand would end to the right of the target location [20, 22, 29, 30, 103].

Although the relationship between intended human motion and produced human motion has been heavily studied, it is interesting that only a few robotics researchers have studied the relationship between intended motion and produced motion of a human operator controlling a remote robot. This dearth of research is even more surprising when one considers the fact that the three representations needed to accurately produce intended motions are necessarily degraded by current limitations in teleoperator technology. First, the operator's understanding of the space of the remote environment is degraded because he or she must view it through a 2D or 3D display instead of through direct vision. Second, the operator needs to rely heavily on proprioception when completing a task using a teleoperator because his or her vision will be focused on the display of the remote environment, rather than on his or her own limb. In a teleoperator with perfect presence, or a perfect sense of being physically located in the remote environment, the visual feedback from the remote environment would be as useful to the operator as the view of his or her own limbs in a direct manipulation task. However, limitations in current technology, including delays in the teleoperator and imperfect visual displays, preclude perfect presence in teleoperators and necessitate reliance on proprioception to a certain extent. Relying solely on proprioception over vision has been shown to cause subjects to produce large directional errors in targeting tasks [20, 22]. Although teleoperators provide some visual feedback, I still expect that the directional errors produced when completing a targeted reaching experiment via teleoperation would be larger than if one were to complete the targeted reaching task directly. Third and finally, the user of a telerobotic system must account not only for the dynamics of his or her own arm but also for the dynamical properties of the master device and the slave device, including dynamics introduced by any control laws. While it is well known that teleoperation interfaces should have as little inertia as possible [62], Nisky et al. showed that the dynamics of even a well designed, highly transparent system still affect the motion of novice users [70].

For these reasons, it is reasonable to expect human arm motion to be inaccurate when a person is using a teleoperator. Therefore, I hypothesized that bijective positional motion mappings that correct for systematic reaching errors may be preferable to the Cartesian-scaling motion mapping traditionally used in teleoperation. In this chapter I seek to discover such data-driven motion mappings by analyzing human and robot motion data recorded by having human subjects mimic the motion of a virtual robot.

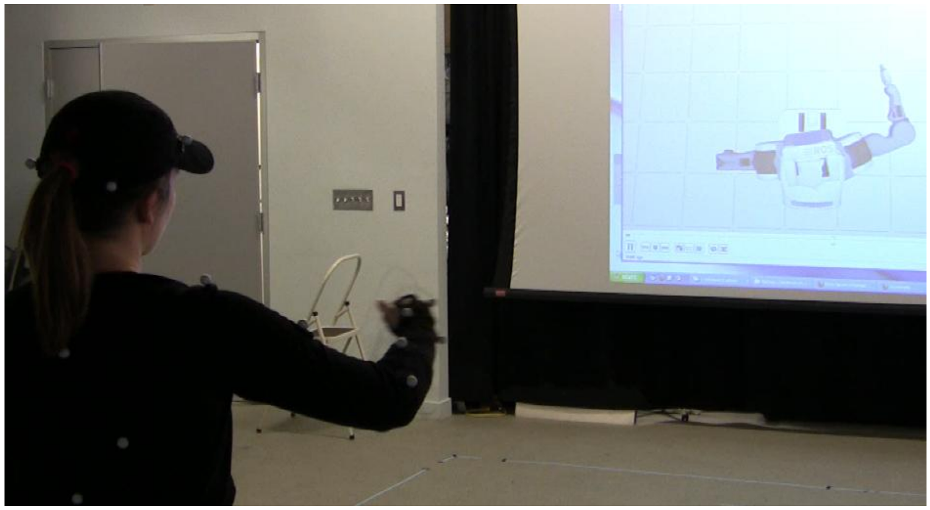

Figure 2.1: A video of the PR2 making planar motions with its right arm was projected on a large screen at the front of the motion capture space. The subject mimicked the robot motion in real time using comfortable motions of her right arm.

2.2 Experimental Setup

To test the hypothesis that data-driven motion mappings can be deduced by having a subject mimic the motion of a robot, I created a system that could record synchronized robot and human movements. Willow Garage's Robot Operating System (ROS) [80] was a natural choice for use in this project, since a major goal of the work was to make extensible algorithms to semi-automatically deduce motion mappings from an operator to a variety of robotic platforms. The algorithms developed in this section are independent of the method used to capture the human's arm movement; optical tracking, magnetic tracking, inertial measurement units, and sensors such as the Microsoft Kinect would all work.

I note that in graphics, retargeting recorded human motion to animate virtual characters has become a standard method for creating realistic movements [23]. Techniques from computer animation have also been adapted to animate humanoid robots, e.g., [6, 14, 77]. However, the goal of this body of prior research has been to create human-like robot motion to enhance human-robot interactions, while this work uses retargeting techniques to allow humans to intuitively teleoperate robotic platforms in real time.

Virtual Robot

ROS's modular, multi-lingual, and open-source packages facilitate the development of algorithms for use on several different robotic platforms. Willow Garage's humanoid, the PR2, is one of the best supported robots in ROS and is available in the University of Pennsylvania's GRASP lab. I recorded the PR2 moving its arm through commanded trajectories using Gazebo, a three-dimensional multi-robot simulation environment supported by ROS [50]. Fig. 2.1 shows the recorded view of the simulated robot presented to the subject. Equivalent alternatives would have been to record the actual robot moving or to physically locate it with the operator during testing.

This work focuses on identifying transformations between human motion and robot motion for trajectories confined to a horizontal plane, since this is the plane in which Ghez et al. [21] found systematic distortions. Planar robot arm motion was produced using ROS's real-time joint controller. The shoulder and elbow joints were controlled to follow pre-set trajectories over time, and the other joints were com-

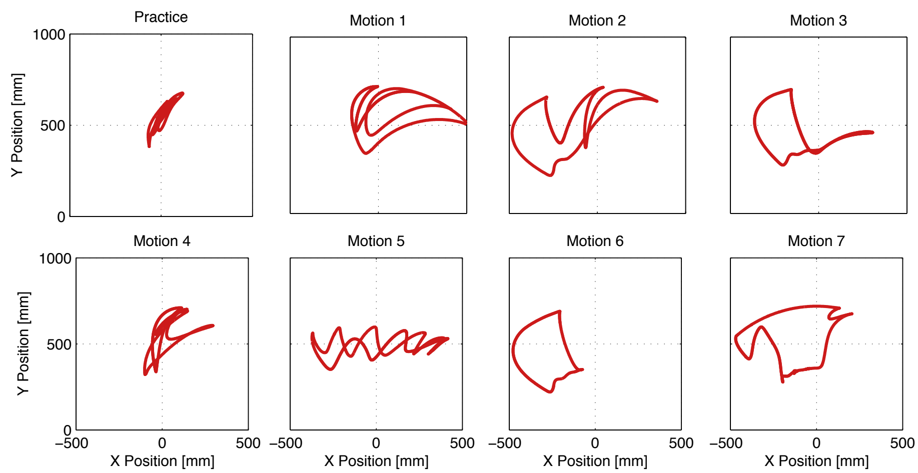

Figure 2.2: Trajectories of the eight motions created by the PR2's right hand.

manded to stay at fixed angles. Fig. 2.2 shows the trajectories of the PR2's hand for the eight motions used. The robot's hand moved with approximately constant speed in motions 1 through 5 and at varied speed in motions 6 and 7. The PR2 was recorded making each motion from six to ten times over approximately 90 seconds. The view point in the movie was overhead looking down, as shown on the screen in Fig. 2.1.

Motion Capture

Human movement was recorded using the Vicon motion capture system in the Penn SIG Center. The subjects wore a full-body suit covered with 53 passive retroreflective fiducial markers. These markers are individually placed adjacent to all major joints in the body, to provide a stationary reference point when the corresponding joint is moved. Because [22] and [21] describe systematic errors in hand positions and velocities, I decided to focus the analysis on comparing the position of the human's hand to the position of the robot's hand. The position of the subject's hand was taken to be the location of the marker on the wrist by the base of the thumb.

2.3 Experimental Procedures

All study procedures were approved by the University of Pennsylvania IRB under protocol #815023. Nine subjects participated in the study (seven male and two female). All subjects were right-handed and between the ages of 20 and 31. Each subject gave informed consent before participating.

As shown in Fig. 2.1, the videos of the PR2 making arm planar motions were projected onto a large screen at the front of the motion capture space. The subject was instructed to mimic the PR2's motion as closely as possible, using only comfortable motions of the right arm. The instruction of comfortable motions was important to the objective of this work because a major goal was derive human-robot motion mappings that could be used for hours on end with minimal physical and mental fatigue. The subjects were given no specific instruction on how to accomplish this task, since it was important that each picked the mapping that was most natural to him or her. The subject was first shown the constant-speed practice motion from Fig. 2.2, then each of the numbered motions twice. The seven motions were presented in random order for each subject, and the two viewings of each motion occurred sequentially.

This procedure yielded motion recordings of the subject attempting to mimic the robot repeatedly performing each trajectory in Fig. 2.2. The subject's motion data was recorded at a constant rate of 120 Hz, while the PR2's motion was recorded with time stamps at an irregular rate of approximately 1000 Hz. The robot data stream was down-sampled to 120 Hz via linear interpolation. The two data streams were then aligned in time by finding the segment of human data that yielded the smallest average Cartesian distance to the corresponding robot data stream under a similarity transformation. Once aligned in time, both data streams needed to be described in a right-handed reference frame with its origin at the center of rotation of the right shoulder. The X-axis of this reference frame is directed from the left shoulder to the right shoulder, the Y-axis points out from the chest, and the Z-axis points up. A visual examination of the captured data showed that there were often very large discrepancies between the human and robot motions at the beginning of each data set, during the time when the human was learning the periodic motion of the robot, as would be expected. Additionally, subjects often stopped mimicking the robot just before the end of each video. Therefore, the first twenty seconds and the last two seconds of each data set were excluded from analysis.

At the end of the study, each subject completed a short questionnaire to explain the strategies and methods they used to accurately reproduce the robot's motions. Subjects also completed a NASA Task Load Index (NASA-TLX) [37] to rate the difficulty of the task. The questions posed by the NASA TLX and the associated rating scales are given in Table 2.1.

Question	Endpoints
How mentally demanding was the task?	Very Low–Very High
How physically demanding was the task?	Very Low–Very High
How hurried or rushed was the pace of the task?	Very Low–Very High
How successful were you in accomplishing what you were asked to do?	Failure–Perfect
How hard did you have to work to achieve your level of performance?	Very Low–Very High
How insecure, discouraged, irritated, stressed, and annoyed were you?	Very Low–Very High

Table 2.1: NASA TLX Rating Scale Definitions [37]

2.4 Proposed Motion Mappings

Once synchronized in time and space, the motion data obtained during the study was analyzed to look for trends in the differences between each subject's motion and that of the robot. These differences can be attributed to the motion mapping chosen by the subject, as well as unintentional spatial distortions made by the subject while mimicking the robot's motion. Four models of increasing complexity were fit to map the motion made by the subject to the motion of the robot, as described below.

2.4.1 Traditional: Predefined Uniform Scaling

To handle kinematically dissimilar robots, the position of the master device is typically scaled and offset to better allow the user to perform a task in the slave's environment [69]. In the Cartesian plane this mapping can be represented as

$$\vec{x}_r = s\vec{x}_h + \vec{\gamma} \tag{2.4.1}$$

where $\vec{x}_r$ is the robot's desired position and $\vec{x}_h$ is the human's. I set the scale factor, s, to be the ratio of the robot's arm length to the human's arm length, while the offset, $\vec{\gamma}$ is the vector from the mean of the scaled human position to the mean of the robot position.

2.4.2 Similarity Transformation

In transformation geometry, a similarity is an operation for which the distance between two points is proportional to the distance between the two transformed points [61]. A similarity transformation consists of a scaling, a rotation, a reflection, and/or a translation. In the Cartesian plane, a similarity can be expressed as follows, where s is a scale factor, T is a 2×2 orthogonal matrix, and θ is the rotation angle.

$$\vec{x}_r = sT\vec{x}_h + \vec{\gamma} \tag{2.4.2}$$

$$T = \begin{bmatrix} \cos(\theta) & -\sin(\theta) \\ \sin(\theta) & \cos(\theta) \end{bmatrix} \tag{2.4.3}$$

The least-squares method developed by Schonemann [88] was used to find the similarity transformation that best fits the human's motion to the robot's.

2.4.3 Affine Transformation

An affine transformation is a colineation that preserves parallelness between two lines; it can consist of a strain, a shear, a rotation, a reflection, and a translation. In the Cartesian plane, the transformed point, $\vec{x}_r$, can be expressed as a linear combination of the X and Y components of the measured point, $\vec{x}_h$

$$\vec{x}_r = T\vec{x}_h + \vec{\gamma} \tag{2.4.4}$$

$$T = \begin{bmatrix} a & b \\ c & d \end{bmatrix} \tag{2.4.5}$$

The best fit affine transformation from the human trajectory to the robot trajectory can be solved for in the same manner as the best fit similarity transformation, relaxing the constraint that T be an orthogonal matrix.

2.4.4 Variable Similarity

The final and highest dimensional proposed motion mapping is a position-based egocentric variable-similarity motion mapping designed to correct the systematic directional errors that humans make when completing a targeting task while relying only on proprioception, were a directional error is defined to be the angle between the desired displacement vector and the produced displacement vector. It has been shown that subjects make directional motion errors as large at $20°$ when completing a targeted reaching task without being able to view their arm [20, 21, 31], where the directional error is defined to the be the angle between the desired displacement vector and the actual displacement vector. The directional errors made by people when performing such a blinded-reaching task strongly depend on the location of the hand, especially the lateral position. If either the left or the right hand is laterally aligned with the corresponding shoulder, reaching motions tend to be accurate. When either hand is displaced to the left of the corresponding shoulder, large counter-clockwise directional errors are made. Conversely, when either hand is displaced to the right of the corresponding shoulder, large clockwise errors are made.

To look for similar errors in the motion data recorded in this study, I partitioned the human and robot data into half-second segments and found the best fit similarity transformation for each matched pair. The rotation, scale, X offset and Y offset (θ, c, γ_1, and γ_2 from (2.4.2) and (2.4.3)) were plotted against the X and Y position of the first data point in the time segment. The function for each of the four fitted parameters is in the form of a plane because the results of Ghez et al. found that directional errors made by humans vary fairly linearly with human hand position [20, 21]. The variable-similarity motion mapping can be written as follows,

$$\vec{x}_r = s(\vec{x}_h)T(\vec{x}_h)\vec{x}_h + \vec{\gamma}(\vec{x}_h) \tag{2.4.6}$$

$$T(x,y) = \begin{bmatrix} \cos(\theta(\vec{x}_h)) & -\sin(\theta(\vec{x}_h)) \\ \sin(\theta(\vec{x}_h)) & \cos(\theta(\vec{x}_h)) \end{bmatrix} \tag{2.4.7}$$

$$\vec{\gamma}(\vec{x}_h) = \begin{bmatrix} \gamma_x(\vec{x}_h) \\ \gamma_y(\vec{x}_h) \end{bmatrix} \tag{2.4.8}$$

$$s(x,y) = a_s x_h + b_s y_h + c_s \tag{2.4.9}$$

$$\theta(x,y) = a_\theta x_h + b_\theta y_h + c_\theta \tag{2.4.10}$$

$$\gamma_x(x,y) = a_{\gamma x} x_h + b_{\gamma x} y_h + c_{\gamma x} \tag{2.4.11}$$

$$\gamma_y(x,y) = a_{\gamma y} x_h + b_{\gamma y} y_h + c_{\gamma y} \tag{2.4.12}$$

I note that while studying pilot data, I also tested a motion mapping scheme that transforms the direction and magnitude of the user's velocity as a function of the position of the user's hand. This mapping in the velocity domain creates robot motions that depend on the path of the subject. Thus, certain human motions could cause the mapping in the velocity domain to command desired positions beyond the robot's workspace. Additionally, only rotation angle and scaling could be fit in the velocity domain, while the warping presented in this study can also fit the X offset and the Y offset. In the variable similarity transformation, the X offset and Y offset describe both global translation and differential scaling.

2.4.5 Summary of Mappings

All of the proposed data-driven motion mappings will be used to find the best fit transformation from the human motion data to the robot data. Applying the fitted mapping to human motion will calculate the desired robot trajectory for each data set. The four motion mappings investigated in this paper are summarized in Table 2.2. This table includes a visualization of how the space around the human will be morphed to command a desired robot pose. The traditional position mapping uniformly scales and offsets human motion to map it to a desired robot position. The similarity mapping uniformly scales, offsets, and rotates the human motion, while the affine transformation adds differential scaling and shear. Finally, the variable similarity motion mapping smoothly warps, scales, and offsets the human position to calculate desired robot motion.

Model	**Fitted Parameters**	**Visual Effect**
Traditional	s γ_x γ_y	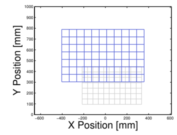
Similarity	s θ γ_1 γ_2	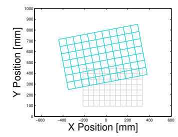
Affine	a b c d γ_x γ_y	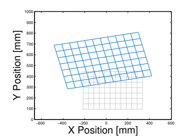
Variable Similarity	$a_s, a_{\gamma x}$ $b_s, b_{\gamma x}$ $c_s, c_{\gamma x}$ $a_\theta, a_{\gamma y}$ $b_\theta, b_{\gamma y}$ $c_\theta, c_{\gamma y}$	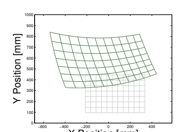

Table 2.2: The four motion mappings considered in this work.

2.5 Preliminarily Evaluation of Motion Mappings

Preliminary analysis of the data showed that all of the motion mapping schemes were capable of transforming human motion to the general shape of the robot motion, but they were unable to fit the global position. For each of the three data-driven models, more than 20% of the error in initial within-trial tests was explained by the offset centers of the transformed human and robot motion. This effect greatly worsened when human motion was transformed using a model trained on different data sets, rising to more than 35% for all four motion mappings. This discrepancy is due to the fact that one's proprioceptive estimation of arm position drifts significantly over time [104]. However, even with a large drift in proprioception, the direction and extent of motion remain relatively constant [7]. This effect is clearly evident when humans blindly draw repeated shapes: subjects render several nearly identical shapes with offset centers [102,111]. In the post-study survey, subjects were asked to estimate the percentage of time that they focused the center of their vision on their arms. The mean response to this question was 9.2% with a standard deviation of 13%, indicating that subjects relied heavily upon proprioception to complete the task. Thus, it was not surprising that a similar drift was found in this data set. For this reason, all fittings are evaluated by translating the center of the transformed human motion to the center of the robot motion.

The quality of each motion mapping model was determined using four tests that differed in their choice of training and validation data. In each test, the parameters of the three data-driven motion mappings were determined by fitting human motion from a training set to the corresponding robot motion. The identified mappings were then used to transform the validation set's human motion to a predicted robot motion for comparison to the actual robot motion. The scale factor in the traditional fittings was always taken as the ratio of the length of the PR2's arm to the length of the validation subject's arm. In the first test, the models were trained and tested on the same data; each trial represented one of the fourteen recordings for one subject. Second, the training data was set to be the first half of each recording, and the second half of the recording was used as the validation set. Third, a leave-one-out cross validation test was performed: for every subject, each of the fourteen data sets was used as the validation data for models trained on the combined data of the remaining thirteen sets. Fourth, a leave-one-out cross validation test was performed across all subjects; the combined data of each of the nine subjects was used as the validation set for motion mappings trained on the combined data for the other eight subjects. The median of the Cartesian distance from the transformed human position to the robot's actual position was used as the metric to evaluate the goodness of each fit.

The errors yielded by the four validation tests for each of the four motion mapping schemes are shown in Fig 2.3. A two-way analysis of variance (ANOVA) was implemented on the average values of the motion mapping errors for each test, using the fixed factor of mapping type and the random factor of subject number. These

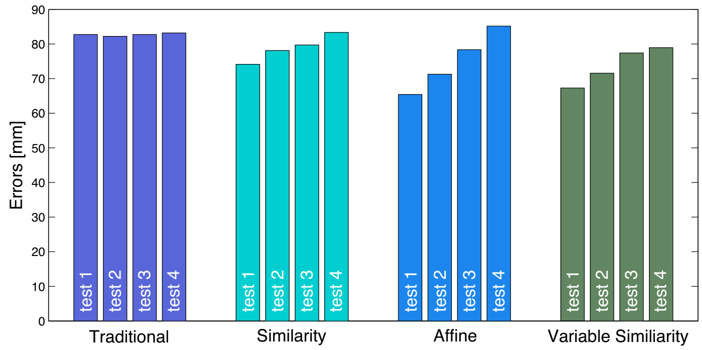

Figure 2.3: Average errors for tests 1 through 4 on the four tested motion mappings.

ANOVAs determines whether the motion mapping models yielded significantly different errors in each test, taking $\alpha = 0.05$. If model errors were found to differ significantly, a Tukey-Kramer post-hoc multiple comparison test was conducted at a confidence level of $\alpha = 0.05$ to determine which models produced significantly different errors. When the training and validation sets were the same (Test 1), the similarity, affine, and variable similarity transformations produced significantly lower error than the traditional fitting ($\mathrm{F}_1(3{,}35) = 26.96$, $p_1 < 0.0001$, $\eta_1^2 = 0.2717$), as one would expect from the higher dimensionality of these fittings. When a mapping trained on data from a given subject was tested on previously unseen motion data recorded from the same trial (Test 2) or a different trial (Test 3), the three data-driven mappings yielded similar errors, with the variable similarity performing slightly better than the similarity and affine transformation. All three data-driven mappings were again statistically significant improvements over the traditional fitting ($\mathrm{F}_2(3{,}35) = 17.33$, $p_2 < 0.0001$, $\eta_2^2 = 0.1462$; $\mathrm{F}_3(3{,}35) = 4.76$, $p_3 = 0.0096$, $\eta_3^2 = 0.0168$). The errors yielded by the cross-subject validation (Test 4) did not differ significantly from each other ($F_4(3,35) = 1.58$, $p_4 = 0.2201$). Though not significantly better, the variable similarity mapping is the only one that performs better than the traditional fitting in Test 4.

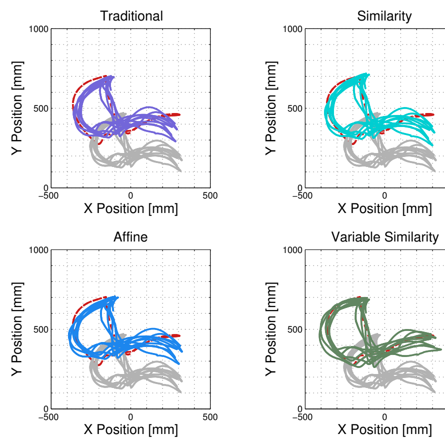

Figure 2.4: Transformed human motion (solid colored line) overlaid on robot data (dashed line) for subject 6, motion 3 (test 1). The original human data is also displayed in light gray. In test 1, the training and validation sets are the same.

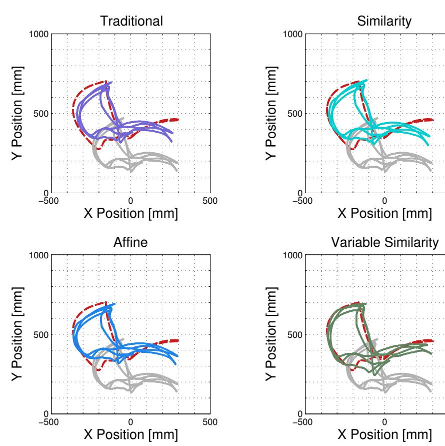

Figure 2.5: Transformed human motion (solid colored line) overlaid on robot data (dashed line) for the within-trial validation test for subject 6, motion 3 (test 2). The original human data is also displayed in light gray. Test 2 splits each trial in half to form the training and validation sets.

Figs. 2.4–2.7 show how the model trained in each one of the validation methods

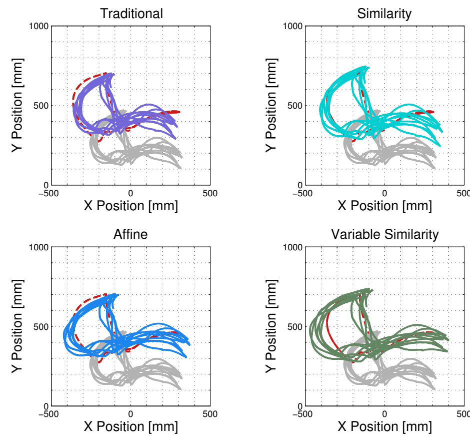

Figure 2.6: Transformed human motion (solid colored line) overlaid on robot data (dashed line) for the leave-one-out validation test for subject 6, motion 3 (test 3). The original human data is also displayed in light gray. Test 3 involves a standard leave-one-out cross-validation within each subject.

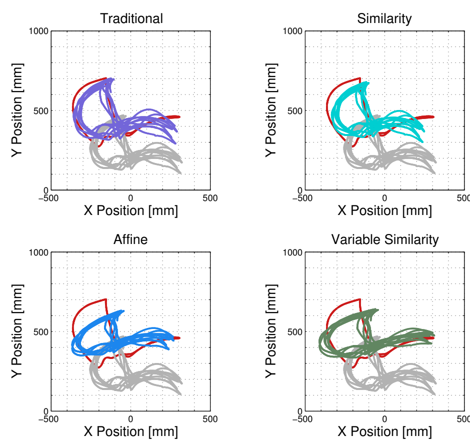

Figure 2.7: Transformed human motion (solid colored line) overlaid on robot data (dashed line) for the leave-one-out validation test across subjects for motion 3 (test 4). The original human data is also displayed in light gray. Test 4 involves leave-one-out cross-validation across subjects.

transforms a sample movement by Subject 6 to that of the robot. These plots make it clear that the variable similarity fitting can better match the features of human motion data to those of the robot motion data. In the same vein, Figs. 2.8–2.10 visually displays the distortion of space around each of the nine subjects' bodies when

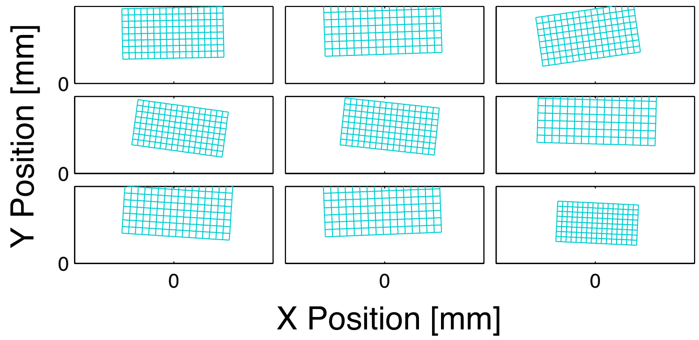

Figure 2.8: Visualization of all nine subjects' similarity mappings.

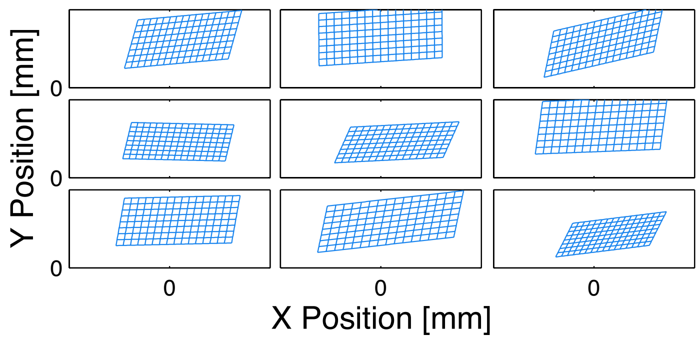

Figure 2.9: Visualization of all nine subjects' affine mappings.

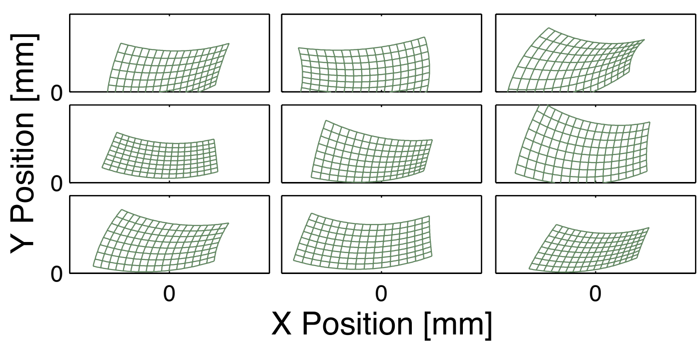

Figure 2.10: Visualization of all nine subjects' variable similarity mappings.

mapping human motion to robot motion under the data-driven similarity, affine, and variable similarity transformations trained on the combined data of each subject. These figures show that the similarity and affine transformations can be viewed as local approximations to the total spatial warping around the subject's body. Thus, if the similarity and affine transformations are trained on data recorded when the subject's hand is in a certain region, the resulting mappings may not be able to map human motion to robot motion when the subject's hand moves to another region. Since the global position of the subject's hand drifted over time, which was likely caused by the fact that they were using proprioception to estimate their arm positions, it will be important to accurately model a human's entire workspace when performing longer data captures.

The fact that the variable similarity fitting performed slightly better than the traditional mapping in the cross-subject leave-one-out validation study means that some parameters of this transformation are consistent across subjects. Though the variable similarity fittings shown in Fig. 2.10 clearly differ across subjects, there are some striking similarities among all of the identified mappings. Notably, these similarities are in general agreement with the systematic rotational errors described by Ghez et al. [21]. Fig. 2.10 shows how the human's motion would have to be transformed to best match the robot's motion. Thus, if the findings from this study are consistent with those described by Ghez et al., the variable-similarity transformation will appear to be an inversion of the distortions they described. Looking again at Fig. 2.10, we see that the angle of rotation error of the subject is consistent with the previously reported results: the magnitude of the direction error grows with lateral displacement and is increasingly counterclockwise to the left and clockwise to the right. Furthermore, the rotational errors made by subjects when the hand was between the body midline and the right shoulder were fairly small. With the exception of points very near to the body for subjects 1 (top left in Fig. 2.10) and 3 (top right in Fig. 2.10), the lateral location where the directional errors change from clockwise to counterclockwise is within 30 cm of the shoulder at all points over all nine subjects, which is consistent with the findings of Ghez et al. Additionally, much like their described distortions, the variable-similarity fittings show a large dependence on the lateral position of the subject's hand and a much smaller dependence on the extension of the subject's hand.

2.6 Task Difficulty

Fig. 2.11 shows the subjects' NASA Task Load Index ratings of the difficulty of the motion mimicking task. Overall subjects found the task to require relatively little mental effort. They also indicated that they were successful when completing and felt little insecurity while completing the task. However, subjects found the task to be moderately physically taxing and indicated they needed to work at moderately hard to complete the task. Some subjects also felt that they were felt hurried or rushed when completing the task. The higher than expected physical exertion are likely due to the subject's arm position. Although each subject was instructed to complete the mimicking task using only natural and comfortable motions, several completed the entire task while constraining his or her arm to the horizontal plane at shoulder height, which is a very tiring arm position. In future studies, I avoided this issue by more heavily emphasizing that subjects should stay comfortable during the experiment.

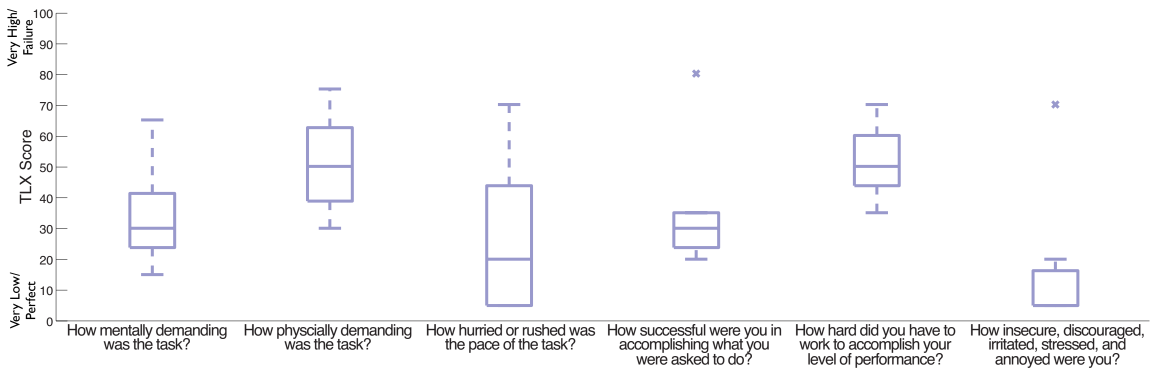

Figure 2.11: NASA NLX ratings of the difficulty of the motion mimicking task..

2.7 Conclusion

This chapter presents the first work to consider non-traditional data-driven motion mappings for teleoperation. A standard semi-automatic paradigm was created to determine motion mappings from the recordings of a human mimicking a target robot that was autonomously moving through a trajectory. Simultaneously measuring the motions of the human and the robot allows us to model how a subject systematically distorts space around his or her body while imitating the robot. I hypothesize that these models can be used to better enable the subject to naturally teleoperate the robot.

Three new motion mapping models were discussed in this paper: similarity, affine, and variable similarity. To validate these models, each was trained and validated in four tests: the same data set, portions of the same data, data from other trials by the same subject, and finally data recorded from other subjects. In the tests where mappings were trained and validated on motion data from the same subject, the three data-driven motion mappings all yielded significantly lower errors than the traditional motion mapping. The variable similarity fitting was the only motion mapping that yielded a lower error than the traditional mapping for the cross-subject validation study, although the difference was not significant.

The validation tests used for this study were an appropriate starting point, but to see the true effectiveness of each motion mapping model, I implemented them on a teleoperation platform for use by human operators. Chapter 3 describes a user study in which data-driven motion mappings were derived for each subject and tested against the traditional Cartesian-scaling motion mapping and a data-driven variable-similarity motion mapping fit to the aggregate data from the nine subjects who participated in the study described in this chapter.

Chapter 3

Evaluation of Data-Driven Motion Mappings

A teleoperation system with high transparency enables the operator to focus on completing the task at hand instead of on controlling the robot. In Chapter 2, I proposed that modifying the mapping from human movement to desired robot movement might improve the transparency of teleoperators in ways similar to adding sensory feedback. Specifically, I created non-Cartesian motion mappings that correct for systematic reaching errors made by humans, so that the robot motion resembles the operator's intent rather than his or her produced movement. This chapter presents a study that compares subjects' performance in a virtual teleoperated targeting task under three different motion mappings: the Cartesian-scaling motion mapping that is typically implemented in teleoperators, a corrective variable-similarity motion mapping that is fit to aggregate data from subjects in the previous study, and a corrective variable-similarity motion mapping that is fit to calibration data collected from each subject. Twelve participants reached toward 120 targets under each of the three motion mappings with balanced random presentation order and a washout task between conditions. Subjects were able to complete the targeting task with higher accuracy in initial direction of robot motion, at higher speeds, and with more natural and efficient reaching movements under the variable-similarity motion mappings. Subjects also overwhelmingly preferred the variable-similarity motion mappings. These results indicate that subjects experienced a higher level of transparency when using the virtual teleoperator with the variable-similarity motion mappings than with the standard Cartesian mapping. Therefore, mappings that correct for systematic errors in human motion, such as the variable-similarity motion mappings tested here, should be considered in teleoperator design.

This chapter first discusses the motion mappings investigated in this study in Section 3.1. I then provide detail about the experimental materials and methods in Sections 3.2 and 3.3. Sections 3.4 and 3.5 present the results from this experiment and interpret their meaning. Finally, I leave the reader with the main conclusions in Section 3.6. The research presented in this chapter was published as an article in the journal Presence: Teleoperators and Virtual Environments [48].

3.1 Tested Motion Mappings

The validation tests discussed in Section 2.5 were an appropriate starting point, but to see the true effectiveness of different motion mappings, they needed to be implemented on a teleoperation platform and used by human operators. Given the variable-similarity motion mapping's promising performance in the preliminary tests, I designed a study to elucidate how data-driven variable-similarity motion mappings affect a human's ability to perform remote tasks using a teleoperator, especially when compared to their performance using a traditional Cartesian-scaling motion mapping. Secondarily, we sought to discover whether there were any measurable differences in task performance when the subject uses a population-fit variable-similarity motion mapping, which corrects for the average distortions made by a group of subjects, versus an individually-fit variable-similarity motion mapping, which is based on data collected during a calibration routine.

In this study subjects performed a targeted-reaching task under three different motion mappings; a Cartesian scaling motion mapping described in Section 2.4.1, and two variable-similarity motion mappings described in Section 2.4.4. The scale factor of the Cartesian-scaling motion mapping was chosen to be the ratio of the length robot's arm to length of the subject's arm. This choice of scale factor most closely transforms the workspace of the subject to the workspace of the robot. The first data-driven variable-similarity motion mapping was calibrated using the aggregate data of the population of the nine subjects discussed in Chapter 2, so it corrects for average directional errors. As a reminder, the variable-similarity motion mapping can be written as follows,

$$\vec{x}_r = s(\vec{x}_h)T(\vec{x}_h)\vec{x}_h + \vec{\gamma}(\vec{x}_h) \tag{3.1.1}$$

$$T(x,y) = \begin{bmatrix} \cos(\theta(\vec{x}_h)) & -\sin(\theta(\vec{x}_h)) \\ \sin(\theta(\vec{x}_h)) & \cos(\theta(\vec{x}_h)) \end{bmatrix} \tag{3.1.2}$$

$$\vec{\gamma}(\vec{x}_h) = \begin{bmatrix} \gamma_x(\vec{x}_h) \\ \gamma_y(\vec{x}_h) \end{bmatrix} \tag{3.1.3}$$

$$s(x,y) = a_s x_h + b_s y_h + c_s \tag{3.1.4}$$

$$\theta(x,y) = a_\theta x_h + b_\theta y_h + c_\theta \tag{3.1.5}$$

$$\gamma_x(x,y) = a_{\gamma x} x_h + b_{\gamma x} y_h + c_{\gamma x} \tag{3.1.6}$$

$$\gamma_y(x,y) = a_{\gamma y} x_h + b_{\gamma y} y_h + c_{\gamma y} \tag{3.1.7}$$

The fitted parameters for the population-fit variable similarity motion mapping are given in Table 3.1

The second variable-similarity motion mapping was fit individually for each subject in this study, based on data from the calibration described in Section 3.3.1. A geometric representation of the population-fit variable-similarity motion mapping is shown in Fig. 3.1. The individually fit motion mappings are shown in Fig. 3.4.

Parameter	Value
a_s	-0.000188 $\frac{1}{mm}$
b_s	0.000163 $\frac{1}{mm}$
c_s	1.159217
a_θ	-0.000107$\frac{1}{rad}$
b_θ	-0.000610$\frac{1}{rad}$
c_θ	-0.003591
$a_{\gamma x}$	-0.063688
$b_{\gamma x}$	-0.077315
$c_{\gamma x}$	279.937082 mm
$a_{\gamma y}$	-0.174457
$b_{\gamma y}$	0.448195
$c_{\gamma y}$	89.506589 mm

Table 3.1: The fitted parameters of the population-fit variable similarity motion mapping. These parameters were derived in a right shoulder centered coordinate frame, with the X-axis pointing forward and the Y-axis pointing to the left. When used with equations (3.1.1)-(3.1.7), the X and Y position of the human's hand should be given in millimeters.

3.2 Experimental Setup

I created a teleoperator that would allow different motion mappings to be introduced when calculating the desired robot hand position from the human's measured hand position. For the master device, I simply needed an accurate motion capture system, as I was not trying to provide any haptic feedback to the user. Because I sought to improve the accuracy, speed, and intuitiveness with which one can control a remote robot, we needed a robot that responds to position commands, but it did not need to manipulate objects in its environment. Therefore, I chose to use a simulated robot in this experiment.

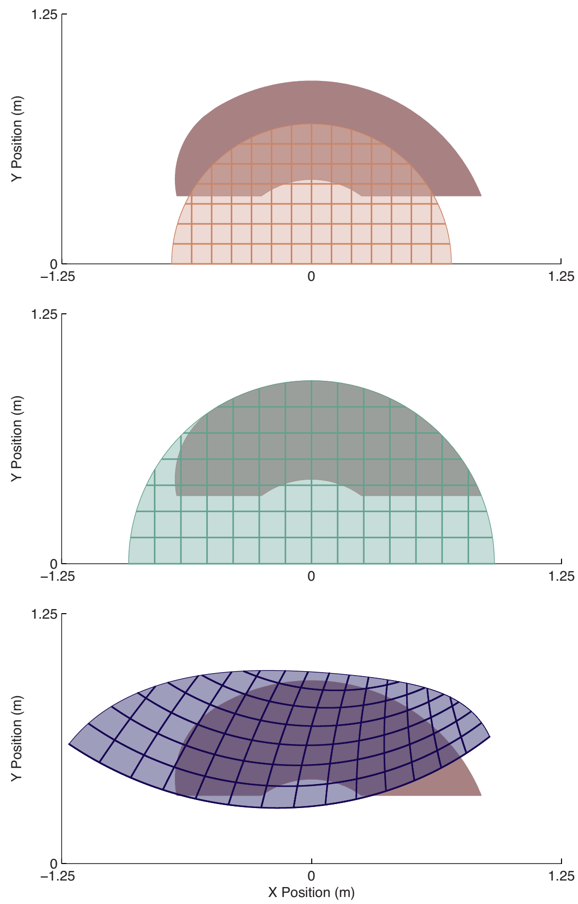

Figure 3.1: A sample subject's workspace (top), the subject's workspace transformed using the traditional Cartesian-scaling motion mapping (middle), and the subject's workspace transformed by the population-fit variable-similarity motion mapping (bottom).

3.2.1 Virtual Robot

A virtual version of Willow Garage's humanoid robot, the PR2, was once again chosen for use in this experiment as it is fully supported by ROS (Robot Operating System) [80] and is readily available for use in Gazebo, an open-source, three-dimensional multi-robot simulator [50]. The virtual PR2 robot was presented to the user using ROS's Robot Visualizer (RViz) [38], which allowed me to control objects in the robot's environment. Fig. 3.2 shows the view of the robot presented to the user. The robot's

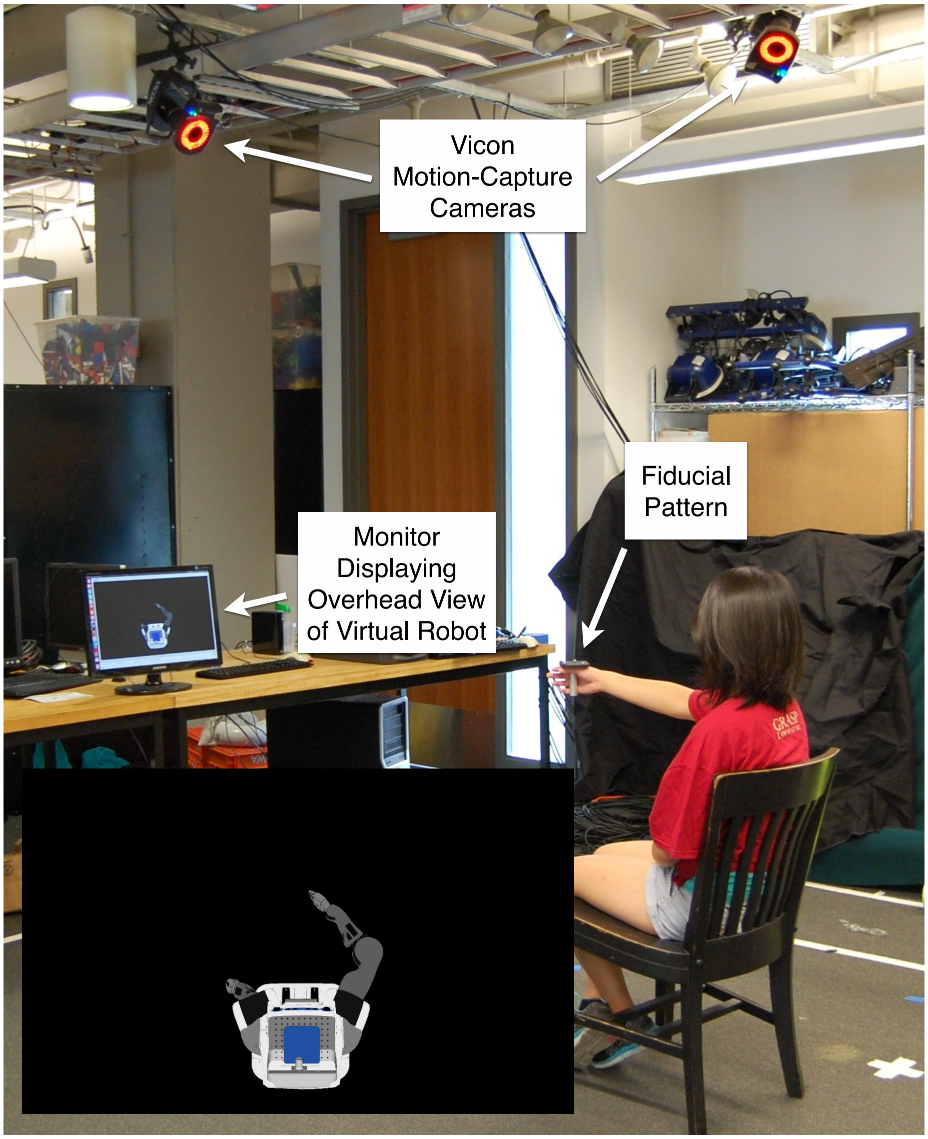

Figure 3.2: The subject controlled the hand position of a virtual PR2 robot during the study. An overhead view of the robot was displayed on a monitor approximately 1.5 m away from the subject's chair. A Vicon motion capture system was used to track the position of the subject's hand relative to his or her shoulder.

arm position was commanded using a real-time joint controller that ran in ROS's hard realtime control loop. For all three motion mappings, the desired position of the PR2's hand was constrained to the horizontal plane passing though the robot's shoulders. The robot's arm was always configured such that the entire robot arm was also contained in this horizontal plane. Additionally, the joints of the robot's spherical wrist were fixed so that the hand acts as a rigid extension of the robot's forearm. In this configuration, the PR2's arm is reduced to a two link manipulator with revolute joints at the robot's shoulder and elbow. The inverse kinematics for this two-link manipulator can be solved analytically to find the desired shoulder and elbow angles given a desired hand position. The control loop explicitly solved this inverse kinematics problem with each iteration, always choosing the elbow-out solution. The resulting desired shoulder and elbow angles were then commanded to the virtual robot using a PD control law on each joint. Although the controller ran at a regular rate of 1000 Hz in simulation time, irregular scaling between real time and simulation time means that the controller was running at an irregular update rate that averaged 792 Hz in real time.

As shown in Fig. 3.2, the overhead view of the robot allowed the subject to view the plane in which the robot's arm was contained without any distortions. The robot was placed in a solid black virtual environment to avoid giving the subject any spatial context, which could affect their performance in both the targeting task and the mimicking task.

3.2.2 Motion Capture

We used a Vicon MX motion capture system with six cameras to measure the human's hand position. To allow the Vicon system to measure the position and orientation of the subject's right shoulder and right hand, we created two patterns of retro-reflective markers for the Vicon system to track. One marker pattern was placed at the subject's shoulder; it was attached via velcro to a t-shirt worn by the subject over their own clothes. To ensure that the shoulder marker pattern would remain stationary when the subject moved his or her arm, I placed the marker pattern on top of the clavicle bone, as close to the shoulder joint as possible. The second marker pattern was attached to a handle that was held by the subject during the experiment. The Vicon system measured the position and orientation of each pattern at a rate of 120 Hz.

3.2.3 Teleoperator Integration

The Vicon motion capture system and the virtual PR2 robot were integrated using ROS. Each time new position data was measured by the Vicon motion capture system, a ROS topic was used to send the subject's hand position to the robot's software controller. The positions of the marker patterns were first used to calculate the position of the subject's hand in a coordinate frame centered at the right shoulder. The controller then transformed the position of the subject's hand using one of the three motion mappings tested in this experiment.

3.3 Experimental Procedures

All experimental procedures were approved by the University of Pennsylvania's Institutional Review Board under protocol number 817343. Twelve subjects between the ages of 19 and 31 participated in all experimental procedures. Three of the subjects were female, and the remaining nine subjects were male. Eleven of the subjects were right handed, and one was left handed; all subjects completed the study tasks using their right arm. At the beginning of each session, the experimenter reviewed all experimental procedures and obtained informed consent. The subject then completed a short survey on demographic information. The survey also asked the subject to confirm having normal motor control of the right arm and normal or corrected-to-normal vision, both of which were required for participation in this study. Once deemed eligible for participation, the subject completed the three activities described below.

3.3.1 Motion Mapping Calibration

In this phase of the study, data was collected for both the Cartesian-scaling and the individually-fit variable-similarity motion mappings. The population-fit motion mapping was fit to data recorded in Chapter 2 and was not changed for any of the subjects. As defined by Equation (2.4.1), the Cartesian-scaling motion mapping scales the human's motion by the ratio of the length of the robot's arm to that of the subject's. Therefore I needed to measure the length of each subject's arm. The subject held his or her arm straight out, and I measured the distance between the

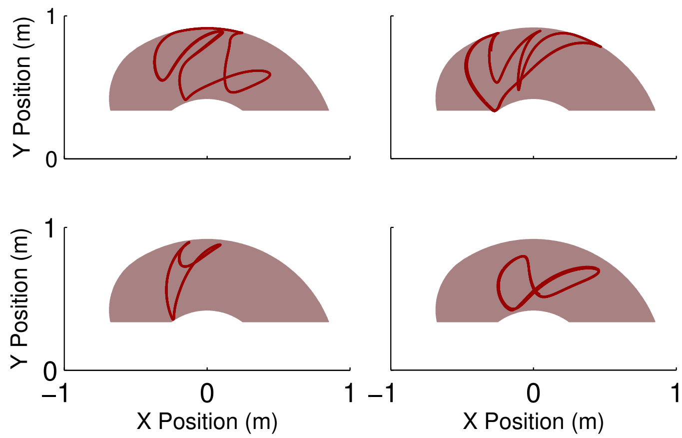

Figure 3.3: The four robot trajectories that the human mimicked in the calibration stage.

marker pattern placed at the shoulder and the marker pattern held in the subject's hand.

The calibration routine used to determine an individual motion mapping for each subject was nearly identical to the procedure described in Section 2.3. The subject was seated in a chair in the center of the Vicon space approximately 1.5 meters away from a 24-inch-diagonal computer monitor displaying an overhead view of the robot, as shown in Fig. 3.2. The robot then moved its right arm through the four pre-programmed periodic trajectories shown in Fig. 3.3. Each motion was traced by the robot's hand four to six times over approximately one minute. Subjects were instructed to follow the motion of the robot as closely as possible using only comfortable and natural movements of their right arm. During this task, each subject mimicked each set of trajectories twice consecutively, for eight total trials. A computer program was used to record all seven joint angles of the PR2's right arm and the subject's shoulder and hand position at an irregular rate of approximately 1000 Hz, although the human position data was updated at a rate of only 120 Hz. After the calibration phase of the study, the subject rested while I calculated the individually-fit variable-similarity motion mapping, according to the methods described in Section 2.4.

3.3.2 Teleoperation Targeting Task

The subject completed a targeted reaching task to determine how each motion mapping affected his or her ability to control the simulated robotic arm. A video showing an example of the targeted reaching task is available at http://haptics.grasp.upenn.edu/index.php/Research/Data-DrivenMotionMappings. The subject was told that three different motion mappings would be introduced during the targeting task, but was given no information about the motion mappings. The motion mappings were referred to only by the order in which they were presented.

The targeting task took place in the same Vicon motion capture space as the calibration task, and all data collection procedures were also the same. At each time step, the human's hand position was transformed through one of the three motion mappings to obtain the desired robot hand position, which was then commanded to the virtual PR2 robot.

The targeting task started with a green circle appearing in the robot's workspace. The green target was displayed on the screen for 0.25 seconds in simulated time, which yielded an average 0.23 seconds in real time. Once the target disappeared from the screen, the subject moved the center of the robot's hand to the location the target had occupied as quickly and accurately as possible. The subject then held the robot's hand as still as possible at the final location. After the robot's hand remained still for more than 0.1 seconds in simulated time, the next target appeared on the screen. The location of successive targets was chosen randomly from a set of possible targets at five distances (5, 10, 15, 20, or 25 cm) and sixteen directions (0, $\frac{\pi}{8}$, $\frac{\pi}{4}$, ..., $\frac{15\pi}{8}$ rad) from the ending location of the robot's hand. The location of the target was checked to ensure it was in the robot's workspace; if it lay outside of the reachable workspace, another target location was randomly chosen, and its location was checked for validity. The next target was then displayed to the user as a green circle in the robot's workspace. Once this target disappeared, the subject again moved the robot's hand to the space the target had occupied. This process was repeated until the subject had reached to 40 targets. The subject then rested for as long as he or she desired before starting the next set. The subject completed three sets of 40 targets for each motion mapping.

After doing all three sets for the first motion mapping, the subject completed the surveys described in Section 3.3.3 and the mimicking washout task described in Section 3.3.4. The subject then repeated the targeting task, the surveys, and the mimicking washout task for the remaining two motion mappings. Each of the six possible motion mapping orders was tested by two subjects to minimize the effects of learning and fatigue.

The data collected in the targeting task was split into two files, each recorded in a separate ROS node. The first data set contained the robot's commanded position, the robot's actual position, the human's position, and a time stamp. The second data set contained the target locations and time stamps. The timers used to record the time stamps for each data set were synchronized.

3.3.3 Survey Data

The subject indicated the difficulty of the targeting task in the six domains of the NASA Task Load Index (TLX) [37]: mental demand, physical demand, temporal demand, performance, effort, frustration. Subjects were not asked to rank the importance of the six domains due to time constraints in the experiment.

3.3.4 Mimicking Washout Task

After filling out the TLX survey for a motion mapping, the subject did a mimicking task similar to the calibration. The setup for this activity was identical to that used in the calibration phase. The subject mimicked the robot completing the trajectory shown in the top right plot of Fig. 3.3 for two one-minute segments. If completing the targeting task under different motion mappings causes any after effects, performing this task between sets should help the subject return to his or her natural arm motions. The data for this task was recorded in the same manner as the calibration data.

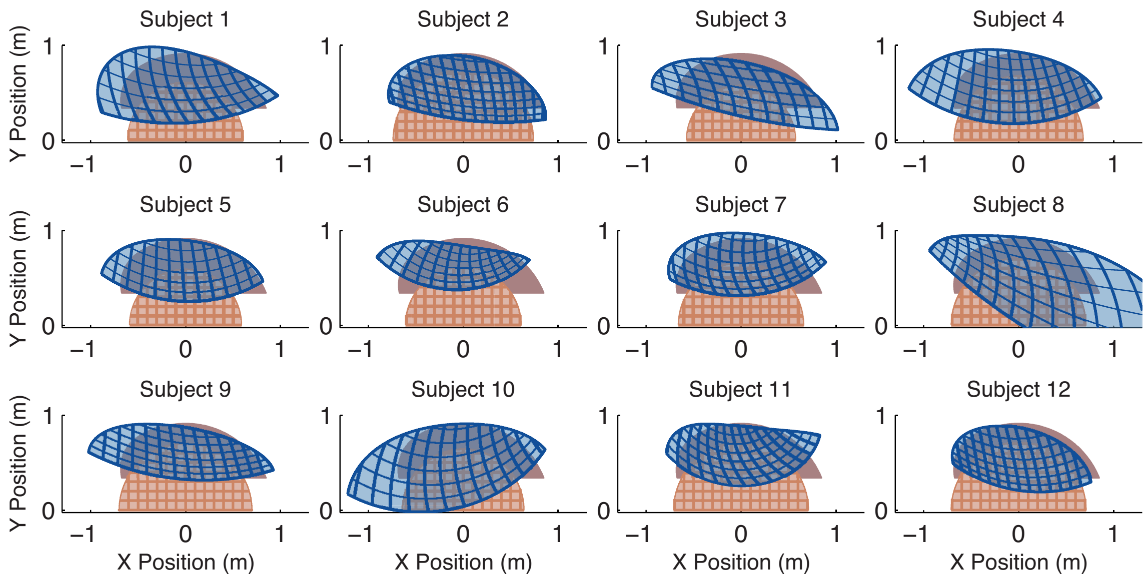

Figure 3.4: The workspace of each of the 12 subjects (tan) is transformed using the individually-fit variable-similarity motion mapping (blue). The robot's workspace is also displayed (brown).

3.3.5 Final Preference

After the entire experiment was complete, nine of the subjects were asked "Which motion mapping did you prefer?" The final nine subjects were asked this question after an early subject volunteered this information after completing the study.

3.4 Results

Motion Mapping Calibration

All twelve subjects successfully completed the calibration phase of the study. Fig. 3.4 displays a visual representation of the individually-fit variable-similarity motion mappings for each of the twelve subjects. In each plot, the human's workspace is represented as a semicircle with a radius equal to the subject's arm length. This is a reasonable representation of the projection of the subject's workspace onto the horizontal plane because the subject's arm was never constrained during the study, allowing the subject to reach all points in this semicircle. A Cartesian grid is overlaid on the human's workspace to help visualize how the area within the subject's workspace is transformed by the individually-fit variable-similarity motion mapping. The human's workspace and the Cartesian grid are transformed using each subject's individually-fit motion mapping to obtain the area of the robot's workspace that the human can reach with this mapping. The robot's workspace is also displayed on each plot.

3.4.1 Teleoperation Targeting Task

Thirteen metrics were chosen to measure how well the subjects completed the targeting task under the three different motion mappings. The first three metrics describe how accurately the subject moved the robot's hand from the starting position to the target location. The remaining ten metrics describe aspects of the human's and the robot's trajectory as the subject moved the robot's hand from the starting position toward the target location.

For each of the presented targets, the metrics were calculated using only the data collected during the time when the subject was actively moving the robot's hand toward the target location. To determine this period of time, I first roughly segmented the data by creating a separate data file of human motion and robot motion for each target presented; this file includes a stationary period before the subject started moving the robot's hand, the active period when the subject was moving the robot's hand, and a stationary period after the subject completed his or her move and was waiting for the next target to be presented. I refined this segmentation by determining the onset of motion by finding the point in time when the speed of the user's hand rose above a threshold, δ. Similarly, I determined the time of motion completion by finding the point when the speed of the user's hand fell below the threshold δ. I chose to set a default threshold value of $\delta = 0.002$ m/s, which is just higher than the noise level observed in the human's speed data. However, since subjects were only verbally asked to hold still between targets, and they had to do so without any physical support, some segments had a small initial and final velocity, causing the segmentation to fail with $\delta = 0.002$ m/s. For these trials, the threshold value δ was incremented by 0.0001 m/s until the threshold was high enough for the segmentation method to find the period of active motion. I believe this approach is better than using a single threshold value that is higher than necessary for the majority of the trials because a lower threshold value more accurately detects the beginning and end of the human's motion. The average threshold value used was 0.00205 m/s with a standard deviation of 0.00024 m/s. The onset and completion times found by the above method were visually inspected for all presented targets to ensure accuracy. Fig. 3.5 shows a sample trajectory from the first subject moving the robot's hand

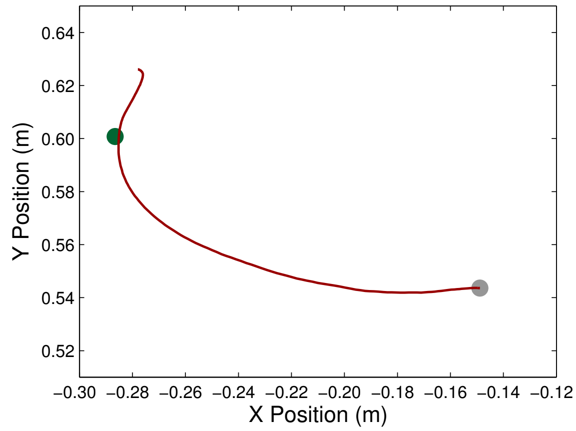

Figure 3.5: A sample robot motion trajectory. The starting location of the robot's hand is shown by the light gray circle and the goal location is shown by the dark green circle. The origin of this plot is located at the center of the subject's right shoulder. This trajectory will be used to illustrate several of the metrics used to analyze the subjects' performance.

toward a target under the Cartesian-scaling motion mapping.

Once the period of active motion was accurately determined, I was able to compute the thirteen metrics for each target under each of the three motion mappings. The following paragraphs describe all of the metrics and explain whether subjects obtained significantly different metrics under the three motion mappings. For the following analyses all metrics were calculated for each of the 120 targets presented per motion mapping. I then eliminated non-representative trials in which any one metric was more than 1.5 standard deviations away from the mean for that subject for that motion mapping. Once the trials that contained outlier metrics were removed, I calculated the mean value of each metric for each subject under each motion mapping. A two-way analysis of variance (ANOVA) was performed for each metric using the factors of subject number and the motion mapping that the subject used to complete the targeting task. This analysis allows me to determine whether the factor of motion

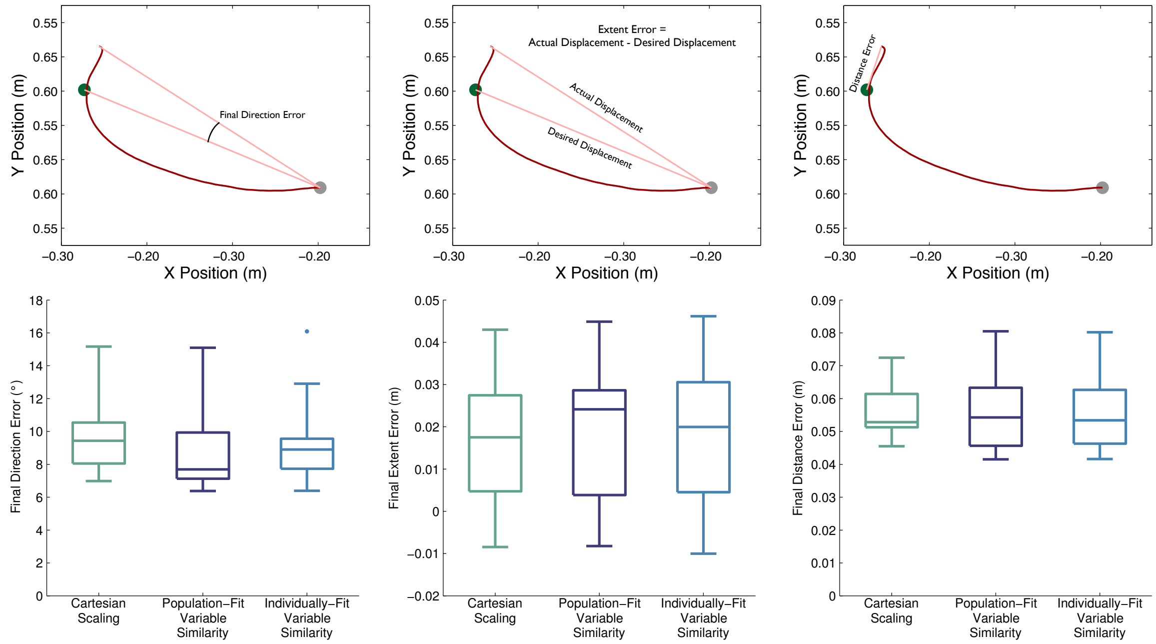

Figure 3.6: (Top) Illustrations of the final direction, final extent, and final distance errors. (Bottom) There were no statistical differences in the subjects' final direction error (F = 2.90, p = 0.076), the final extent error (F = 0.24, p = 0.79), or the final distance error (F = 0.0089, p = 0.99).

mapping affected how the subjects performed the task. When a significant difference in subject performance was found, a Tukey-Kramer post-hoc multiple comparison test was performed at a confidence level of $\alpha = 0.05$ to determine which mappings led to significant differences in the metric. Significant pairwise difference are marked with brackets in the figures.

The three metrics that describe how accurately the subject was able to move the robot's hand to the target location are final direction error, final extent error, and a final distance error. These three metrics are illustrated in Fig. 3.6. The direction error is defined to be the magnitude of the angle between two lines originating at the starting location of the robot's hand: one line ends at the target location and the other line ends at the final location of the robot's hand. The extent error is taken to be the difference between the actual and the desired displacement of the robot's hand. Finally, the distance error is the distance between the target location and the location of the robot's hand after the subject stopped moving. The distribution of the direction, extent, and distance errors are shown in Fig. 3.6. There were no statistically significant differences between how well the subject completed the targeting task under the Cartesian-scaling motion mapping, the population-fit variable-similarity motion mapping, or the individually-fit variable-similarity motion mapping as measured by the final direction error ($F = 2.90$, $p = 0.076$), the final extent error ($F = 0.24$, $p = 0.79$), or the final distance error ($F = 0.0089$, $p = 0.99$), although the final direction error is close to significance.

In addition to considering metrics regarding the final position of the robot's hand, I also considered metrics that describe the human's trajectory and the robot's trajectory as the subject moved the robot's hand from the starting location to the target location. The first of these metrics is an initial direction error, which is shown in Fig. 3.7. I was interested in such a metric because the variable-similarity motions mappings were designed to help correct for the systematic position-dependent direction errors that humans make when performing a targeting task while relying solely upon proprioception. I defined the initial direction to be the angle of the line connecting the robot's starting position to the point where the robot's hand is first displaced 1 cm. The initial direction error is then defined as the magnitude of the angle be-

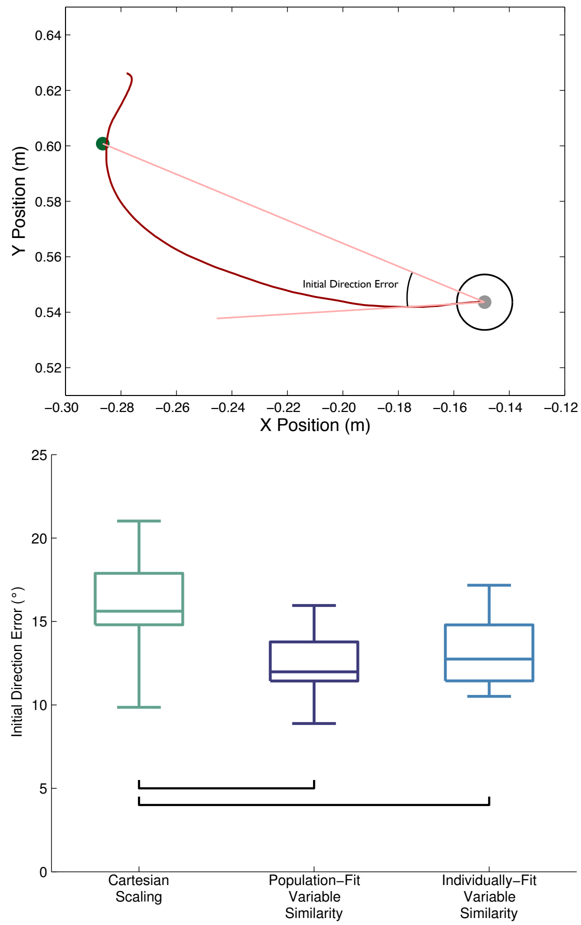

Figure 3.7: (Top) The initial direction is defined as the angle at which the robot's hand leaves a 1 cm circle. The initial direction error is the difference between the initial direction and direction from the starting position to the goal. (Bottom)The subjects' initial movement were more accurate when completing the task under both the population-fit and the individually-fit variable-similarity motion mappings ($F = 7.86$, $p = 0.0027$).

tween the initial direction and the direction of the line connecting the robot's initial hand position and the target location. Fig. 3.7 is a box plot showing the average initial direction errors for the twelve subjects when completing the targeting task under the three different motion mappings. Subjects had significantly smaller initial direction errors when completing the targeting task with both the population-fit variable-similarity motion mapping and the individually-fit variable-similarity motion mapping than when completing the task using the traditional Cartesian-scaling motion mapping ($F = 7.86$, $p = 0.0027$).

In addition to the accuracy of the initial movement, I sought a metric describing how naturally the subjects moved their arms when completing the targeting task under the different motion mappings, to gain insight into how each motion mapping affected the user's performance. It is well established that humans make arm movements using trajectories that minimize the time integral of the magnitude of jerk [17]. Therefore, if subjects are moving their arms in a natural fashion, their paths should follow a minimum jerk trajectory. It has also been established that humans will make curved trajectories when reaching with neither any physical external constraints acting on their arms nor any instruction about the straightness with which they should move [16]. Therefore, rather than comparing the subjects' motion trajectories to the models presented in [17], which state that the human's hand movement will be in a straight line, I compared the subjects' movements to a model that allows for curvature. The curved minimum jerk trajectory that we created states that the path length through which the hand moved should follow the quintic trajectory of a minimum jerk movement. In other words, the path length traveled should be:

$$S(t) = \sum_{n=0}^{5} c_n t^n \tag{3.4.1}$$

where the coefficients c_n can be found by setting the initial and final position, velocity, and acceleration of the minimum jerk trajectory to the initial and final position,

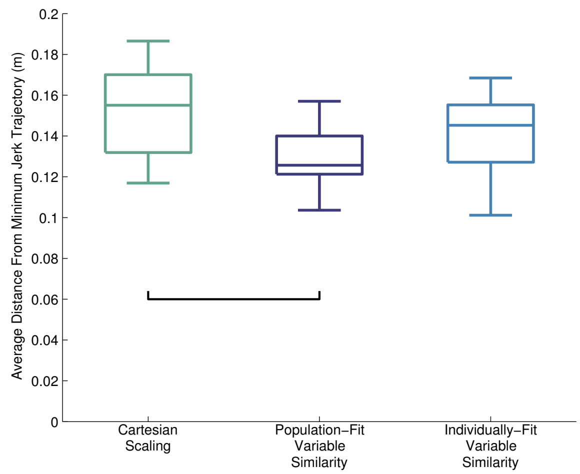

Figure 3.8: Subjects' trajectories were closer to a minimum jerk trajectory when completing the task under the population-fit variable-similarity motion mapping than with Cartesian scaling (F = 7.86, p = 0.0027).

velocity, and acceleration of the human's trajectory. I chose this metric because the data presented in [106] show that the velocity profiles of curved movements made by subjects are similar to the velocity profile predicted by the straight-line quintic models of [17]. To determine how close the subject was to the minimum jerk model, I calculated the average path length distance that the human's hand was away from the curved minimum jerk trajectory. The average minimum jerk errors are shown in Fig. 3.8. When completing the task under the population-fit variable-similarity motion mapping, subjects' trajectories were significantly closer to the minimum jerk trajectory than they were under the Cartesian-scaling motion mapping (F = 9.67, p = 0.00096). Although not significant, the average distance to the minimum jerk trajectory is also smaller when the subjects were completing the task with the individually-fit variable-similarity motion mapping than when completing the task using the Cartesian-scaling motion mapping.

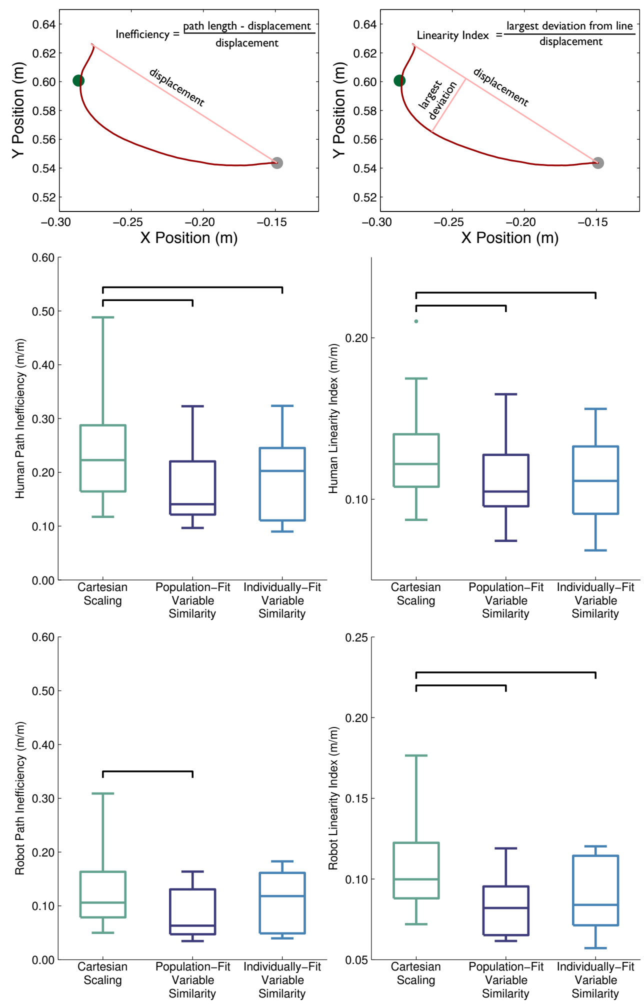

Figure 3.9: (Top) Definitions of the two metrics that measure path inefficiency and linearity. (Bottom) Both the subjects' and the robot's trajectories were more efficient under the variable-similarity motion mappings.

Analysis of the efficiency of the subject's movements will lend further insight into how well the subjects completed the targeting task using the different motion mappings. To measure movement efficiency, I defined two metrics; the first measures movement inefficiency and the second measures movement linearity. Each of these two metrics was computed for both the human's motion and the robot's motion. As shown in Fig. 3.9, I defined movement inefficiency as the difference between the path distance traveled and the displacement of a movement. Since several target distances were presented, I normalized this metric by the displacement of the movement. Movement linearity is measured by the linearity index, as first defined in [1]. The linearity index is the ratio of the largest deviation of a trajectory from the straight line that connects the beginning and end of the motion to the displacement of the movement, as illustrated in Fig. 3.9. The distributions of these two metrics are shown in Fig. 3.9. When completing the targeting task using both of the variable-similarity motion mappings, the subjects moved their arms with significantly lower movement inefficiency ($F = 9.30$, $p = 0.0012$) and lower linearity indices ($F = 6.34$, $p = 0.0067$). The robot's movements had significantly lower inefficiencies when the subject was completing the task under the population-fit variable-similarity motion mapping ($F = 4.30$, $p = 0.027$). I also evaluated the robot's motion using the two efficiency metrics because efficiency in the robot's motion is desirable, especially in teleoperators where the remote robot has limited battery life and power consumption is a key factor in the system's success. The motion of the robot had significantly lower linearity indices when the subject was completing the targeting task with both the population-fit and individually-fit variable-similarity motion mappings ($F = 10.46$, $p = 0.00064$).

Finally, I investigated how quickly the subjects completed the targeting task by evaluating both the average and peak speed of both the human's and the robot's hand. As shown in Fig. 3.10, the human's average speed and peak speed were significantly higher when the subject was completing the targeting task under the population-fit

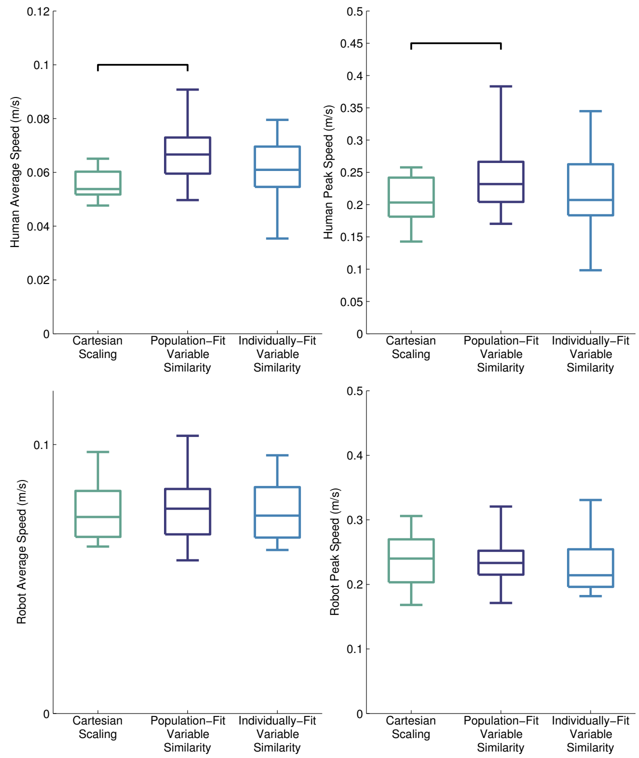

Figure 3.10: The subjects' and robot's peak speeds were highest under the population-fit variable-similarity motion mapping. No statistical differences were found in the subjects' and robot's average speeds.

variable-similarity motion mapping than with the Cartesian-scaling motion mapping (F = 11.17, p = 0.00045), (F = 4.50, p = 0.023), respectively. There were no significant differences between the mappings for either the average speed of the robot's hand (F = 1.06, p = 0.36) or the peak speed of the robot's hand (F = 0.34, p = 0.72).

3.4.2 Survey Data

Subjects rated the cognitive workload of the task using the NASA Task Load Index (TLX) [37] after finishing the targeting task under each of the three motion mappings. The perceived difficulty of the task, as measured by subject responses to the six TLX

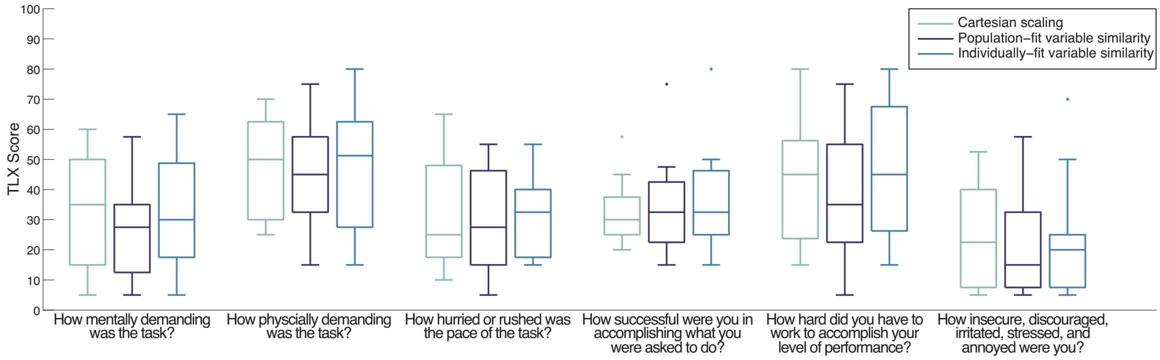

Figure 3.11: Subjects rated task difficulty using the NASA Task Load Index (TLX). For all questions, a lower rating indicates less difficulty. Numbering the questions from left to right, a rating of 0 corresponds 'very low' for questions 1, 2, 3, 5, and 6 and 'perfect' for question 4, while 100 corresponds to 'very high' and 'failure'. No significant differences were found in task difficulty as measured by TLX ratings.

questions, is shown in Fig. 3.11. A three-way ANOVA was performed on the responses to each of the six questions using the factors of mapping, set number (1, 2, or 3), and subject. No significant differences were found for any of the questions for the mapping and set number factors.

3.4.3 Washout Task

For each subject we collected two mimicking data sets containing human motion and robot motion for each mapping tested. I analyzed this data to determine if the subject's performance in the mimicking task was affected by the motion mapping that had just been used in the targeting task. Since there was a small time delay in the human's reaction to the robot's motion, I first aligned the human's motion to the robot's in time. To do so, I eliminated the first two seconds and final half second from the robot's motion data. I then found the segment of human data that

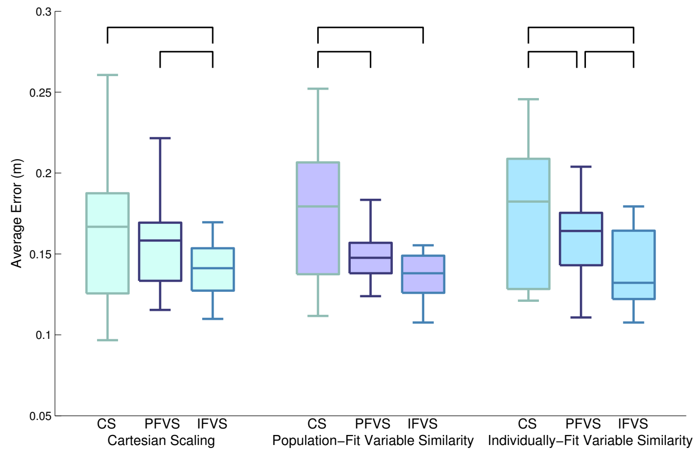

Figure 3.12: The subjects mimicked the motion of the robot after each motion mapping was tested in the targeting task. For each motion mapping tested (box fill color), the motion data was transformed using each of the three motion mappings (box outline color). The washout task showed a small after-effect due to the motion mapping tested in the targeting task.

best transformed to the robot's under a similarity transformation, which effectively removes the time delay of the human.

I transformed each human motion dataset using the Cartesian-scaling motion mapping, the population-fit variable-similarity motion mapping, and the individually-fit variable-similarity motion mapping. To compare how close the transformed human data was to the corresponding robot motion, I computed the average Cartesian distance between the transformed human motion and the corresponding robot motion. Since subjects mimicked the motion of the robot two times after each targeting set, I obtained one error metric by averaging the resulting error values for the two data sets. As shown in Fig. 3.12, the human data transformed with the individually-fit variable-similarity motion mapping is always closer to the corresponding robot data than when the same human motion data is transformed using the Cartesian-scaling

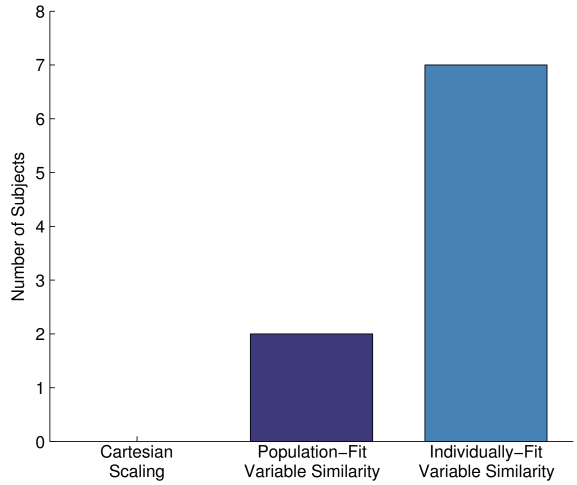

Figure 3.13: Subject's responses to the question "Which motion mapping did you prefer?"

motion mapping or the population-fit variable-similarity motion mapping. Furthermore, the average distance between the transformed human motion and the robot motion is smallest for each motion mapping after that motion mapping was tested in the targeting task.

3.4.4 Final Preference

After the final motion mapping was tested, nine of the subjects answered the question"Which motion mapping did you prefer?" Subjects responded with either the first, second, or third motion mapping tested, and I recorded this preference. I began to collect this data only after the fourth subject volunteered this information after completing the study. Preference data was not collected for the first three subjects. The subjects' preferences are shown in Fig. 3.13. Seven subjects responded that they most liked doing the targeting task under the individually-fit variable-similarity.

Two subjects responded that they most liked doing the targeting task under the population-fit variable-similarity motion mapping. No subjects indicated that they preferred the Cartesian-scaling motion mapping.

3.5 Discussion

Motion Mapping Calibration

Each subject mimicked the movement of the robot during the calibration activity, enabling us to calculate his or her individually-fit variable-similarity motion mapping. The calibration was successful for several reasons. First, the identified transformations were able to map the human's workspace to cover nearly the entire portion of the robot's workspace in which targets could have been presented (mean 90.4%, standard deviation 8.4%), meaning the subjects were able to use their individually-fit motion mappings to reach a large percentage of the robot's workspace. Furthermore, the individually-fit motion mappings allowed each subject to reach a large percentage of the robot's workspace using only a subset of his or her own workspace (mean 65.6%, std. dev. 12.4%).

The results from the calibration phase of this study also contain information that is relevant to the secondary research question: is it important to fit an individual motion mapping for each subject, or does a population-fit motion mapping suffice? It is difficult to make analytical comparisons between the 12-degree-of-freedom variable-similarity motion mappings fit to the different subjects. Therefore, I interpreted the mappings geometrically by analyzing how each subject's workspace is transformed under the variable-similarity motion mappings. I also used this geometric analysis to compare the individually-fit variable-similarity motion mappings between subjects, as well as to the population-fit variable-similarity motion mapping.

The first geometric metric that we analyzed was the scale factor, given by

$$S = \frac{A'_h}{A_h} \tag{3.5.1}$$

where A'_h is the area of the transformed human's workspace and A_h is the area of the human's workspace. The mean scale factor for the individually-fit variable-similarity motion mappings, 1.51±0.70, is not stastically different from the mean scale factor for the population-fit scale factors, 1.38±0.12 ($p = 0.5185$). Therefore, the population-fit motion mapping may capture the average behavior of the subjects in this study.

A similar trend was found in the other two geometric interpretations of the variable-similarity motion mappings. The first is the inversion point of the motion mapping, which I defined as the point where the X-axis of the human's workspace is mapped with a zero rotation. To the left of the inversion point, the variable-similarity motion mapping will correct for counter-clockwise directional errors. To the right of the inversion point, the variable-similarity motion mapping will correct for clockwise directional errors. Ten of the twelve individually fit motion mappings had an inversion point. The average inversion point of these ten subjects is 0.0122±0.17 m to the left of the subject's right shoulder. Although there is a lot of variation among the subjects, the mean value of the inversion point of the individually-fit motion mappings is not significantly different from the inversion point of the population-fit motion mapping, which is 0.0512 m to the left of the shoulder ($p = 0.4830$). The inversion points found in the individually fit motion mappings and the population-fit motion mappings are both in general agreement with the findings of [21].

The final geometric interpretation is the overall rotation of the transformed human workspace, which we defined as the orientation of the line connecting the endpoints of the transformed X-axis of the human's workspace. Much like the first two metrics, the mean value of the overall rotations of the individually-fit motion mappings of $-3.18 \pm 11.30°$ is not statistically different from the rotation value for the aggregate motion mapping of $1.17 \pm 0.24°$ ($p = 0.2077$).

These analyses show that although there is variation between the individually-fit motion mappings, it does seem likely that the population-fit motion mapping fit to subjects from the previous study discussed in Chapter 2 is capturing the average behavior of the subjects in this study, just as the population-fit mapping was intended to. Although this finding may seem obvious, it was important to confirm given the nonlinearity of the variable-similarity motion mapping and the fact that no subject who participated in this experiment had participated in the previous study from which data for the population-fit motion mapping was taken. A further comparison of the population-fit and individually-fit motion mappings regarding how these mappings affect subject performance is given in Section 3.5.2.

3.5.1 Teleoperation Targeting Task

The thirteen metrics used to evaluate the subjects' performance in the targeting task shed insight into how the three different motion mappings affect targeted reaching. Since there were no significant differences found in the final direction error, final extent error, or final distance error, the subjects were able to move the robot's hand to the desired target location equally well under the Cartersian-scaling, population-fit variable-similarity, and individually-fit variable-similarity motion mappings. This result is expected because subjects had visual feedback of the robot's hand during all trials and could make corrections as they moved. Therefore the three metrics evaluating the subjects' final performance are actually measuring how well the subjects could remember the desired target location and how accurately they were able to move the robot's hand.

For this reason, the ten metrics that describe the human and robot motion trajectories provide more insight into how the different motion mappings affected the subjects' performance during the targeting task. The first trajectory metric is the initial direction error, which was defined to be the direction in which the subject moved the robot's hand before any path correction could be made. The initial direction error was smaller for both the population-fit and the individually-fit variable-similarity motion mappings than for the Cartesian-scaling motion mapping, indicating that the

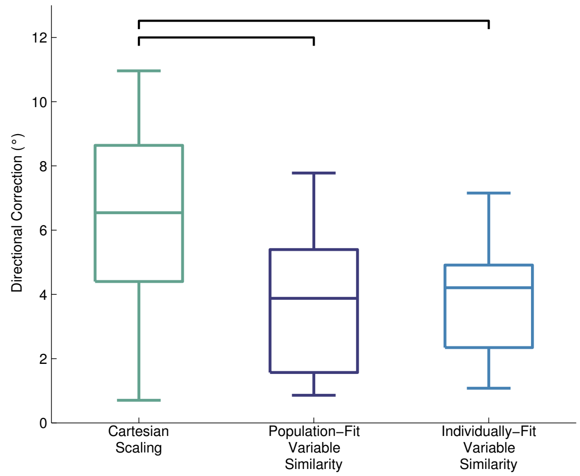

Figure 3.14: Subjects needed to make smaller directional corrections under both the population-fit and individually-fit motion mappings (p = 0.0180 f = 4.853).

subject's initial movement of the robot's hand was more accurate under the variable-similarity motion mappings. Furthermore, since there were significant differences in the initial direction errors, but none in the final direction errors, the subjects made larger corrections to their path direction when completing the targeting task under the Cartesian-scaling motion mapping. In fact, defining the direction correction as the difference between the initial direction error and the final direction error, subjects did make significantly larger directional corrections under the Cartesian-scaling motion mapping (F = 4.8530, p = 0.0180). Fig. 3.14 shows the distribution of the average directional corrections for the twelve subjects under each of the three motion mappings. Since subjects needed to make smaller corrections to their paths while using the variable-similarity motion mappings, using the variable-similarity motion mappings will prove to be less cognitively taxing on operators than the Cartesian-scaling motion mapping.

The fact that subjects' trajectories are closer to minimum jerk trajectories when completing the task using the population-fit variable-similarity also supports the fact that subjects were able to complete the targeting task under this motion mapping with fewer path corrections. It is known that if a subject was to complete the targeting task directly using his or her arm, the trajectory would be very similar to a minimum jerk trajectory [17]. Since subjects' trajectories were farthest from the minimum jerk trajectory under the Cartesian-scaling motion mapping, we can conclude that subjects made the least natural reaching movements under this condition. Some of the loss of naturalness in the reaching movements can be attributed to the fact that subjects were more heavily relying upon visual feedback to correct the robot's motion under the Cartesian-scaling motion mapping than under the population-fit variable-similarity motion mapping. Additionally, if subjects were to complete the targeting task using a completely transparent teleoperator, they would make motions identical to those made when directly performing the targeting task. Therefore, the closeness to minimum jerk trajectories also measures the transparency of the system. This finding leads the conclusion that the virtual teleoperation system was most transparent to users under the population-fit variable-similarity motion mapping.

Analysis of the movement inefficiency metric, which measures unnecessary human and robot movement, and the linearity index, which measures curvature of the human's and robot's path, further support the above conclusion: subjects were able to complete the targeting task in a more feedforward manner under the population-fit and the individually-fit variable-similarity motion mappings. The excess motion made when completing the targeting task under the Cartesian-scaling motion mapping was caused by the fact that subjects needed to make more path corrections under this condition. Under this mapping, the initial movement of the robot's hand was in an unexpected direction. Once the subjects observed this behavior, they corrected their own trajectory to more accurately complete the targeting task with the teleoperator. Such corrections require subjects to move less efficiently. A similar trend is observed in the fact that the linearity indices of the subjects' paths are highest when completing the targeting task under the Cartesian-scaling motion mapping. Although it is known that unconstrained human motion won't follow a straight path, and all linearity indices shown in Fig. 3.9 are well within the range of the data presented in [16], straighter paths with low linearity indices are still more efficient and therefore desirable. This study was designed to present a similar range of targets to the subject under each motion mapping. Since subjects had the worst linearity indices under the Cartesian motion mapping, again leading to the conclusion that subjects moved less efficiently under this condition.

The final path metrics analyzed the speeds at which the subject and the robot moved during the targeting task. Subjects' average and peak velocity were significantly higher when completing the task under the population-fit motion mapping than under the Cartesian-scaling motion mapping. Since this increase in speed did not cause a decrease in motion accuracy, I conclude that the subjects had more confidence that their input motion would produce the robot motion they expected in these conditions.

3.5.2 Population-Fit vs. Individually-Fit Variable-Similarity Motion Mappings

According to the ten trajectory metrics, the population-fit variable-similarity motion mapping often allowed subjects to complete the targeting task better than the individually-fit variable-similarity motion mapping, although the differences between the two were never significant. There are some desirable features of the population-fit variable-similarity that are not present in some subjects' individually-fit motion mappings. First, the population-fit motion mapping transforms the user's workspace in a more uniform way. The local scale factors of the population-fit variable-similarity motion mapping are fairly constant for the subject's entire workspace, visually shown by the uniformly sized blocks of the transformed Cartesian grid in Fig. 3.1. While some subjects have a uniformity of local scale factors in their individually-fit mappings, such as subjects 4 and 5, others have widely varying local scale factors, such as subjects 1, 3, 7, and 8. While better individually-fit motion-mapping could have been achieved though a more extensive calibration process, it seems that a population-fit motion mapping allows subjects to perform at least as well as, if not better than, the individually fit motion mappings.

3.5.3 Subject's Workspace

I was initially concerned that some of the improvements in the subjects' performance as measured by the thirteen metrics were simply due to the fact that the subjects completed the task using a more comfortable portion of their workspace, close to their right shoulder where directional errors in targeted reaching tasks are smallest [20–22]. Therefore, I performed the ANOVA analysis described in Sec. 3.4.1 using only trials during which the subject moved through the common workspace of all three motion mappings. All metrics that had significant differences when including all targets still retained significance when only including targets in this common workspace. Furthermore, a Tukey-Kramer post-hoc multiple comparison test showed that the same mappings allowed subjects to perform the targeting task significantly better when including either all targets or only those common to the workspace of all three motion mappings.

3.5.4 Survey Data

Although the subjects were better able to perform the targeting task using the population-fit and individually-fit variable-similarity motion mappings, ratings of task difficulty did not depend on the motion mapping used in the targeting task. One explanation for this finding is that subjects were not able to accurately indicate the difficulty of the task using the TLX survey. A second explanation is that the differences in difficulty between performing the targeting task under the three different motion mappings were too small to measure using the TLX. Either explanation makes sense because changing the motion mapping used in the targeting task altered only a small part of the task. Subjects still had to use the same teleoperator to produce similar motions, using similar concentration levels to complete the task.

3.5.5 Mimicking Washout Task

Analysis of the washout task data allows us to understand whether there were any lasting after effects from using the different motion mappings in the targeting task. As shown in Fig. 3.12, the motion mapping used in the targeting task has a slight effect on the subjects' motion when performing the mimicking task. The individually-fit variable-similarity motion mapping always most closely transformed the human's motion to that of the robot, regardless of which motion mapping was tested in the targeting task. The Cartesian-scaling motion mapping always transformed the human's motion to be the farthest from the robot's motion. Although the trend is not statistically significant, each motion mapping best transformed the human's motion to the robot's after the same motion mapping was tested in the targeting task. For these reasons, I conclude that the subjects slightly adapted to the motion mapping implemented in the targeting task. The after effects are small given that the motion mapping used to transform the human motion data is a much stronger predictor of average error than the motion mapping that was tested in the previous set of the targeted reaching task.

3.5.6 Final Preference

All queried subjects self-reported that they preferred the variable-similarity motion mappings over Cartesian scaling. I trust these subjective reports of motion mapping preference because the motion mappings that subjects preferred were the same motion mappings that best allowed them to perform the targeting task. Furthermore, the presentation order was balanced across subjects, and the subjects were never told which motion mapping was being used.

An anecdotal finding from pilot testing further supports that subjects reported their preferences without bias. Another member of the Haptics Group participated in this study as a pilot subject. He was aware that at least one motion mapping would distort his motion when translating his movements to the motion of the robot. He also knew that at least one motion mapping would preserve his motion. When he finished piloting the experiment, he was reluctant to tell me his opinion of the motion mappings because he had incorrectly guessed which motion mapping was preserving his motion. He strongly preferred the variable-similarity mapping, which he guessed was preserving his motion, to the Cartesian scaling mapping, which he had guessed was distorting his motion.

3.6 Conclusion

This study tested the influence of three motion mappings on human completion of a planar targeting task conducted through a virtual teleoperator. Subjects were equally good at placing the robot's hand at the target location when performing the task under the Cartesian-scaling, population-fit variable-similarity, and individually-fit variable-similarity motion mappings. More interestingly, the subject's and robot's motion trajectories were better when the subject completed the task under both of the variable-similarity motion mappings; subjects had smaller initial direction errors and therefore had to make fewer corrections to their chosen paths. In addition to making fewer path corrections, subjects moved more naturally and moved the robot more efficiently when using the variable-similarity motion mappings. Subjects also moved more quickly, which may indicate that they were more confident during the targeting task. Finally, subjects liked the variable-similarity motion mappings more than the traditional Cartesian-scaling mapping.

Given these differences, I conclude that the data-driven variable-similarity motion mappings are preferable to the commonly used Cartesian-scaling motion mappings in teleoperation. However, I do not claim that we have found the best possible motion mapping. This chapter simply has proven that it is important to consider human factors when designing the mapping from human motion to robot motion, a teleoperator design factor that has rarely been explored.

Chapter 4

A Wearable Device for Controlling a Robot Gripper with Ungrounded Haptic Feedback

An artist sculpting a block of marble, a magician pulling a card from thin air, and a surgeon performing an emergency surgery all rely on their sense of touch to push the limits of human capability. While touch is particularly important in these extreme undertakings, this often overlooked sense is also vital in mundane tasks such as buttoning a shirt and packing a bag. One rarely, if ever, contemplates the multi-faceted haptic sensations that are produced by physical interactions with the world. The unified experience of touch is produced by the combination of four distinct tactile modalities sensed by mechanoreceptors in the skin, plus the kinesthetic sense, working seamlessly together [46, 71].

The rich touch sensations of direct manipulation contrast starkly with most teleoperation systems, which allow an operator to complete a task using a remotely located robot. The vast majority of teleoperators provide either no haptic feedback or only a single modality. I hypothesize that including multiple modalities of haptic feedback would aid teleoperated task performance in ways analogous to how the distinct modalities of touch aid direct task completion.

To test this hypothesis, I created a wearable haptic device that gives an operator bilateral control over the gripper of a remote robot. This device is the first to provide kinesthetic grip force feedback along with independently controllable fingertip contact, pressure, and vibrotactile feedback, all of which are known to be of vital importance to humans when directly manipulating objects. The device is worn on the user's index finger and thumb and allows him or her to control the grip aperture of the robot using a pinching motion. Simultaneously, the operator receives kinesthetic grip-force feedback from a geared DC motor and fingertip contact, pressure, and vibrotactile feedback from a pair of linear voice-coil actuators.

I describe the design of the wearable haptic device and the implemented control algorithm in this chapter and Chapter 5 gives the details and results of the user study designed to interrogate the main hypothesis.

I open this chapter by motivating this project and summarizing relevant prior work in Section 4.1. I then describe the design of the device and the full teleoperation system in Section 4.2. In Section 4.3 I propose a controller that closely links the human's hand to the sensory signals measured by kinesthetic and tactile sensors on the robot's gripper. Initial feasibility of the device is shown in Section 4.4 by having a user teleoperate a PR2 humanoid robot to repeatedly pick up and set down five diverse objects. This research was initially published in the proceedings of the 2014 IEEE Haptics Symposium [75].

4.1 Background

Adding high-quality haptic feedback to teleoperation interfaces has been a long-standing goal of the robotics and haptics communities. The majority of the work contributing toward this goal has been focused on force-feedback systems, which measure the forces acting on the end effector of the slave robot and apply a proportional force to the user, e.g., [36]. This form of haptic feedback has proven to be useful in many studies; for example Hannaford et al. showed that operators completed a peg-in-hole insertion task more quickly and with lower translational forces under force feedback than with no haptic feedback [36]. Wildenbeest et al. found that translation low-bandwidth force feedback improved subject performance of a tool-mediated bolt-and-spanner task, but higher-bandwidth force feedback produced diminishing benefits [105]. However, a major drawback of such single-point-of-contact force-feedback systems is that they cannot haptically inform users about interactions that produce a zero net force between the robotic end-effector and the environment, such as when the robot is gripping a stationary object, like a door handle. This lack of grip force feedback can make certain manipulation tasks difficult, as the user can easily apply too little grip force and drop the object during the manipulation, or apply too much grip force and damage fragile objects. The latter case is evident in results presented in [49], which showed that subjects applied unnecessary pressure to durable rubber pieces when using the da Vinci surgical system to complete a peg transfer task with no grip force feedback.

To remedy this problem, researchers began to investigate ways to display manipulation forces to the user. Barbagli et al. created a desktop haptic device capable of providing both translational and grip force feedback to users interacting with virtual environments [2]. Verner et al. created a similar haptic interface to serve as the master device in a telemanipulation system, which was used to study the different effects of translational and grip force feedback in teleoperation [101]. In this study, subjects used the telemanipulator to complete a peg-in-hole insertion task with either (1) no haptic feedback, (2) only grip force feedback, (3) only translational force feedback, or (4) both grip and translational force feedback. While the combination of translational and grip force feedback led to the best task performance, grip force alone led to an increased number of unrecoverable drops of the manipulated peg [101]. This result is surprising because good haptic feedback is generally believed to facilitate manipulation tasks [35]. The finding is also disappointing because the force sensors needed for translational force feedback are generally too expensive and fragile to include in most robotic platforms. Fortunately, improvements to teleoperation systems with grip force feedback, but without translational force feedback, are possible. For example, Griffin et al. showed that shared control can be used to improve operator success during teleoperation with ungrounded grip force feedback in [32]. Griffin et al. also implemented several modalities of haptic, auditory, and visual feedback in an attempt to aid task performance. These researchers found that all three types of feedback have the potential to improve subject performance, but that auditory feedback (playing tones) and visual feedback (blinking lights) can also confuse subjects..

The hypothesis explored in this chapter is that adding tactile feedback to an ungrounded grip force-feedback device offers another solution to improving teleoperation without translational force feedback.

The design of the device is informed by the extensive neuroscience research, reviewed by Johansson and Flanagan [46], that details how humans use tactile afferents conveyed by mechanoreceptors during object manipulation. Johansson and Flanagan explain that it is fast adapting signals, both type I (FA-I) and type II (FA-II) that humans rely on most heavily to monitor task progress while lifting an object off of a table and setting it back down. The FA-I signals fire when the human's fingers make and break contact with the object, while the FA-II signals respond to the high-frequency accelerations produced by the handheld object making and breaking contact with the table. The slowly adapting type I (SA-I) and type II (SA-II) signals are also vital in the completion of this task. SA-I signals monitor steady-state grip force, and SA-II signals inform the human of skin deformations caused by shear forces at the fingertips and hand movement. Since each of the four types of tactile afferent signals provide important information during manipulation tasks, we sought to include as many tactile feedback modalities as possible.

As outlined by Romano et al. [84], the accelerometer and pressure sensors available on Willow Garage's humanoid robot, the PR2, allow for the measurement of tactile signals similar to FA-I, FA-II, and SA-I afferents in the human. Furthermore, inexpensive MEMS-based accelerometers, such as those added to a da Vinci surgical robot in [64], and MEMS-based barometers, such as those used in [45], make it realistic to equip most robot manipulators with tactile sensors similar to those available on the PR2. Since FA-I, FA-II and SA-I tactile signals are readily obtainable on robotic platforms, we sought to create a device that will naturally stimulate the user's FA-I, FA-II, and SA-I mechanoreceptors, in addition to providing grip force feedback. Unfortunately, the PR2's tactile sensors are unable to measure mechanical contact signals similar to SA-II afferents, so SA-II tactile feedback is not included in the design of the device.

The design of this tactile display builds on previous successes of researchers who have shown that kinesthetic and tactile feedback combine synergistically to improve a user's ability to perform tasks in a virtual environment. Most recently, Chinello et al. created a three-degree-of-freedom fingertip display that informs the user of the orientation of a virtual object's surface and the applied force [10]. This device was further tested in the context of virtual object manipulation by Pacchierotti et al. [72]; subjects could complete a virtual peg-in-hole insertion task best under a combination of cutaneous feedback provided by the device and kinesthetic translational and grip force feedback provided by two desktop haptic devices. Another tactile device designed by Provancher et al. [79] and refined by Kuchenbecker et al. [54] displays the making and breaking of contact and contact location of a virtual object on a user's finger. In [54] the authors showed that the contact location display allowed subjects to follow a virtual contour more quickly and with less force than when following the contour with single-point-of-contact force feedback. Another fingertip contact display was created by Solazzi et al. [92]. In the evaluation of this device [18], subjects wore one contact display on the index finger and one on the thumb. The subject then pinched and slid his or her fingers over two virtual planes to determine their parallelism under contact display, kinesthetic force display provided by another haptic device, and a combination of contact and kinesthetic display. The authors found that kinesthetic and tactile information was combined according to a Bayesian model, meaning that subjects were best able to determine parallelism using the combined feedback. Each of these three fingertip display devices are notably validated in virtual tasks, as they require more advanced sensing than is readily available in teleoperation systems. However, simplified feedback modes of each of these three devices could be used to display the making and breaking of contact between a robot's fingers and an object or the forces acting on a robot's pressure sensors. This includes tactile

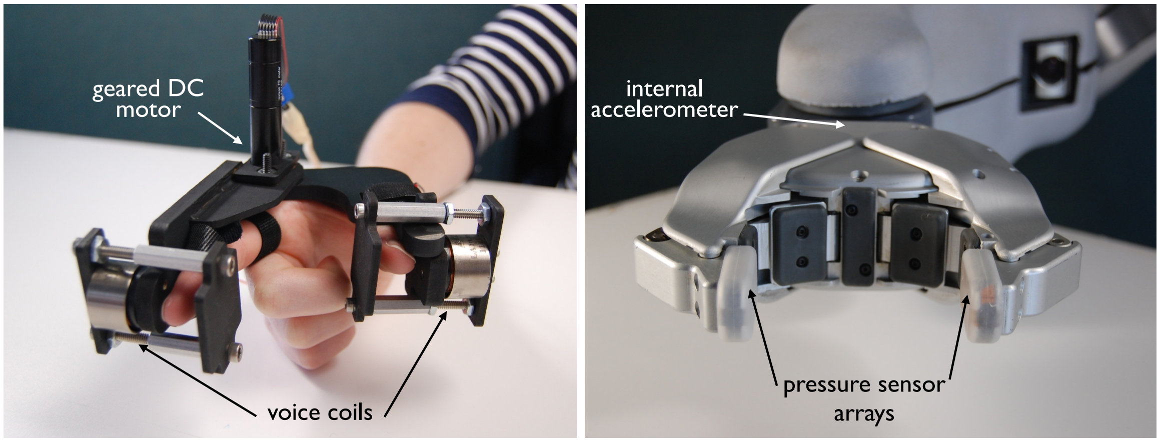

Figure 4.1: The wearable haptic device (left) and the PR2 robot gripper (right).

fingertip feedback of both contact and pressure display.

In addition to fingertip contact and pressure display, I also chose to include high-frequency acceleration feedback, as previous work has shown these cues can significantly improve the usability of teleoperation systems. As first demonstrated in [51], vibration feedback greatly aids users in completing tasks where high-frequency feedback is of vital importance, such as feeling for the grinding produced by a bad bearing. When used in conjunction with force feedback, vibrotactile feedback greatly improves the realism of virtual and real interactions, as shown by Kuchenbecker et al. [53] and McMahan et al. [66], respectively. Acceleration can also be a useful stand-alone haptic feedback modality when force feedback is not possible, for example [64], where McMahan et al. added tool vibration feedback to the da Vinci surgical system.

Figure 4.2: A PR2 humanoid robot acts as the slave in this teleoperation system. The opening of the robot's right gripper is controlled by the custom wearable haptic device.

4.2 Gripper Teleoperation Hardware

4.2.1 Robot

A Willow Garage PR2 humanoid robot was chosen to be the slave robot in the teleoperator. As shown in Fig. 4.1, the PR2's hand consists of a parallel-jaw gripper instrumented with two pressure sensor arrays mounted on the fingertips and an internal three-axis accelerometer mounted near the robot's wrist. A brushless motor, equipped with an encoder, actuates the robot's gripper via a planetary gearbox and a custom mechanism that converts the rotary motion from the motor to linear motion of the fingertips. Willow Garage supplies a PD controller for the distance between the robot's fingertips, allowing users to easily set the desired grip aperture. The high gear ratio of the gripper limits the rate of change of the grip aperture to be no greater than 0.04 m/s, which is relatively low compared to the speed of the human hand. Furthermore, the large gear ratio gives the PR2's gripper a high mechanical impedance, making it easy for the manipulator to crush nonrigid objects.

Fortunately, the tactile data supplied by the pressure sensor arrays and the three-axis accelerometer make it possible for the robot to interact with even the most delicate objects, including raw eggs and ripe peaches, as demonstrated in [84]. The pressure sensor arrays (from Pressure Profile Systems, Inc.) each consist of 22 pressure cells: a 3×5 array of the flat gripping surface of the fingertip, 1 pressure cell on the back surface of the array, and 6 pressure cells arranged along the sides of the fingertips. Pressure data describing the perpendicular forces applied to each of the 22 cells is simultaneously available at a rate of 24.4 Hz. A single pressure reading is obtained from the 15-unit array on the robot's finger pad by summing the simultaneous readings from these tactile 15 units. Although the pressure data contains very little noise, there is hysteresis and drift. Therefore, the pressure sensors are rezeroed each time the teleoperator is started by setting the mean of the first 0.25 seconds of pressure data to zero. The two pressure sensor arrays also have a tendency to measure different values when identical forces are applied.

The accelerometer (Bosch BMA150) measures accelerations between ± 78 m/s^2 at a rate of 3 kHz. This data is made available by the PR2 at a rate of 1 kHz, with each data packet containing three accelerometer readings. Much like FA-II mechanoreceptors [46],these accelerations can be used to capture the high-frequency vibrations produced by contacts between the robot's arm, hand, or handheld objects and other objects in the robot's environment, such as a table surface..

SA-I, FA-I, and FA-II tactile feedback were all provided to the user based on this sensor data, as discussed in Section 5.2.2. No SA-II (skin stretch) feedback was provided because the PR2 does not have a way to measure such a signal. Furthermore, we are most interested in SA-I, FA-I, and FA-II feedback because these tactile cues can be measured by low cost, robust sensors that can realistically be included on any robotic platform. The Bosch BMA150 on the PR2 can be purchased for less than $20. The TakkTile TakkStrip measures similar information as the PR2's pressure sensors and can be purchased for $150 a pair [97]. The force sensors needed to measure SA-II signals would be much more expensive and relatively fragile.

4.2.2 Design of Haptic Device

As shown in Fig. 4.1, I designed a lightweight, hand-wearable haptic device that allows a user to control the parallel-jaw gripper of the PR2 while receiving haptic feedback conveying information measurements from all of the kinesthetic and tactile sensors of the robotic hand, as laid out in Table 4.1. The total mass of the device is 205 grams.

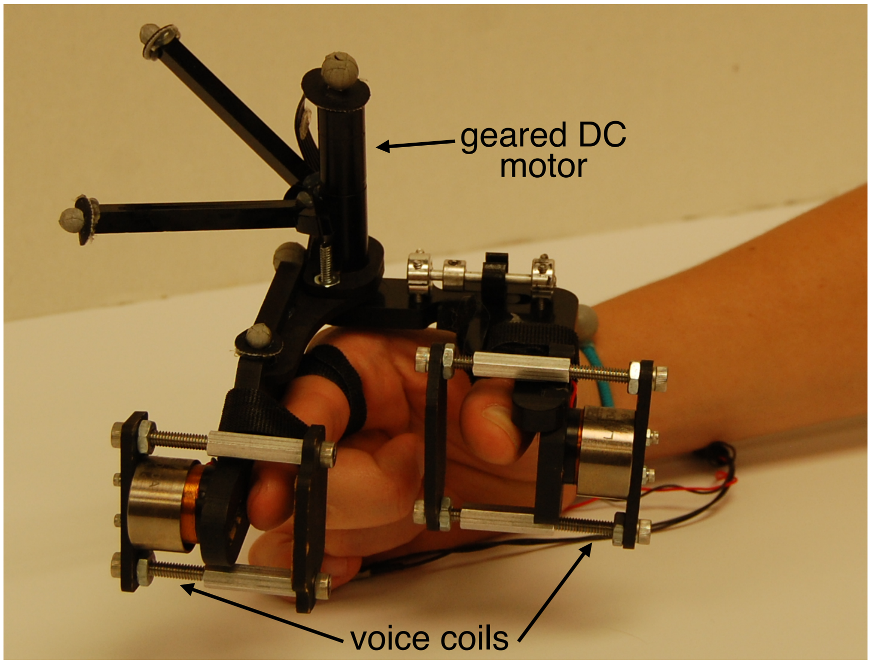

Figure 4.3: The second iteration of the wearable haptic device contained a lockable sliding linkage in the thumb piece to allow the device to fit more hand sizes. The position of the thumb and index coils are adjustable via slots and bolts.

The device is worn over the user's right index finger and thumb and constrains his or her gripping motion to one degree of freedom. The device has a rotational joint whose axis is aligned with the metacarpophalangeal (MCP) joint of the user's index finger. The first link of the device is firmly secured using a velcro strap placed around the proximal phalange of the thumb. This part contains a lockable sliding linkage, shown in Fig. 4.3, to set the distance between the MCP joint and the side of the thumbpiece, allowing the device to fit a wide range of hand sizes. The second link of the device is attached to the user's index finger via two velcro straps placed over the proximal phalange and the distal interphalangeal (DIP) joint; the second strap also prevents bending of the user's index finger.

A geared DC motor equipped with an optical encoder (Maxon, Motor: RE13-118423, Gearbox: GP13A: 275:1-110316, Encoder: 110778) is used to actuate the revolute joint of the device and can apply a continuous torque of up to 0.363 Nm to the user's hand. The torque provided by the motor is transmitted through the device and converted to a normal force felt at the user's index finger and thumb through the velcro straps, which naturally actives the user's SA-I mechanoreceptors to display grip force. The low friction of the motor and its 275:1 gearbox allow the user to easily change the angle between the index finger and the thumb when little or no current is sent through the motor. The motor's encoder enables us to measure the position of the device with a resolution of 4400 counts per revolution of the output shaft of the gearbox. I note that in contrast to other grip force feedback devices [2, 101], the decision to display the grip force with the motor at a location other than the finger pad allows us to add tactile feedback that can be displayed at the fingertips, where mechanoreceptors are most dense.

In addition to the motor, the device has two voice-coil actuators (BEI Kimco Magnetics: LA10-08-000A) placed behind the distal phalanges of the thumb and index finger using slots and bolts. As shown in Fig. 4.1 and more closely in Fig. 4.4, the current-carrying coils are mounted directly to the back of the device, and the magnets are rigidly attached to movable platforms via screws that allow us to easily adjust the distance between the magnet and the platform to fit different users. Using an arbitrary sign convention, when a negative current is sent through the coil, a

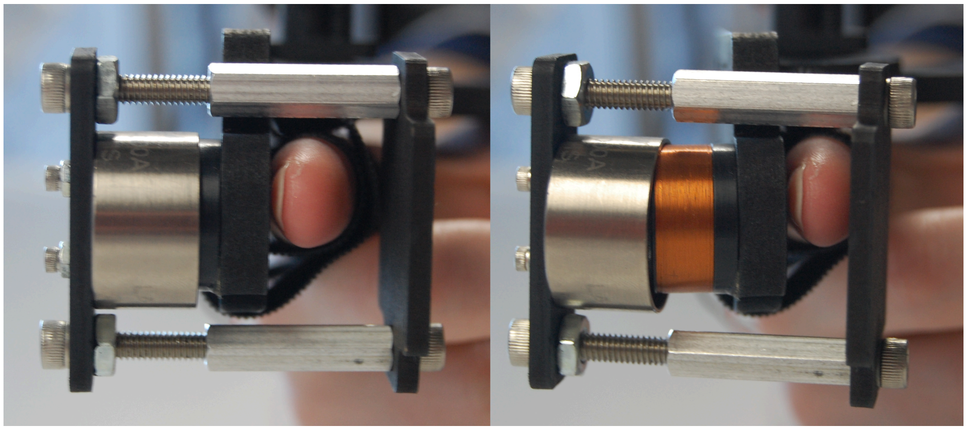

Figure 4.4: The fingertip voice-coil actuators move platforms that are rigidly attached to the magnet to make and break contact and apply pressure to the fingertip. The voice coil actuators are also used for vibration feedback. In the above picture, the distance between the user's finger and the platform is extended for visual clarity.

magnetic field is created that attracts the magnet to the coil and stably holds the platform away from the finger pad. When a positive current is sent through the coil, the resulting magnetic field repels the magnet from the coil, bringing the platform in contact with the user's finger. The parallel platforms contact the user's index finger and thumb in the same way an object with flat parallel sides would when held in a pinch grasp. The forces that the platforms apply to the user's finger and thumb are proportional to the applied current and can reach up to 6.7 N for short durations and 2.7 N continuously. The making and breaking of contact between the user's finger and the platform activates the FA-I mechanoreceptors, while the steady-state force applied to the finger by the voice coil activates the SA-I afferents.

Although the voice coils produce a reaction force on the back of the user's finger when the platform is in contact with the user's finger. Fortunately, this reaction force does not hinder the quality of the tactile feedback since it is much less perceptible

Feedback	Actuator	Measurement	Afferent
grip force	motor	difference between human and robot hand aperture	SA-I and Golgi tendon organs
fingertip pressure	voice coils	pressure at robot's two fingertips	SA-I
fingertip contact	voice coils	pressure at robot's two fingertips	FA-I
vibrations	voice coils	accelerations at robot's wrist	FA-II

Table 4.1: Modalities of haptic feedback provided by the device.

than the force acting on the user's finger pad for two reasons. First, the reaction force acts on the user's nail and on the back of the hand, which are less sensitive than the finger pad. Second, the reaction force is transmitted to the user's hand through a larger area than the area through which the platform contacts the user's finger pad, meaning that not only will the reaction force act on the user at lower pressure level, but also that changes to this pressure will be less perceptible to the user [95]. Additionally, I note that fingertip contact and pressure feedback can be coupled with grip force feedback and presented using a single actuator, such as is done in [67]. However, the decision to use a dedicated actuator for fingertip contact and pressure feedback allows for independent control of the tactile and kinesthetic feedback modalities, which is necessary to create the haptic feedback described in Section 4.3. Furthermore, voice coils can be used for vibration feedback because they are high-bandwidth vibration actuators [64]. Adding high-frequency signals with a zero mean to low-frequency force commands allows us to activate the FA-II afferents when the platform is both in and out of contact with the finger. I added a thin layer of neoprene foam between the magnet and the voice coil to allow for vibration feedback without rattling when the magnet is being attracted to the coil.

4.3 Control and Haptic Feedback

There are numerous ways that the described haptic device can be used to control the PR2's gripper. I sought to create a stable, direct-control, bilateral teleoperation system that haptically immerses the operator in the robot's environment in an intuitive manner.

4.3.1 Bilateral Gripper Controller

Early testing revealed that the fast rate at which humans naturally open and close the device makes position-position control better suited than a position-force controller for bilateral control of the PR2 gripper with our device. When grasping an object under position-force control, the human is prone to close the device at a rate much faster than the 0.04 m/s that the robot's gripper can move, thus commanding the robot's grip aperture to be much smaller than the width of the object. When the robotic fingers finally contact the object en route to the smaller commanded aperture, the high-impedance gripper crushes all nonrigid objects. Avoiding this undesirable behavior requires the user to visually observe the position of the robot's fingers and try to keep her grip aperture similar to that of the robot, a difficult task that distracts from the manipulation itself.

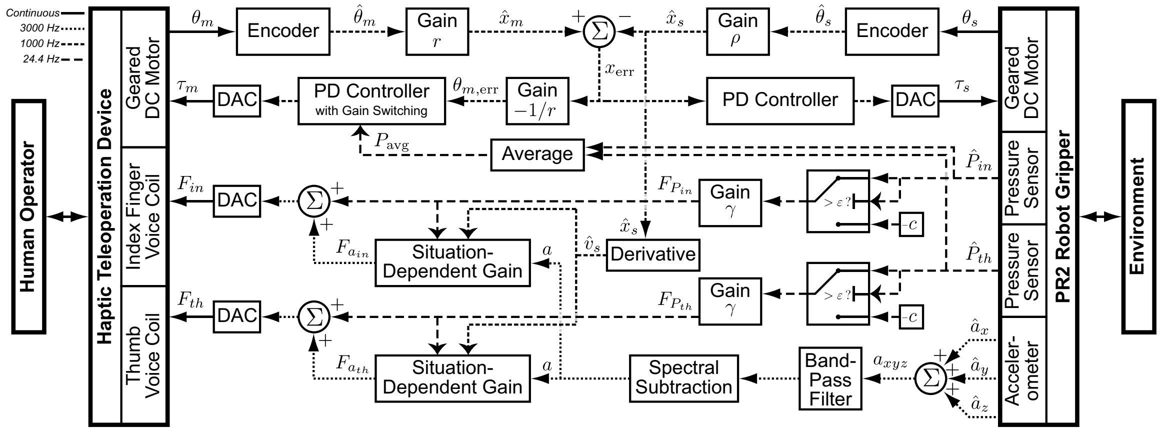

Figure 4.5: Diagram of the proposed controller, which enables the human to control the aperture of the PR2 robot gripper while receiving kinesthetic grip force feedback plus tactile fingertip contact, pressure, and vibrotactile feedback.

Therefore, I decided to implement a position-position controller. This control scheme, described in detail in [69] and illustrated in the top part of Fig. 4.5, applies a resistive force to the operator's hand when she has closed her hand too far or is attempting to close her hand too quickly, naturally keeping the human's and robot's grip apertures close together. A PD controller is used to drive the grip aperture of the robot to match the human's present grip aperture, as measured by the encoder on the motor. A second PD controller is used to drive the grip aperture of the human's hand to the present grip aperture of the robot. I convert between rotational and translational commands using the length r = 0.056 m. The gains for the robotic control loop were unchanged from the default gripper controller provided by Willow Garage. The derivative feedback gain on the device's PD controller was tuned so that it is easy for the user to open and close the device to control the PR2's gripper position as long as she is moving the device at approximately the same rate that the robot is opening and closing its gripper.

Unfortunately, the well known fact that linear time-invariant position-position control schemes provide poor transparency, as first discussed in [58], made it much more difficult to tune the proportional feedback gain in the haptic device's control loop. When the proportional gain on the device's PD controller is low, the operator is easily able to move her hand to change the commanded grip position of the robot, which is desirable when opening and closing the gripper in free space. However, the operator will also be able to effortlessly command the robot's pose when the gripper is squeezing an object, not only preventing the user from feeling that the robot's gripper is holding an object, but also allowing the operator to crush the potentially fragile object. In an attempt to remedy this problem, the gains of the haptic device's PD controller can be increased to make it more difficult for the user to change the robot's hand pose; however, it then becomes difficult for the operator to change the robot's grip aperture in free space.

Fortunately, as proposed and demonstrated in [68], a gain-switching position-position control scheme can be used to provide a good sense of transparency to the user. When the gain-switching PD control loop is implemented on this device, a low proportional feedback gain in used when the robot's hand is in free space, allowing the user to easily control the robot's grip aperture. Once the robot's hand begins to grasp an object, the proportional gain is switched to a higher value, haptically alerting the user that the robot's fingers are in contact with the object, both via the user's FA-I afferents, responding to the quick change in the level of force applied by the motor, and the user's SA-I afferents, responding to the steady-state forces commanded by the PD controller with a high proportional feedback term.

The pressure sensor arrays on the PR2's fingertips provide a natural and accurate method to determine gain-switching conditions. An average of the force applied to the left and right pressure sensors, as determined by methods described in Section 4.3.2, is compared against predetermined thresholds to tell if the robot's hand is squeezing an object. When closing the robot's gripper in a grasp attempt, the proportional gain is switched to high once the average pressure rises above the threshold, ϵ. While this high gain makes it difficult for the user to further close her hand, it also makes it difficult for the user to release the grasped object and can create the illusion of adhesion between the robot's fingers and the object. Therefore, the system detects when the user is opening her hand using the motor's encoders and switches the proportional gain back to the lower level once the force applied to the pressure cell arrays falls below a higher threshold value, $\epsilon + \delta$. Even though this gain-switching scheme has the potential for fast switching of control gains, which could lead to stability issues, I have yet to encounter problems caused by fast gain switching, largely due to the low noise of the pressure sensors. Hysteresis may be added in future versions if problems are encountered.

4.3.2 Tactile Feedback Modes

Contact and Pressure Feedback

The contact and pressure feedback provided by the voice-coil actuator activate the user's FA-I and SA-I tactile afferents in a similar way that a directly manipulated object would activate these afferents. This feedback mode informs the user if either or both of the robotic fingers are contacting an object and gives the user an idea of the amount of force the robot is applying to the object. The system independently controls the force of the voice-coil actuator on the index finger and thumb based on the corresponding robot finger's sensor reading. The robot's symmetric hand and infinitely rotatable wrist make it necessary to assign the corresponding finger. I chose to assign the fingers based on the robot's arm configuration so that the robot's index finger is chosen to be the robotic finger that is closer in position to the human's index finger. For example, when the gripper is facing directly outward, as in Fig. 4.1, the lateral finger is labeled as the index finger.

To calculate appropriate commanded forces to the voice coil, I first process the data from the index and thumb pressure sensor arrays in the same way as in [84]. I obtain one reading from the pressure cell arrays on the robot's thumb and index finger by finding the total force applied to the 15 pressure cells on the finger's flat gripping surface. Although this reading contains little noise, there is a noticeable drift caused by deformations in the rubber covering the pressure sensor arrays and other sensor imperfections. To help negate the drift, I tare the sensors during an initialization routine by setting the average of the first 0.25 seconds of data to zero. To determine whether or not the platform attached to the voice coil magnet should be contacting the finger, I compare the resulting pressure reading to 1 N, a level slightly higher than the drift observed in the sensors during typical interactions. When the pressure reading is below this level, the controller commands a current to the voice coil to keep the platform away from the user's finger, as shown in the left picture of Fig. 4.4. If the pressure reading rises about this level, the controller commands the platform to contact the finger with a force proportional to the force at the robot's finger, up to 6.7 N, as shown in the right picture of Fig. 4.4. In this version of the controller, I set this proportionality constant so that when the robot's gripper is stalled while attempting to crush a rigid object, the voice coils output their maximum 6.7 N. In the future, rigorous testing of this feedback mode will help refine this proportionality constant. Finally, I note that although the platform attached to the voice coil's magnet applies a force to the user's finger, this force is matched by an equal and opposite reaction force applied to the back of the finger. Since these internal forces negate each other, the fingertip contact and pressure feedback does not greatly influence the dynamics or stability of the system.

Acceleration Feedback

Acceleration feedback was used to stimulate the user's FA-II afferents by playing processed accelerations measured by the PR2's accelerometer through the voice coils;

these signals naturally convey important information about contact events in the robot's environment. Drawing heavily on previous work conducted in the Penn Haptics Lab, I digitally process the accelerometer data to obtain clear signals that can readily reveal important contact events. First, the three axes of acceleration data are summed to obtain a single accelerometer reading, a computationally efficient method that introduces no time delay while still providing a good temporal and spectral match with the original three-axis signal [57]. The resulting acceleration signal is filtered using a fourth order 150 to 750 Hz Butterworth bandpass filter to remove the low frequency gravity component and a strong signal at 1000 Hz. The filtered signal contains both accelerations caused by contact events and accelerations caused by the motors and cooling of the PR2. To isolate the important contact accelerations from the ego-vibrations of the robot, I implemented an adaptive spectral subtraction method, similar to the method described in [65]. In adaptive spectral subtraction, short segments of the time domain acceleration signal are transformed to the frequency domain, where a continually updated estimate of the robot's ego-vibration spectrum is subtracted from the total spectrum of the signal. The remaining signal content, which contains the spectrum of contact events, is then converted back to the time domain. The resulting processed acceleration signal is then scaled to command appropriate levels of current to the voice coil.

I sought to scale the vibration feedback so that a processed vibration signal containing only robot ego-vibrations would be barely perceptible by the user, allowing the contact acceleration transients to be most salient. I found two main factors that each independently affect the strength of the vibration feedback. First, the acceleration feedback feels drastically different depending on whether or not the voice coil's magnet is being attracted to or repelled from the coil. When the magnet is being attracted to the coil, the vibrating magnet is in direct contact with the neoprene foam, and the vibrations are transmitted throughout the device. Somewhat surprisingly, this creates stronger vibrotactile feedback than when the magnet is being repelled from the coil and the platform is in direct contact with the fingertip. Second, although the adaptive spectral subtraction removes much of the robot's own vibrations, a discernible acceleration signal caused by the opening and closing of the PR2's gripper is not eliminated, as seen in Fig. 4.6; this sustained vibration is unpleasant to feel. For these reasons, a different scale factor is used for each of the four combinations (attraction or repulsion between the coil and the magnet and movement or stationarity of the robotic gripper). The acceleration gains for the finger and thumb are switched independently.

4.4 Preliminary Validation and Conclusion

To validate the design of our wearable haptic device, I integrated it into a full teleoperation system that controls the PR2's right arm. The teleoperation system consists of the device, the control and haptic feedback methods described in Section 4.3, a real PR2 robot, a keyboard controller adapted from [96] to move the robot's hand,

and visual feedback from one of the robot's head-mounted cameras, viewed using the open-source Robot Visualizer (RViz) software [38]. I used this integrated platform to conduct a simple validation experiment in which one of the authors of [75] teleoperated the PR2 to lift several objects off of a table and set them gently back down. To complete this task, the operator first maneuvered the robot's hand to a grasping position using the keyboard controller and then used our gripper controller to grasp the object with the robot's hand. Once she was confident that she was firmly grasping, but not crushing, the object, she used the keyboard arm controller to lift the object approximately 0.1 m above the table. She then set the object back down and opened the gripper to release the object.

The experience level and personal bias of the operator in this study preclude it from serving as proof, and more extensive testing is certainly required to fully validate the functionality of the device. Still, the results from this preliminary experiment indicate that our haptic grip controller can be used to successfully manipulate objects with the PR2. The operator was able to complete this lift-and-replace task a total of more than 40 times with the following objects: an empty paper gift bag, a Solo cup, a champagne glass, a soft block of foam, and a hard plastic cup. Although no object was ever dropped or damaged, one of the completed trials resulted in a failure when a champagne glass that was grasped by its stem rotated in the robot's hand upon lift.

This initial testing also validated that the control and haptic feedback methods described in Section 4.3 worked as intended. The data shown in the top plot of

Fig. 4.6 was recorded during a trial when the operator lifted a rigid cup with a relatively high grip force, while the data shown in the bottom plot of Fig. 4.6 was recorded during a trial when the operator gently grasped a flimsy Solo cup. In both trials the robot's grip aperture tracked that of the human's hand very well. While the user's prior knowledge of the robot's speed limitations influenced her use of the device, the derivative feedback made it difficult for her to open and close her hand at a rate faster than the robot's hand, enabling this good tracking. In both trials the gain-switching controller produced a step increase in the amount of force applied to the user's hand by the geared motor when the robot's fingers first contacted the object. The recordings also show that the tactile feedback worked as intended. The voice coils properly applied a force proportional to the force measured by the pressure cell arrays on the robot's 'index finger' and 'thumb' to the human's index finger and thumb. Although the acceleration transient caused by the hard plastic cup contacting the table (at 9 seconds in the top plot of Fig. 4.6) is the only contact event captured in the presented trials, the vibrotactile feedback did properly alert the user each time a hard contact was made.

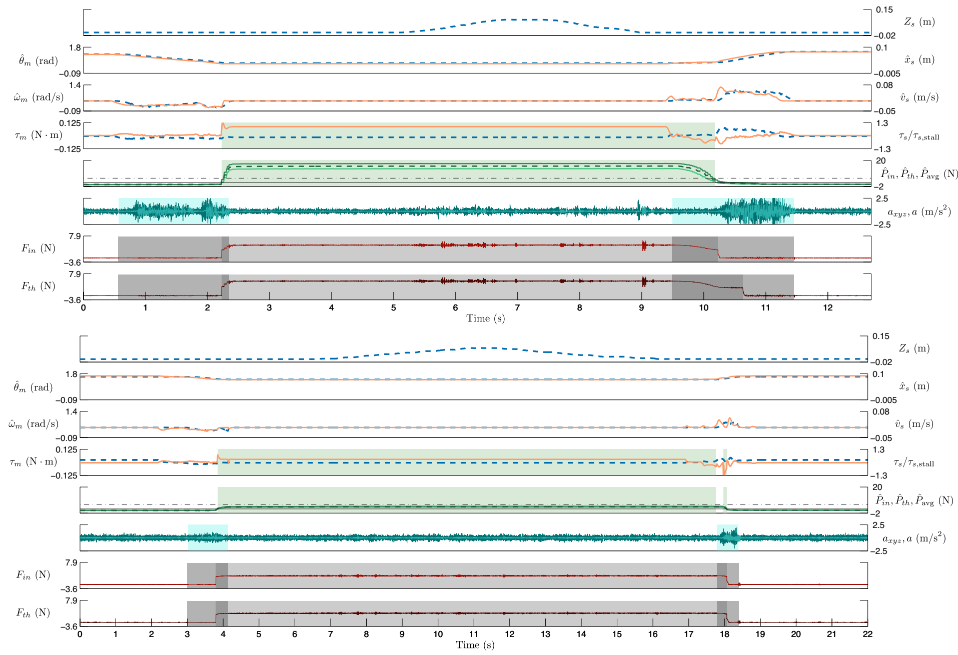

Figure 4.6: Sample data recorded during the validation experiment described in Section 4.4. The robot was teleoperated to grasp a rigid plastic cup (top) and a flimsy disposable plastic cup (bottom). The scale of the data associated with the human and the wearable haptic device is given on the left Y-axes, while the scale of the data associated with the robot is shown on the right Y-axes. Using a numbering convention so that *Plot 1* corresponds with the top plot for each data set, *Plot 1* shows the height of the slave robot's hand above the table's surface. *Plot 2* shows the master device's grip aperture (solid peach) and the slave robot's grip aperture (dashed blue). *Plot 3* shows the rate of change of grip aperture for the master and slave using the same line formats. *Plot 4* shows the torque commanded by the master device's PD controller (solid peach), and the torque output of the robot's PD controller normalized by the gripper's stall torque (dashed blue). The green shading in *Plots 4* and *5* shows the period of time during which the high gain was active in the device's gain-switching PD controller. *Plot 5* also shows the pressure measured at the robot's index finger (solid light green) and thumb (solid dark green), as well as the average of the two pressure readings (green dashed). Additionally, *Plot 5* shows the pressure threshold used to switch the device's PD controller's proportional gain to high when the user is closing the device (solid black) and the pressure threshold used to switch the proportional gain to low when the user is opening the device (dashed black). *Plot 6* shows the acceleration measured at the robot's gripper before (dark teal) and after (light teal) spectral subtraction. The teal shading in *Plot 6* shows the period in time when the robot's gripper was moving. Finally, the force output of the voice coils on the index finger and the thumb are shown in *Plots 7* and *8*, respectively. On these plots the gray shading indicates the situation-dependent acceleration gain used during that period of time. On each plot, the white background indicates that the gripper was still and the voice coil's platform was held away from the finger, the light gray indicates that the gripper was still and the voice coil's platform was contacting the finger, the medium gray indicates that the gripper was moving and the voice coil's platform was held away from the finger, and the dark gray indicates that the gripper was moving and the voice coil's platform was contacting the finger.

Chapter 5

Effects of Ungrounded Haptic Feedback on a Teleoperated Pick-and-Place Task

This chapter tests the hypothesis that ungrounded grip-force, fingertip-contact-and-pressure, and high-frequency acceleration haptic feedback, provided by the device described in Chapter 4, will improve human performance of a teleoperated pick-and-place task. Thirty subjects used a teleoperation system consisting of the haptic device worn on the subject's right hand, a remote PR2 humanoid robot, and a Vicon motion capture system to move either a flexible plastic cup or a rigid plastic block to a target location. Each subject completed the pick-and-place task ten times under each of the eight haptic conditions obtained by turning on and off grip-force feedback, contact feedback, and acceleration feedback. The results indicate that the addition of grip-force feedback with gain switching enables subjects to handle objects more delicately, hold objects more stably, and better control the motion of the remote robot's hand. Although certain aspects were improved, such as sensing when the object is in the remote robot's hand, the addition of contact feedback generally led subjects to handle the object more roughly. Finally, adding acceleration feedback slightly improved the subject's performance when setting the object down, as originally hypothesized; interestingly it also allowed subjects to feel vibrations produced by the robot's motion, causing them to be more careful when completing the task. This study supports the utility of grip-force and high-frequency acceleration feedback in teleoperation systems. An article documenting this research has been submitted to the IEEE Transactions on Haptics [47].

This chapter begins in Section 5.1 by providing detailed background information about the human sense of touch, specifically on how its different modalities enable completion of a simple pick-and-place task. The main hypothesis of this chapter is that the haptic feedback provided by the wearable device will aid the operator's performance just as the different touch modalities aid direct task completion. Sections 5.2 and 5.3 describe the teleoperation system and the experimental procedures of this study. I present the results in Section 5.4, interpret them in Section 5.5, and summarize the main conclusions and plans for future work in Section 5.6.

5.1 Background on Human Touch

Extensive neuroscience research, reviewed by Johansson and Flanagan [46], has found that there are four distinct tactile afferents conveyed by mechanoreceptors in the glabrous (non-hairy) skin of the hand. Two of the tactile modalities are fast adapting (FA); they respond when a sensation is first experienced but stop relaying information when it persists. Type I afferents have small receptive fields ($\sim$3-50 mm^2), while type II have large receptive fields ($\sim$10-100 mm^2) [100]. The FA-I afferents respond to dynamic loading and skin deformation over the entire hand, but they are most dense at the fingertips. FA-II afferents respond to high frequency vibrations ranging from 40 to 400 Hz [46]. The other two tactile modalities are slowly adapting (SA); they continually relay information even after the tactile stimulus has reached steady state. SA-I afferents are sensitive to low-frequency loading and skin deformation, while SA-II afferents respond to low-frequency skin stretch.

Johansson and Flanagan highlight the value of each of the tactile afferent modalities by examining the task of picking an object up from a table and placing it back down [46]. This pick-and-place task is broken into six action phases: reach, load, lift, hold, replace, and unload. The tactile afferents convey important information not only during the action phases, but also to trigger transitions to the next action phase. The reach phase begins when a person starts moving his or her hand and ends when the fingers make contact with the object. Both FA-I and SA-I afferents respond strongly to this contact, informing the person of the accuracy with which the movement was executed, which in turn allows him or her to make adjustments in future reaching movements [19, 81, 83]. The response of FA-I and SA-I afferents also causes the person to transition to the load phase, in which grip force and vertical load force increase.

The load action phase ends and the lift action phase commences when the object breaks contact with the table, an event that activates the FA-II tactile afferent. The lift phase transitions to the hold phase when the person lifts the object to the goal height. The replace action phase begins when the person starts lowering his or her hand. Grasp stability is the main goal during the lift, hold, and replace phases. A combination of SA-I and SA-II afferents monitors a stable lift and allows the person to hold the object using a typical grip force of only 10 to 40% more than the minimum allowable grip force. The FA afferents respond if a slip does occur, and the person adjusts his or her grasp accordingly. Finally, the unload action phase begins when the object makes contacts with the table, triggering an FA-II response. The unload action phase ends when the fingers break contact with the object, as sensed by the FA-I and SA-I afferents.

The tactile component of touch is complemented by the kinesthetic sense. Golgi tendon organs and muscle spindles monitor tension experienced by tendons and the length and velocity of muscles [41, 71]. Kinesthesia provides both a sense of applied force and awareness of body position (proprioception). In the context of the pick-and-place task, proprioception allows one to understand the position and orientation of one's hand during the reach action phase. Toward the end of the reach action phase, the proprioceptive sense indicates the degree to which the hand is opened. The kinesthetic measure of force activates during the load phase and allows the person to understand the amount of grip force and vertical load force he or she is applying to the object.

This chapter tests the hypothesis that fingertip-contact (FA-I), pressure (SA-I), and vibrotactile (FA-II) feedback with kinesthetic grip-force feedback will aid a teleoperated task in the same way that tactile afferents are known to play vital roles in direct manipulation.

5.2 Teleoperation Hardware

To test the value of the different modes of haptic feedback provided by our wearable device [75], we integrated it into a teleoperator that gives the operator full control over the arm and hand of a remote robot, as shown in Fig. 5.1. A complete discussion of the Willow Garage PR2 humanoid robot and the custom control device is given in Chapter 4.2. More succinct descriptions of these components are included in Sections 5.2.1 and 5.2.2, respectively, for clarity and completeness. We also describe updates that allow the haptic device to fit more hand sizes. As discussed in Section 5.2.3, a Vicon motion capture system was used to measure the pose of the subject's hand, and the robot's hand was controlled to follow.

Figure 5.1: Our teleoperation system consisted of a PR2 robot, a custom haptic device, a Vicon motion capture system, and a visual display.

5.2.1 Robot

During this experiment the PR2 robot, which is described more fully in Section 4.2.1, was located in a room across the hall from the subject. The robot in its experimental

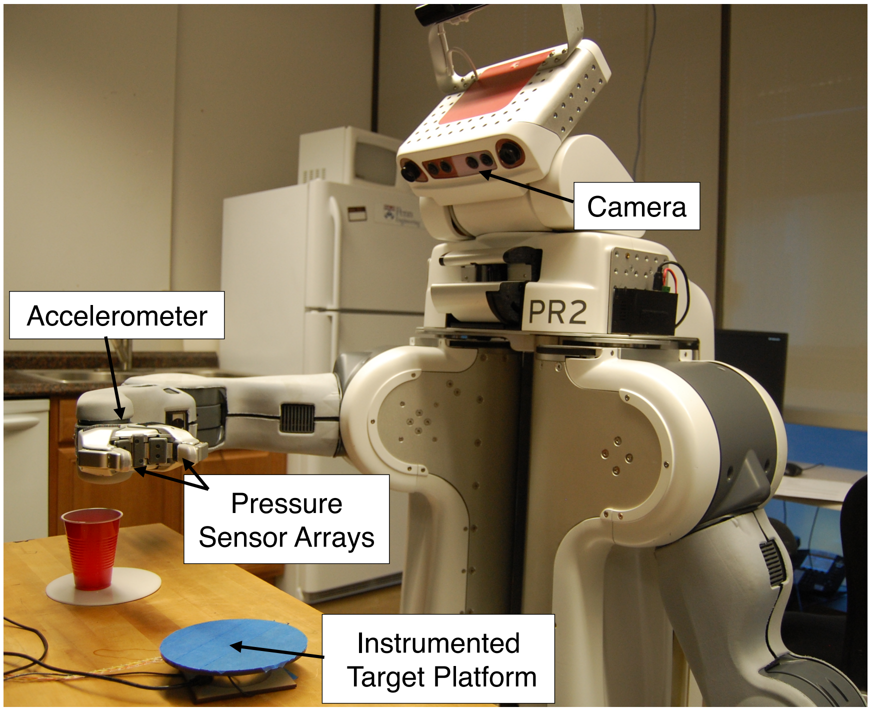

Figure 5.2: The PR2 slave robot was located in a separate room from the subject. Sensors in the robot's gripper were used to provide haptic feedback to the operator, and sensors in the blue platform monitored environment interactions.

environment is shown Fig. 5.2. The robot's base, torso, left arm, and head remained stationary during the study. The robot's right arm was controlled by the subject using methods described in Section 5.2.3.

The PR2 has several cameras that capture information in the visual domain. A head-mounted color ethernet camera with resolution of 752×480 pixels at 15 frames per second was used to record the robot's view. This information was displayed to the user using ROS's Robot Visualizer (RViz) [38] on an LCD monitor approximately 1 m in front of the user, as shown in Fig. 5.1. Displayed images measured 52 cm diagonally.

5.2.2 The Haptic Device

The version of the custom haptic device used in this study is shown in Fig. 4.3. The haptic device allows the operator to control the distance between the robot's fingers while feeling a representation of what the robot feels. Brief details of the implementation of the haptic feedback modalities are given in this section.

A position-position PD controller with gain-switching on the proportional feedback term was implemented to provide kinesthetic grip-force feedback. The proportional gain of this PD controller is changed based on the state of the robot's fingertips to improve the quality of the kinesthetic grip-force feedback provided to the user [68]. The value of a gain-switching PD controller is highlighted by examining the grip-force feedback during the action phases of a teleoperated pick-and-place task. When the user is moving the robot's hand toward the object, the robot's fingertips are in free space, as can be sensed by the robot's fingertip-mounted pressure sensors. During this action phase, the user should feel little or no resistance. Therefore, the proportional gain of the device's PD controller is set to a low value. At the end of the reach phase, the robot's fingertips contact the object of interest. In this teleoperator, we detect when the robot's fingertips are no longer closing in free space by comparing the sum of the readings from the robot's two fingers to a preselected threshold value, $\delta = 2$ N. The task has now entered the load phase, so we switch the proportional gain of the device's control loop to a higher value. The torque commanded to the motor will now make it difficult for the user to continue to close the robot's hand. The gain remains high for the lift, hold, and replace action phases of the task. During the unload phase, the proportional gain will switch back to the lower value when the combined pressure applied to the fingertips falls below $\delta + \epsilon = 7$ N, once again making it easy for the operator to open and close the device.

The derivative feedback term was kept constant regardless of whether the robot was grasping an object. The gain of the derivative feedback was tuned so that the user would encounter very little resistance when opening and closing his or her own hand at a rate achievable by the robot's gripper. If the subject opens or closes too quickly, the derivative feedback resists this motion.

The other two haptic actuators are voice coils (BEI Kimco Magnetics, LA10-08-000A) that deliver contact (FA-I), pressure (SA-I), and vibrotactile (FA-II) cues to the pads of the operator's index finger and thumb. The magnet of each actuator is connected to a platform in front of the user's fingertip. When the corresponding robot finger is in free space, the current commanded though the coil attracts the magnet, holding the platform away from the user's fingertip. The distance between the magnet and the platform is adjustable to allow the platform to be positioned as close as possible to the user's fingerpad without touching. When the force sensed by the corresponding robot finger rises above 2 N, the direction of the current commanded though the coil is switched, repelling the magnet and thus bringing the platform into contact with the user's fingertip. The steady-state force that the platform applies to the user's fingertip is proportional to the force experienced at the robot's fingertip, clipping with a maximum output of 5.4 N when the robot's finger experiences 29.1 N.

Vibrotactile feedback is achieved by adding the filtered acceleration signal with zero mean to the low-frequency signal calculated for contact-and-pressure feedback. The acceleration signal is scaled by four different scale factors depending on whether the platform is in contact with the operator's fingertips and whether the robot's grip opening is changing. Each scale factor was empirically chosen so that the egovibrations of the robot are barely perceptible.

5.2.3 Motion Capture and Arm Control

A Vicon MX motion capture system with six cameras, two of which are visible in Fig. 5.1, was used to track the pose of the wearable haptic device. As seen in Fig. 4.3, five retroreflective markers were placed on the body of the haptic device to allow tracking by the Vicon system. A sixth marker was placed on the lateral side of the subject's wrist via an elastic band to track the X, Y, and Z position of the user's hand. All six markers were used to track the device's orientation.

The subject's hand position and orientation were based on a right-handed Cartesian coordinate system whose origin was the initial position of the subject's hand. The X-axis of this coordinate system pointed forward, the Y-axis pointed to the subject's left, and the Z-axis pointed up. A Jacobian transpose controller was used to control the position and orientation of the robotic gripper in a Cartesian coordinate system centered at the initial position of the robot's end-effector. The position and orientation of the robot's gripper were commanded to match the subject's position and orientation. Because all computers were connected on the same local network, the roundtrip time delay was negligible.

5.3 Experimental Methods

Thirty subjects (20 male, 10 female) participated in this study, ranging in age from 18 to 48 years (mean: 24.2, standard deviation: 5.8). Procedures were approved by the Institutional Review Board of the University of Pennsylvania under protocol 820867. After giving informed consent, each subject completed a demographic survey to ensure eligibility. As required by the protocol, all subjects reported being right handed, having normal or corrected-to-normal vision, and having normal motor function of the right arm and hand.

Each subject completed repeated trials of a pick-and-place task under the eight haptic feedback conditions obtained by turning on and off grip-force feedback, contact-and-pressure feedback, and acceleration feedback. When grip-force feedback was turned off, the device's proportional and derivative feedback gains were set to zero, so the motor was not activated. When contact-and-pressure feedback was turned off, the platform was always held away from the user's fingertip. Lastly, when acceleration feedback was turned off, the high-frequency acceleration signal was not displayed via the voice-coil actuators.

The order in which the eight haptic conditions were presented was randomized before the experiment began. Custom software switched the haptic feedback condition, keeping the two experimenters blind to the displayed type of haptic feedback. Subjects were told that different types of haptic feedback would be presented, but the conditions were not described until after the study. The haptic feedback was only referred to by presentation order.

A block of pick-and-place trials always started with the object located in the center of the white circular target shown in Fig. 5.1. The subject moved his or her hand to match the pose of the robot and the controller was engaged. In a perfect trial, the subject used the teleoperator to first position the robot's gripper near the object in the reach action phase. The subject then used the wearable haptic control interface to close the robot's hand around the object, initiating the load action phase. Next, the subject moved his or her own hand in the motion capture space to lift the object from the table and then move the grasped object from the white target toward the blue target in the hold action phase. The subject then entered the replace action phase and moved the handheld object toward the blue circular target until the object contacted the supporting surface. He or she then used the haptic device to open the robot's hand to release the object in the unload action phase. Finally, the participant moved the robot's gripper away from the object. These actions constituted a single pick-and-place trial. The subject then performed the same sequence of actions to pick the object up from the blue target and move it back to the white target. *Subjects were told to treat the object delicately by using minimal grasping force and not dropping the object.*

Each subject completed one block of ten single pick-and-place trials for each haptic condition, meaning he or she moved the object from the white target to the blue target and back five times. The subject rested as long as he or she liked after each block of ten, typically no more than one minute. Doing all eighty trials took less than than one hour and ten minutes. Subjects were not compensated for participation.

The subject and the robot were located in two different rooms during the study, and one experimenter was present in each location. Before beginning the pick-and-place task, the subject was taken to see the robot and its environment. One of the experimenters explained the capabilities of the PR2 to ensure that the subject had a basic understanding of the robot he or she would be controlling. Subjects also completed at least one pick-and-place trial with their own hand to confirm that they understood the task instructions and to learn the physical properties of the object.

All subjects followed identical experimental protocols, but they were split into two groups that completed the task with different objects. Fifteen subjects used the teleoperation system to manipulate a flexible disposable plastic cup, and the other fifteen subjects used the system to interact with a rigid plastic block. Fig. 5.3 shows both objects and the force-displacement curves obtained from squeezing each object with the PR2 gripper. The first fifteen subjects who enrolled in the study completed the task with the flexibly cup. Preliminary analysis of their performance led us to believe that the visual measure of grip force via the flexible cup greatly affected the subjects' performance. Therefore, we tested a second group of 15 subjects who

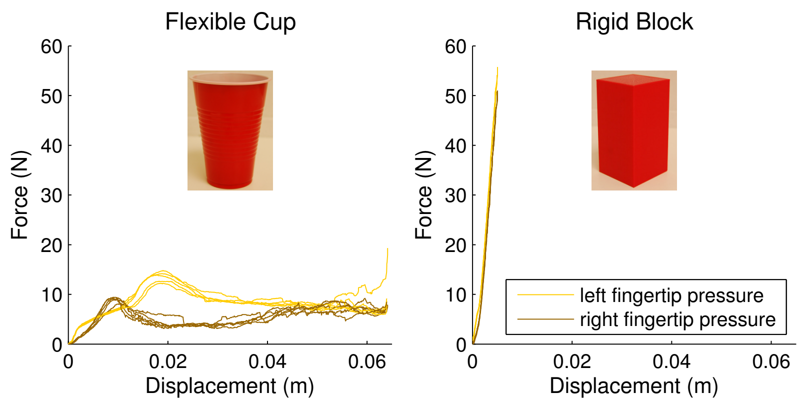

Figure 5.3: The flexible cup (left) and rigid block (right) were the two objects used in this study. The depicted force-displacement curves were recorded in five separate trials in which the robot's gripper was commanded to move from completely open to completely closed.

completed the task with a rigid block in order to investigate how a visual measure of grip force (via the flexible cup) affected task performance. We were careful not change the experimental setup between the two groups of subjects.

5.3.1 Data Acquisition and Task Performance Metrics

In the robot's environment, we collected data from the robot itself and from sensors in the task materials. Naturally, pressure applied to the robot's fingertip pressure sensors and accelerations experienced at the robot's wrist were recorded. The robot's desired and actual grip opening and gripper position and orientation were also logged. The blue circular target (Fig. 5.1) was situated on a one-axis load cell (Loadstar: iLoad Analog) to measure the normal force experienced by the target during different action phases of the pick-and-place task. Two two-axis high-bandwidth accelerometers (ADXL321, ± 18 g) were embedded across from one another in the blue target's platform. One axis on each sensor points upward, along the Z-axis of our frame. The remaining axes of each sensor were placed perpendicular to one another, creating X and Y axes.

One of the experimenters sat in the robot's environment to tally events related to task performance. When the subject was picking up the object, this experimenter counted the number of times the object was knocked over and the number of times the subject began the lift phase before having secured the object in the robot's hand. During the combined load, lift, and hold action phases, the experimenter recorded the number of unstable grasps (slipping) and the number of times the subject dropped the object. For subjects completing the task with the flexible cup, the number of times the cup was slightly deformed and the number of times the cup was crushed were counted. During the replace and unload action phases, the experimenter tracked the number of times the subject dropped the object before it made contact with the table. Finally, the number of times that the robot's hand hit the table was recorded during all action phases. A video camera in the robot's environment recorded the entire experiment. Video documentation was used to double-check the events tallied by the experimenter.

Data recorded in the human's environment included the subject's hand position, orientation, and grip opening. The state of the three haptic feedback modalities was always recorded. If any mode of haptic feedback was turned off, we stored the feedback that would have been experienced by the subject had that mode of haptic feedback been on.

Finally, we obtained subjective ratings of each haptic feedback via identical computer-based surveys completed after each block of ten pick-and-place trials. The subject used a slider to indicate his or her response to five questions on a continuous scale from 0 to 100. The questions posed to the subjects were 'How easy was it to complete the task?', 'How confident were you in sensing the robot's environment?', 'How confident were you in your ability to move the object?', 'How consistent was the task experience with your real-world experience?', and 'How would you rate your overall experience?'. These questions were adapted from Witmer and Singer's Presence questionnaire [107].

5.4 Results

Results are presented by the action phases of the pick-and-place task to highlight how the presence or absence of grip-force, fingertip-contact-and-pressure, and acceleration feedback affected task performance. The load, lift, and hold action phases together and the replace and unload action phases are grouped together because it was not possible to reliably distinguish these action phases from one another given the sensors included in the robot's environment. Additionally, the experimenter tallied events over the entire task performance, so errors that occurred during different phases were coded identically. All performance results are summarized in Tables 5.1 and 5.2. This Section concludes by presenting subjective survey responses.

	Flexible Cup			Rigid Block		
Metric	Grip-Force Feedback	Contact Feedback	Acceleration Feedback	Grip-Force Feedback	Contact Feedback	Acceleration Feedback
Closing Speed	0.70	0.48	0.57	0.023	0.49	0.83
Platform Lift Force	0.95	0.49	0.54	0.20	0.32	0.40
Platform Lift Acceleration	0.55	0.90	0.17	0.42	0.0057	0.31
Reaction Time	0.028	0.41	0.098	0.10	0.57	0.28
Peak Grip Force	0.078	0.025	0.0037	0.013	0.20	0.54
Average Grip Force	0.93	0.21	0.0024	0.0050	0.46	0.51
Average Control Error	NA	NA	NA	<0.0001	0.99	0.16
Platform Place Force	0.29	0.89	0.95	0.0013	0.023	0.60
Platform Place Acceleration	0.21	0.29	0.95	<0.0001	0.062	0.33
Trial Time	0.43	0.30	0.77	0.70	0.72	0.014

Table 5.1: The p-values returned by the repeated measures ANOVA. Positive performance changes caused by the presence of one of the haptic feedback modes are highlighted light gray, while negative performance changes are highlighted dark gray.

Metrics based on sensor data were first calculated for each individual pick-and-place trial. If a metric was more than 1.5 standard deviations away from the mean for that metric for that haptic condition across all subjects, the data point was discarded as an outlier. Each subject's remaining data were averaged, resulting in a single value per subject per haptic condition. Repeated measures analysis of variance (rANOVA), as implemented by [99], was used to determine whether any of the haptic feedback modes affected task performance. The within-subject factors were presence or absence of grip-force feedback, presence or absence of contact feedback, and presence or absence of acceleration feedback. Counted events are presented as the summed tally over all subjects and are not statistically analyzed.

Each plot showing sensor-based metrics or counted events displays the same data three times, once for each of the haptic feedback modes. Each of these presentations breaks the data into a subset that contains all data from when the feedback mode of interest is turned on and a subset when it is turned off. Each of these subsets is

Metric	Flexible Cup						Rigid Block					
	Grip-Force Feedback		Contact Feedback		Acceleration Feedback		Grip-Force Feedback		Contact Feedback		Acceleration Feedback	
	On	Off	On	Off	On	Off	On	Off	On	Off	On	Off
Object Knocked Over	16	13	12	17	14	15	24	32	29	27	30	26
Failed Pickups	4	18	9	13	11	11	10	29	18	21	20	19
Small Deformations	177	189	195	171	170	196	NA	NA	NA	NA	NA	NA
Crushes	5	9	4	10	7	7	NA	NA	NA	NA	NA	NA
Unstable Grasps	26	53	46	33	33	46	3	5	2	6	5	3
Drops	0	4	3	1	1	3	2	3	1	4	2	3
Drops On Placement	34	41	39	36	41	34	64	107	67	104	80	91
Robot's Hand Hits Table	146	139	125	160	136	149	100	145	136	109	119	126

Table 5.2: The number of counted events that occurred in the presence or absence of each of the feedback modalities. An event is highlighted if there is more than 10% change between the counts with and without that feedback modality. Positive performance changes caused by the presence of one of the haptic feedback modes are highlighted light gray, while negative performance changes are highlighted dark gray.

thus the aggregate data from the four conditions of turning the other two feedback modes on and off. Plots showing sensor-based data are presented as box plots. The boxes are filled in if that feedback mode caused a significant difference in subject performance as measured by the metric at the $\alpha = 0.05$ significance level. The total number of times a counted event occurred in each of the eight possible haptic feedback conditions is presented by a rectangular bar whose height is the number of times the event occurred during that feedback mode. Each feedback mode is represented by the following colors: light gray = no haptic feedback, red = grip-force only, green = contact only, blue = acceleration feedback only, yellow = grip-force and contact feedback, purple = grip-force and acceleration feedback, teal = contact and acceleration feedback, black = grip-force, contact, and acceleration feedback.

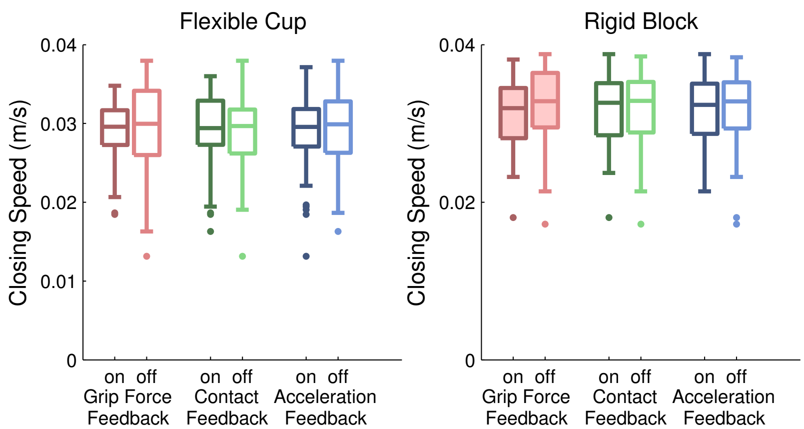

Figure 5.4: The closing speed of the robotic gripper.

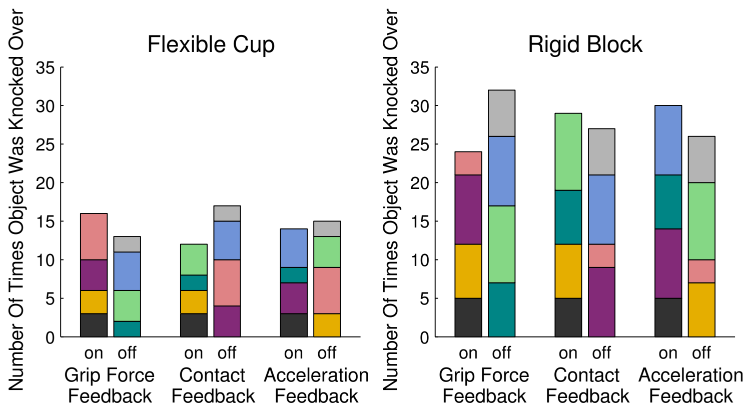

Figure 5.5: The number of times the object was knocked over.

5.4.1 Reach

The analyzed first metric was the rate at which the subject closed the robot's hand during the reach action phase. As shown in Fig. 5.4, grip-force feedback led subjects who completed the task using the rigid block to close the robot's hand more slowly ($F = 6.579$, $p = 0.0225$). Subjects who completed the task with the rigid block also closed the robot's hand more quickly (mean = 0.032 m/s) than the subjects who completed the task with the flexible cup (mean = 0.029 m/s).

The experimenter tallied the number of times the object was knocked over. Al-

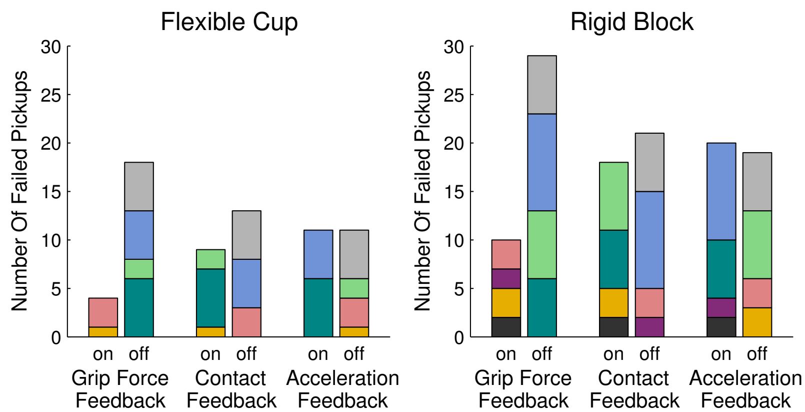

Figure 5.6: The number of times the subject attempted to lift the object without first having successfully grasped the object.

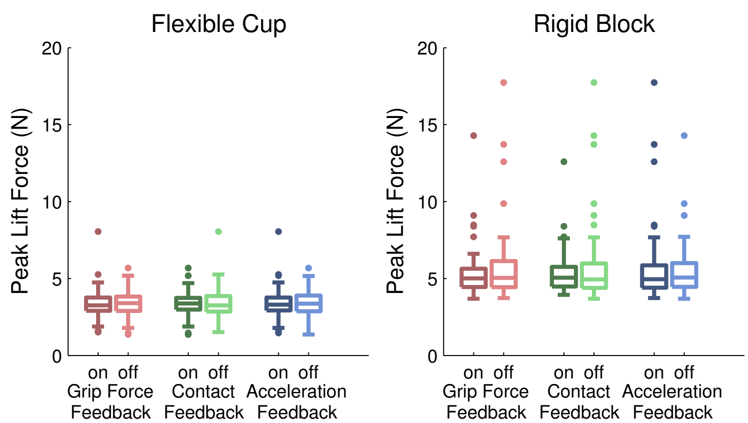

Figure 5.7: The peak force experienced by the sensorized platform during the lift action phase.

though this metric was for the full trial, the vast majority of knock overs occurred in the reach action phase, so we report the data here. As shown in Fig. 5.5, the flexible cup was knocked over slightly more often when subjects received grip-force feedback and slightly less often when they received contact feedback. Subjects who manipulated the rigid block knocked it over fewer times when they received grip-force feedback than when grip-force feedback was turned off. These subjects knocked the rigid block over slightly more when they received acceleration feedback.

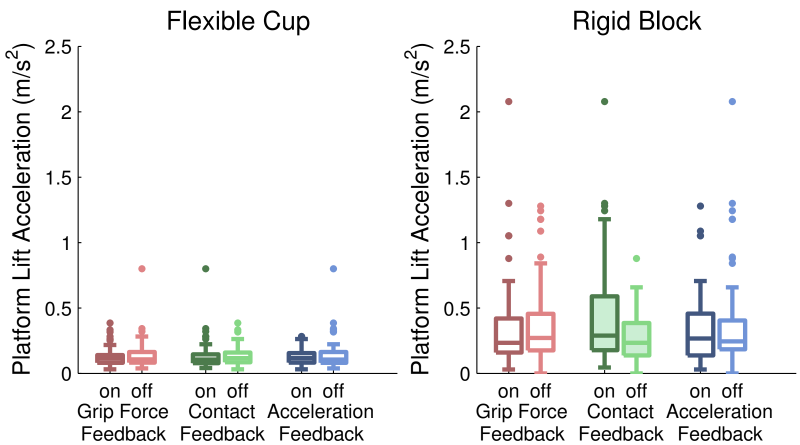

Figure 5.8: The peak platform acceleration during the lift action phase.

5.4.2 Load, Lift, and Hold

Fig. 5.6 presents the number of times the subject attempted to lift the object without first having successfully grasped the object. The number of times the subject attempted to lift the object without first having successfully grasped it was greatly reduced when grip-force feedback was present and was slightly reduced when contact feedback was present for both objects. The rigid object had more failed pick ups.

No form of feedback led to significant differences in the peak force applied to the load cell when the subject was picking up the object, as shown in Fig. 5.7. For the rigid block, but not for the flexible cup, subjects caused higher peak platform accelerations when contact feedback was present, as shown in Fig. 5.8.

We measured the subject's contact reaction speed as the amount of time it took the subject to stop closing the robot's hand after both fingers made contact. As shown in Fig. 5.9, subjects who completed the task with the flexible cup stopped closing the robot's gripper in a significantly shorter amount of time with grip-force

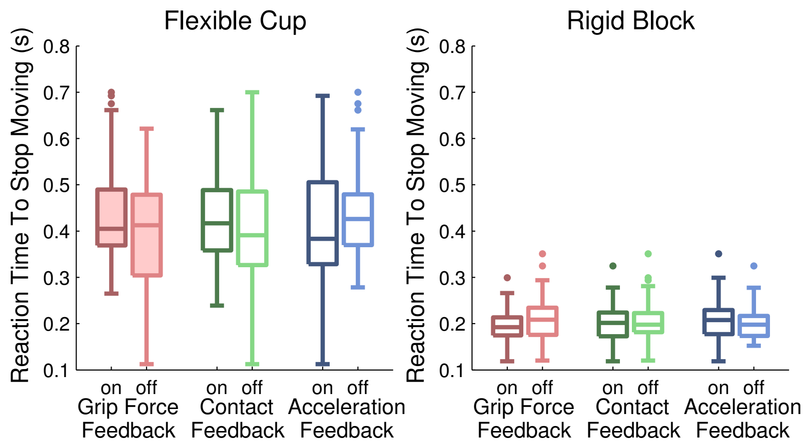

Figure 5.9: The time it took for the robot's hand to stop closing after both fingers contacted the object.

feedback (F = 5.985 p = 0.0282). Although not significant, subjects who completed the experiment using the rigid block also stopped closing the robot's hand more quickly with grip-force feedback (F = 3.025, p = 0.1039).

We analyzed both the peak grip force, shown in Fig. 5.10, and the average grip force, shown in Fig. 5.11, applied to the object. Subjects who completed the task with the flexible cup applied lower peak and average grip forces to the object when they had acceleration feedback (peak: F = 12.131, p = 0.0037, average: F = 13.708, p = 0.0024). These same subjects applied significantly higher peak forces to the flexible cup when receiving contact feedback (F = 6.341, p = 0.0246). Subjects who manipulated the rigid block applied lower peak and average grip force when they had grip-force feedback (peak: F = 7.995, p = 0.00134, average: F = 11.031, p = 0.005).

The final sensor-based metric examined during the load, lift, and hold action phases was the average grip aperture control error, which we defined to be the difference between the robot's grip opening and the subject's grip opening. Using our

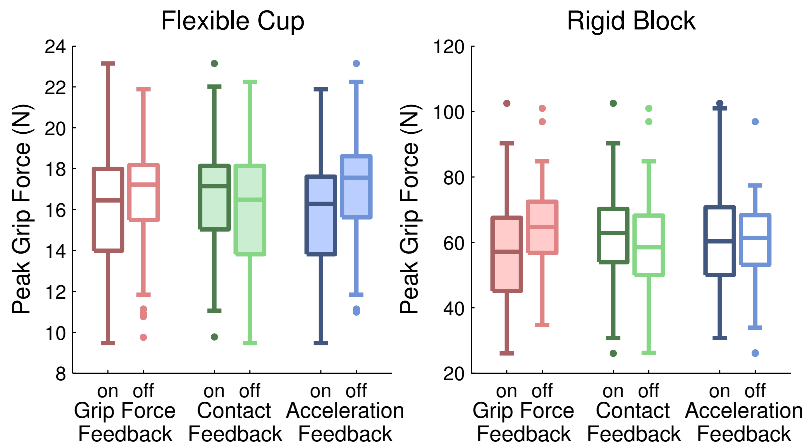

Figure 5.10: The peak grip force exerted on the object.

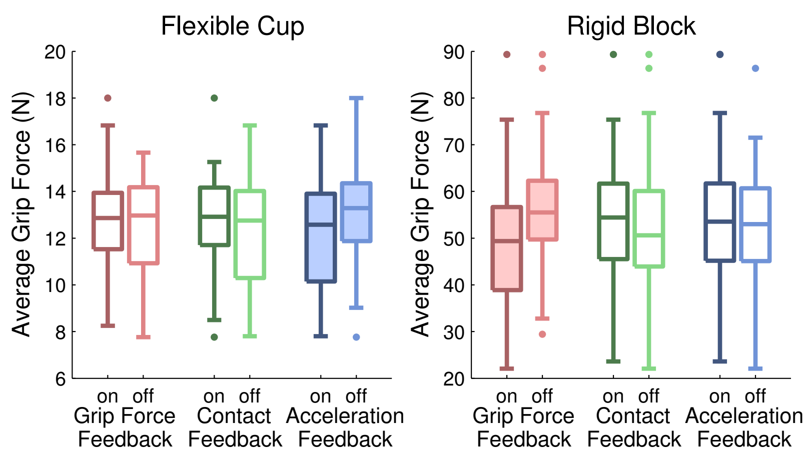

Figure 5.11: The average grip force exerted on the object.

sign convention, a negative error means that the subject's hand was closed more than the robot's. As shown in Fig. 5.12, the control error is very small for subjects manipulating the flexible cup because this object did not impede the robot's gripper. The rigid block did prevent the gripper from closing, so the control errors are much larger. When the subjects manipulating the rigid block had grip-force feedback, they kept their grip opening closer to that of the robot ($F = 38.696$, $p < 0.0001$). Neither contact nor acceleration feedback affected the average control error.

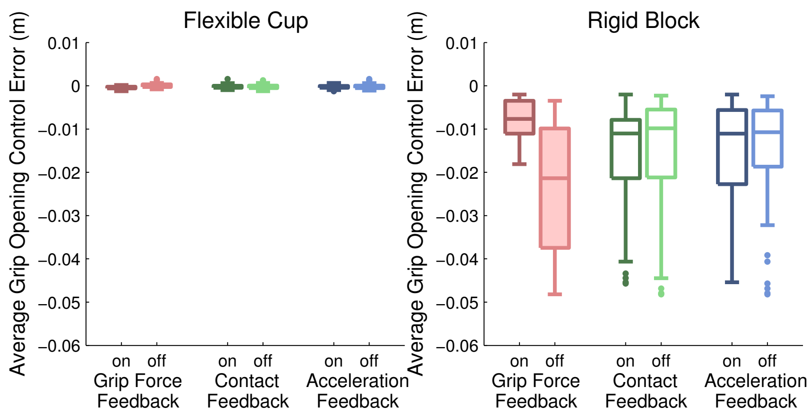

Figure 5.12: The average grip opening control error during the load, lift, and hold action phases.

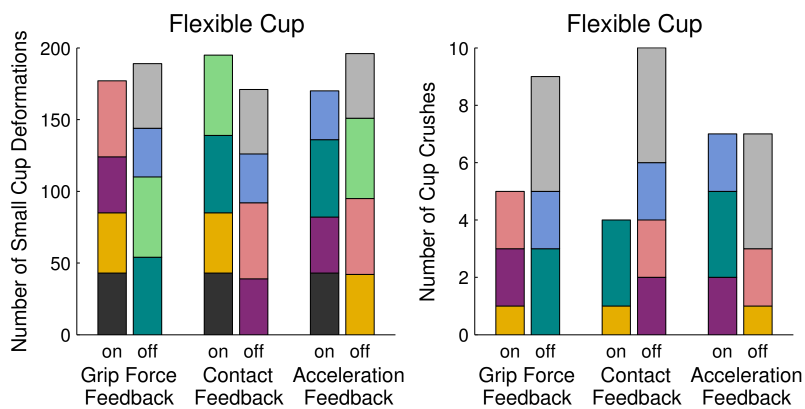

Figure 5.13: The number of times the flexible cup was slightly deformed (left) and crushed (right).

Although the gripper is not impeded by the soft cup, if the subject commands the gripper aperture to be too small, the cup will deform and potentially crush. The number of visible deformations and the number of times the cup was crushed to the point of destruction were counted by the experimenter in the robot's environment, as shown in Fig. 5.13. The number of small deformations was not greatly affected by any of the modes of haptic feedback. However, the number of times the cup was crushed was greatly reduced with the presence of either grip-force or contact feedback.

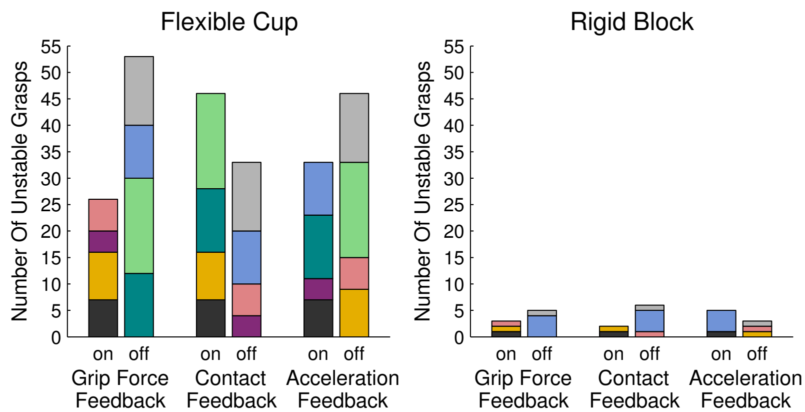

Figure 5.14: The number of times the object slipped or rotated within the robot's gripper without falling.

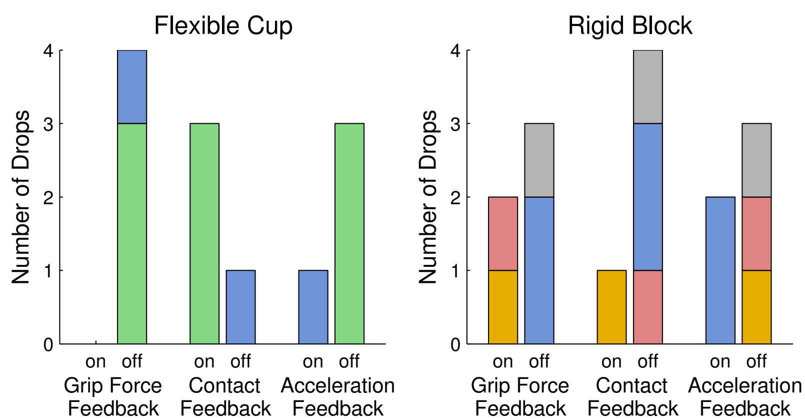

Figure 5.15: The number of times the object was dropped during the lift and hold action phases.

The experimenter in the robot's environment also tallied the number of times the subject lifted the object with an unstable grasp. A grasp was considered unstable if the object rotated or translated in the robot's hand without falling. If the object fell, the event was tallied in a separate category as a drop. The number of unstable grasps and drops are shown in Figs. 5.14 and 5.15, respectively. Subjects who completed the task with the flexible cup had fewer unstable grasps and dropped the cup less often when they had grip-force feedback or acceleration feedback. Conversely, these same subjects had more unstable grasps and dropped the object more often when they had contact feedback. Subjects who manipulated the rigid block had fewer unstable grasps with grip-force or contact feedback, but slightly more unstable grasps when acceleration feedback was on. All three forms of feedback led to slightly fewer drops by the subjects who completed the task with the rigid block.

5.4.3 Replace and Unload

Drops that occurred when the subject released the object before it contacted the table but after the subject had clearly entered the replace action phase were coded separately from normal drops. The total number of times the object was released prior to making contact with the target is shown in Fig. 5.16. Subjects who moved the flexible cup dropped it before making contact with the target location roughly the same number of times regardless of which feedback modes were present or absent. For subjects who completed the task with the rigid block, the presence of each of the three modes of haptic feedback reduced the number of times the object was dropped prior to placement. Overall, the rigid block was dropped more than the flexible cup.

For trials when the subject successfully placed the object on the target without dropping it, data collected by the force and acceleration sensors embedded in the platform reveal how gently the subject placed the object on the target. Fig. 5.17 shows the peak force applied when the subject placed the object on the blue target. Placement force was not affected by any feedback mode for subjects who completed

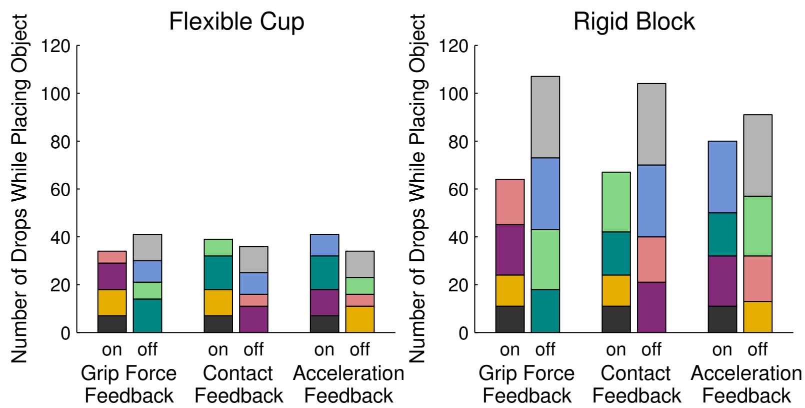

Figure 5.16: The number of times the object was dropped during the replace action phase.

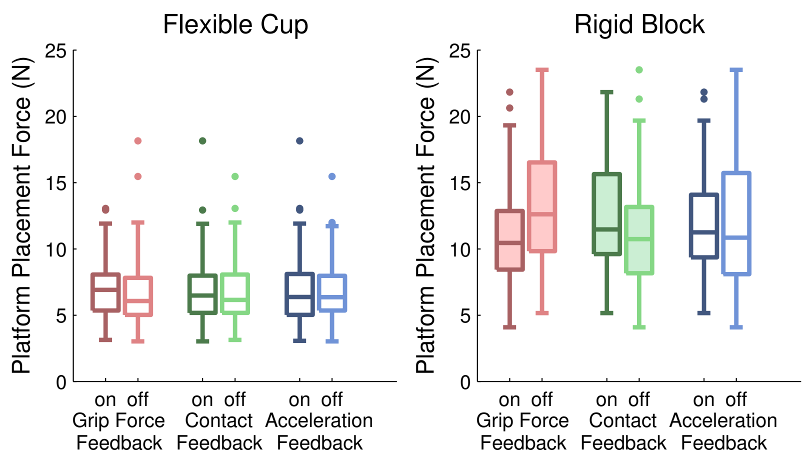

Figure 5.17: The peak platform force during the replace action phase.

the task with the flexible cup. Subjects who manipulated the rigid block placed the object with lower peak force when grip-force feedback was present (F = 16.106, p = 0.0013). Contact feedback caused the same subjects to place the rigid block with a higher peak force (F = 6.513, p = 0.0230). Fig. 5.18 shows the peak acceleration experienced by the target platform. No differences in peak acceleration were observed for subjects who completed the pick-and-place task using the flexible cup. Subjects who completed the experiment using the rigid block produced lower peak acceleration

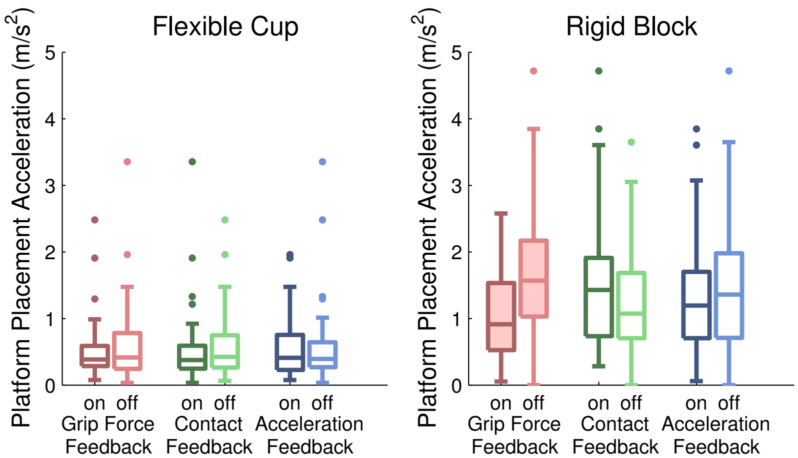

Figure 5.18: The peak platform acceleration during the replace action phase.

when placing the object with grip-force feedback (F = 45.17, $p < 0.001$).

5.4.4 Combined Action Phases

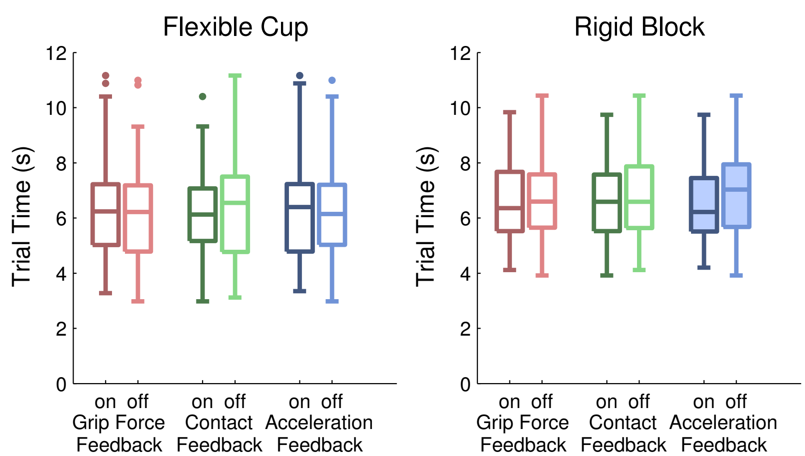

Figure 5.19: The time spent in the load, lift, hold, replace, and unload action phases.

Two metrics span all of the phases. First, we examined the total amount of time the subject took to complete the task. Because subjects performed the pick-and-place task continuously, and because they chose how far to move the robot's hand after releasing the object, we decided to ignore time spent in the reach phase. We define the trial time as the duration the subject was holding the object. No differences were found in trial time for the subjects who manipulated the soft cup, as shown in Fig. 5.19. Subjects who completed the task with the rigid block were faster when receiving acceleration feedback (F = 7.782, p = 0.0145).

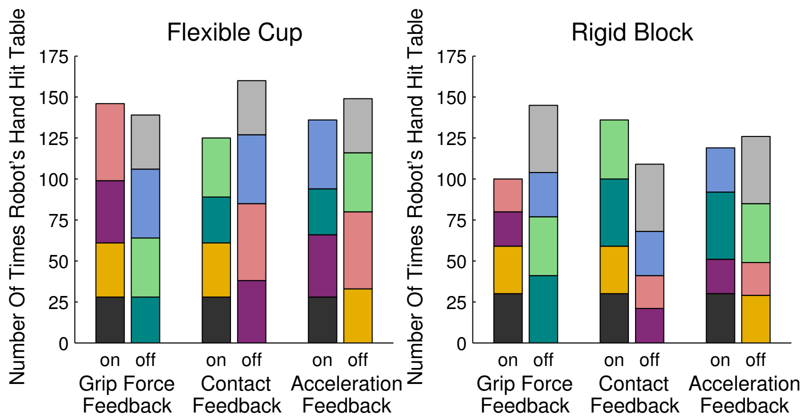

Figure 5.20: The number of times the robot's hand hit the table.

Second, we counted the total number of times that the robot's hand collided with the table. Grip-force feedback led to slightly more collisions for subjects who moved the flexible cup, but it caused many fewer collisions for subjects who moved the rigid block. Contact feedback reduced the number of collisions for subjects who completed the task with the flexible cup, but it led to an increase in the number of collisions for subjects who completed the task with the rigid object. Both sets of subjects completed the task with slightly fewer collisions with acceleration feedback.

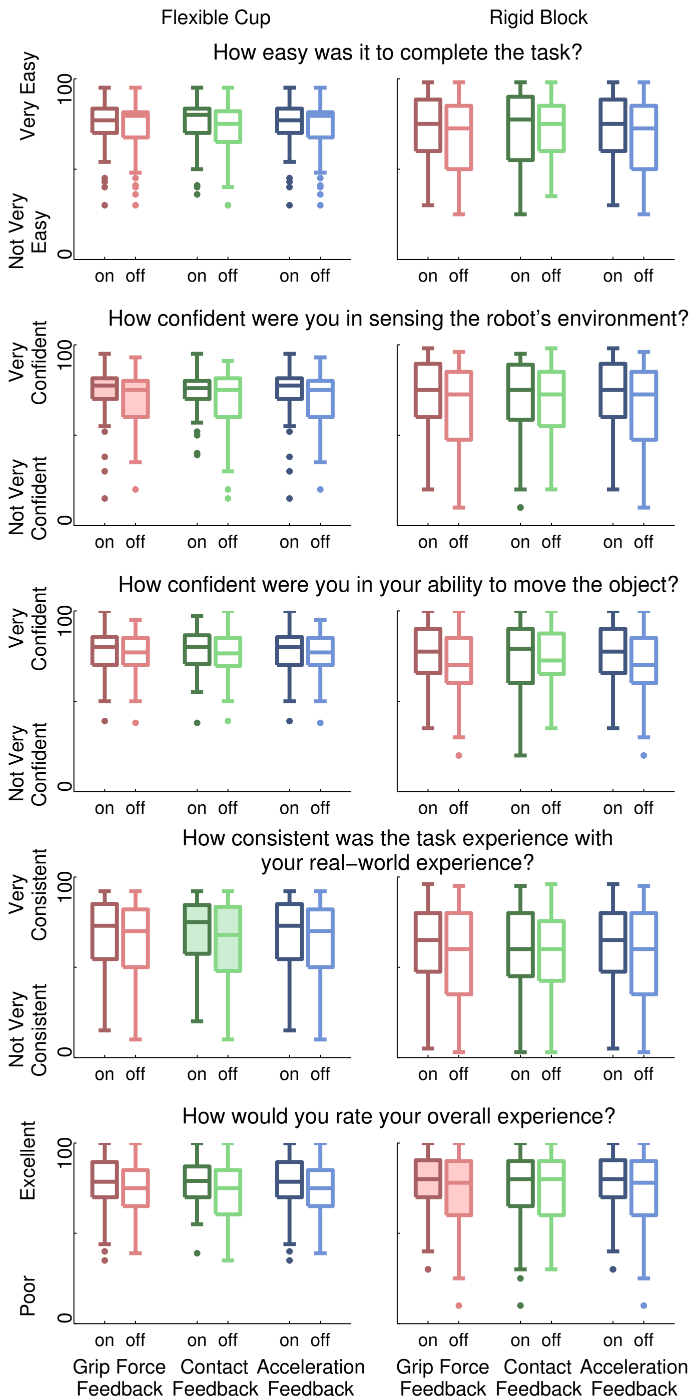

Figure 5.21: Subject responses to survey questions.

5.4.5 Subjective Ratings

The survey completed by the subject after each feedback condition revealed cases where grip-force feedback and contact feedback significantly improved the task experience. These data were analyzed using repeated measures ANOVA with the three within-subject factors of grip-force feedback mode, contact feedback mode, and acceleration feedback mode. The distribution of subject responses in shown in Fig. 5.21. Overall subjects rated the task relatively positively, with mean responses ranging from 58.9 to 76.3 out of 100.

Subjects who completed the pick-and-place task with the cup responded that they felt significantly more confident in sensing the robot's environment when they received grip-force feedback ($F = 8.32$, $p = 0.012$). These subjects also responded that the task was significantly more consistent with their real-world experience when they had contact feedback ($F = 8.07$, $p = 0.0131$). Contact feedback also indicated improvement in subject responses to the questions "How confident were you in sensing the robot's environment?", "How confident were you in your ability to move the object?", and "How would you rate your overall experience?" at the $\alpha = 0.1$ significance level. Acceleration feedback did not lead to differences in subjective ratings for this group.

Subjects who manipulated the rigid block rated the overall experience significantly higher when they received grip-force feedback ($F = 5.50$, $p = 0.034$). These subjects also indicated that grip-force feedback caused them to feel more confident in their ability to move the object and caused the task to be more consistent with their real-world experience at the $\alpha = 0.1$ significance level. The factors of contact feedback and acceleration feedback did not show any differences in the subjective ratings of the task for this group.

5.5 Discussion

As evidenced by the results in Tables 5.1 and 5.2, the different modes of haptic feedback both positively and negatively affected different aspects of the pick-and-place task.

5.5.1 Reach

During the reach action phase, subjects who completed the task with the rigid object closed the robot's hand more slowly when receiving grip-force feedback. Although slower movement may seem inefficient, the excessive grip force and high grip aperture control errors that occurred without grip-force feedback show that subjects were closing the hand too quickly. The desirable slow and careful closure of the robot's gripper under grip-force feedback is due in part to the damping subjects encountered when closing the robot's hand too quickly. It is likely that the subject's increased awareness of the remote object due to grip-force feedback contributed to the more careful behavior.

The number of times the subject knocked the object over indicates how well the subject was able to control the robot's hand in the remote environment, and it may also show the degree to which the robot became integrated with the subject's own body schema [34, 110]. When visual cues gave redundant information about the grip force applied to the flexible cup, grip-force feedback led the subjects to knock the object over more often, while contact feedback led the subject to knock the object over fewer times. When no redundant visual grip force information was present (for the rigid block), subjects knocked the object over more times overall, indicating that this task was more challenging. But grip-force feedback reduced the number of times the rigid block was knocked over, indicating that it gave subjects better control of the robot's hand in the more difficult task condition.

5.5.2 Load, Lift, and Hold

The number of times the subject attempted to lift the object without securing it in the robot's gripper reflects how well he or she was able to sense when the remote object was grasped in the robot's hand. Both grip-force and contact feedback reduced the number of failed pickups for both objects, supporting our hypothesis that grip-force and contact feedback will increase the subject's understanding of the remote environment, allowing a successful transition between the load and lift action phases. With grip-force feedback subjects also stopped closing the robot's gripper more quickly after the flexible cup had been grasped, further confirming our hypothesis that grip-force feedback increases the subject's sense of the remote environment.

When the subjects successfully lifted the object, contact feedback was the only form of haptic feedback that affected the physical interactions between the object and the sensorized platform during the load and lift action phases. Contact feedback caused higher peak accelerations, as measured by the accelerometers embedded in the platform, for subjects who completed the task with the rigid block. The sudden onset of the contact feedback may have startled some subjects, resulting in rougher behavior captured by the peak accelerations.

During the lift and hold action phases, grip-force feedback led subjects to apply lower grip forces to the flexible cup at a $\alpha = 0.1$ significance level and to the rigid object at a $\alpha = 0.05$ significance level. Grip-force feedback also led to fewer small deformations and crushes of the flexible cup. Importantly, grip-force feedback decreased the number of unstable grasps and the number of drops, showing that grip-force feedback allows subjects to hold the object more gently while still applying sufficient force.

Contrary to the hypothesis, subjects applied higher grip forces to the flexible cup when contact feedback was present. Contact feedback also led to more small deformations of the flexible cup, but fewer destructive crushes of the flexible cup. The presence of contact feedback also led to more unstable grasps and drops of the flexible cup, but fewer unstable grasps and drops of the rigid object. Contact feedback may have led to an increased awareness of the remote object, causing subjects to grasp more firmly, explaining the higher grip force and occurrence of small deformations but reduction in the number of times the object was crushed. I note that although contact feedback caused more drops of the flexible object, all three drops occurred during the first block of trials when contact feedback was turned on. Therefore, contact feedback may initially cause subjects to unsafely reduce grip force. However, given the fact that no subjects dropped the flexible object after the first block of pick-and-place trials with contact feedback, I believe that subjects can learn to make proper use of contact feedback with practice. Contact feedback led to fewer unstable grasps and drops of the rigid object, without causing an increase in the overall grip force applied to the object, indicating that contact feedback was beneficial to this set of subjects. However, these subjects were free to apply high grip forces to the rigid object with no negative effects.

Acceleration feedback unexpectedly led to a reduction of grip force applied to the flexible object, resulting in fewer small deformations of the cup. However, acceleration feedback did not affect the number of times the flexible cup was crushed. Acceleration feedback also led to fewer unstable grasps and drops of the flexible cup. Finally, acceleration feedback led to more unstable grasps of the rigid block, but fewer drops. Acceleration feedback was not anticipated to have a positive effect on the subjects' ability to hold the object more more stably with lower applied grip force because the robot's wrist-mounted accelerometer cannot measure any salient signal related to applied grip force during the load, lift, and hold action phases. However, during these action phases the accelerometer does measure vibrations produced by the robot's own motion. Therefore, acceleration feedback let subjects feel not only vibrations caused by interactions between the robot and its environment but also vibrations produced by the robot's own motion. The highly geared PR2 gripper produces significant vibrations when opening or closing. Although acceleration feedback was scaled to reduce these egovibrations, they were still perceptible.The overall positive effects of acceleration feedback during the load, lift, and hold action phases are likely a consequence of subjects having a better appreciation of the robot's movement because they were able to feel the robot's egovibrations.

5.5.3 Replace and Unload

The number of times the object was dropped before it contacted the supporting surface in the replace action phase shows how well subjects understood whether the object in the robot's hand had contacted the target platform. The hypothesis predicted that acceleration feedback would enable subjects to feel the transient vibrations produced when the object contacted the target. Consistent with this hypothesis, acceleration feedback reduced the number of drops of the rigid object during the replace action phase. However, contrary to this hypothesis acceleration feedback increased the number of premature releases of the flexible object. I attribute this difference in performance between subject groups to the physical properties of the objects. The rigid object produces higher peak accelerations than the flexible object for similar contact conditions. Therefore, subjects felt salient vibrations from contacts with the rigid object at lower impact speeds, and acceleration feedback aided user performance.

On the other hand, higher impact speeds were required in order for subjects to feel collision vibrations from the flexible object. Therefore, acceleration feedback acted as negative reinforcement for subjects completing the task with the flexible cup and perhaps led them to release the object before placement.

Subject performance during other action phases has already provided evidence supporting that grip-force feedback improves the subject's control over the robot's hand, while grip-force feedback and contact feedback improve the subject's ability to sense the held object. These conclusions are further supported by the finding that grip-force feedback slightly decreased the number of times the flexible cup was dropped during the replace action phase, and the fact that grip-force and contact feedback both greatly reduced the number of premature releases of the rigid object.

No haptic feedback mode affected placement force and acceleration measured by the platform for the flexible object. However, grip-force feedback reduced both the placement force and acceleration for the rigid block, yet again indicating that grip-force feedback better allowed subjects to control the motion of the remote robot. Contact feedback increased peak placement force of the rigid object at the $\alpha = 0.05$ significance level and peak placement acceleration of the rigid object at the $\alpha = 0.1$ significance level. One explanation is that contact feedback degraded the subject's ability to control the remote robotic hand. An alternative explanation is that contact feedback allowed the subject to better sense the remote object, causing them to avoid dropping it, even at the expense of rougher placements. Contrary to the hypothesis, acceleration feedback did not affect the roughness of object placement for either object, perhaps because it occurs only after impact.

5.5.4 Combined Action Phases

Although no task instructions regarding speed were given to subjects, trial times can still indicate task difficulty. The only haptic condition that improved trial time was acceleration feedback for subjects who completed the task with the rigid block. Noting that trial times were defined to exclude time spent in the reach action phase, we believe that placement cues provided by the acceleration feedback increased subject's confidence when placing the object, decreasing time spent in the replace and unload action phases.

Consistent with results described above, grip-force feedback reduced the number of times the robot's hand hit the table for subjects who completed the task with the rigid object, again indicating that these subjects were better able to control the remote robotic hand with grip-force feedback. Contact feedback reduced the number of robot hand collisions for subjects completing the task with the rigid object, but it increased collisions for subjects completing the task with the flexible object. Contact feedback can both improve and degrade user performance in a teleoperated pick-and-place task.

5.5.5 Subjective Ratings

Survey responses showed that both grip-force and contact feedback improved the subjective experience for participants who manipulated the flexible cup, and only grip-force feedback improved the experience for subjects who completed the task with the rigid block. No mode of haptic feedback degraded the experience for either group. When object deformations were visible (flexible cup), it is interesting to note that grip-force feedback improved one aspect of the task, while contact feedback improved three aspects of the task at the $\alpha = 0.1$ significance level. However, when no redundant visual grip-force information was provided to subjects (with the rigid block), grip-force feedback dominated subject experience, improving three aspects of the task experience at the $\alpha = 0.1$ significance level.

5.6 Conclusion

Grip-force feedback with gain-switching had the most positive effects on subject performance and had very few to no negative effects. It aided task performance in ways consistent with the hypothesis, improving user performance just as the kinesthetic sense of grip force aids a direct pick-and-place task. For example, grip-force feedback reduced the number of failed pickup attempts, the number of unstable grasps and drops during the lift and hold action phases, and the number of drops during the replace action phase for both objects. Grip-force feedback also reduced the number of times that the flexible cup was either slightly deformed or crushed and allowed subjects to apply less grip force to the rigid object. Information provided by grip-force feedback also improved the subject's ability to move the robot's hand through space, although more research is needed to fully understand this effect. Ideally, I would conduct another study investigating subject performance with and without grip-force feedback in a teleoperated reach-to-grasp task to pinpoint how grip-force feedback affects an operator's ability to control the motion of a remote robot.

I hypothesized that contact feedback would improve subject performance in similar ways as grip-force feedback. However, results indicate that aspects of task performance were both improved and degraded with contact feedback. A reduced number of failed pickup attempts of both objects indicates that contact feedback better allowed the subject to determine when the object was grasped in the robot's hand. However, the increased awareness of the remote object seems to negatively affect subject performance in other ways. For example, subjects who completed the task with the flexible cup applied higher grip force and slightly deformed the object more often with contact feedback. Subjects needed time to learn to interpret contact feedback, as evidenced by the fact that all three drops of the flexible cup with contact feedback occurred during the first set of trials that included contact feedback. They were also rougher when picking up and setting down the rigid object with contact feedback. More work is needed to understand the learning curve required for subjects to best make use of contact feedback. In the future, I plan to investigate whether it is possible to improve the method by which contact feedback is presented to improve its effect on operator performance.

I designed acceleration feedback with the goal of informing subjects about physical interactions between the robot's hand and the robot's environment. However, a reduction in the number of drops of the rigid block during the replace action phase and a faster trial time were the only evidence that acceleration feedback improved the subject's ability to place the object. On the other hand, feedback of vibrations caused by the robot's motion had a large impact on subject performance, improving the load, lift, and hold action phases in ways similar to grip-force feedback. I note that Kurihara et al. similarly showed that haptic and auditory feedback of vibrations caused by robot motion increased subjective ownership and the sense of resistance caused by moving a virtual robot arm [55]. I propose to further investigate whether feedback of vibrations caused by robot motion will cause similar effects of increased ownership of the remote robot in teleoperation.

Chapter 6

Conclusion

The ideal teleoperation system would allow an operator to complete a task in environments where human presence is impossible or undesirable as least as easily as if he or she were to directly perform the same task with his or her own hands. To date, all teleoperation systems fall short of this ambitious standard. A few immersive systems that offer high transparency and presence, such as the da Vinci surgical system [33], come close, especially with extensive operator training. However, even the da Vinici surgical system surgical system Furthermore, the da Vinci's immersive display requires the operator to sacrifice awareness of his or her local environment. This tradeoff is acceptable in robotic surgery, but it would be dangerous in many other teleoperation use cases. For example, in a search-and-rescue task, the operator is located in a disaster field and needs to be aware of the local environment [8].

This dissertation presented and evaluated two new methods of improving the usability of teleoperation systems without sacrificing the operator's awareness of the local environment. First, I proposed and proved that data-driven motion mappings that correct for systematic human motion errors improve the usability and transparency of teleoperation systems. Second, I proposed that providing grip-force, finger-tip-contact-and-pressure, and high-frequency acceleration haptic feedback would improve the usability of teleoperation systems by increasing the level of presence experienced by the operator. Analysis of a teleoperated pick-and-place task revealed that grip-force and high-frequency acceleration haptic feedback aided task performance, while finger-tip-contact-and-pressure haptic feedback had both positive and negative effects.

6.1 Contributions

Determining Natural Human-Robot Motion Mappings in Teleoperation

Chapter 2 proposes implementing data-driven motion mappings as an alternative to the typically used Cartesian-scaling motion mapping. The Cartesian-scaling motion mapping falsely assumes that the operator's executed movements identically match his or her intended movement. A data-driven motion mapping that corrects for systematic errors in human movement will result in robot motion that more closely resembles the operator's intent, as opposed to the operator's produced motion. First, I developed and implemented a semi-automatic method to determine such a data-driven motion mapping in which the subject mimics the preprogrammed motion of a virtual robot. The recorded motion data is then used to fit parameters of a data-driven motion mapping model. Three data-driven motion mapping models are proposed and evaluated against a Cartesian-scaling motion mapping. A variable-similarity motion mapping that corrects systematic directional motion errors was found to best transform the recorded human motion to the robot's motion.

Evaluation of Data-Driven Motion Mappings

Chapter 3 confirms the hypothesis that implementing data-driven motion mappings will improve the usability of teleoperation systems. Two forms of the variable-similarity motion mapping model and a Cartesian-scaling motion mapping were used to calculate a virtual robot's desired hand position given the measured human hand position. The first variable-similarity motion mapping was fit to data collected in the study conducted in Chapter 2 and corrects for average motion errors made by a population. The second variable-similarity motion mapping was individually fit to data collected in the calibration phase of the validation user study. Twelve participants reached toward 120 targets under each of the three motion mappings with balanced random presentation order and a washout task between conditions. Subjects were able to complete the targeting task with higher accuracy in initial direction of robot motion, at higher speeds, and with more natural and efficient reaching movements under the variable-similarity motion mappings. Subjects also overwhelmingly preferred the variable-similarity motion mappings. These results indicate that subjects experienced a higher level of transparency when using the virtual teleoperator with the variable-similarity motion mappings than with the standard Cartesian mapping.

A Wearable Device for Controlling a Robot Gripper with Ungrounded Haptic Feedback

In Chapter 4, the focus of the dissertation switches from the feedforward (efferent) channel to the feedback (afferent) channel. An ungrounded wearable haptic device was designed to deliver grip-force, fingertip-pressure-and-contact, and high-frequency acceleration haptic feedback. The device's controller is also developed: a position-position controller with gain switching was implemented to allow the user to control the opening of the remote robot's hand while simultaneously feeling a representation of the grip force that the robot's hand is applying to objects. Signals measured by the robot's pair of fingertip-mounted pressure sensor arrays and a wrist-mounted high-bandwidth accelerometer were processed to drive the tactile fingertip-contact and high-frequency acceleration feedback. Finally, preliminary testing of the device proved that it successfully delivers the intended haptic feedback and enables handling of diverse objects.

Effects of Ungrounded Haptic Feedback on a Teleoperated Pick-and-Place Task

Chapter 5 evaluates each haptic feedback modality that is displayed by the custom device developed in Chapter 4. A user study was designed to test the hypothesis that ungrounded grip-force, fingertip-contact-and-pressure, and high-frequency acceleration haptic feedback will improve a teleoperated pick-and-place task just as the different touch modalities aid direct task completion. I developed a teleoperation system consisting of a haptic device worn on the subject's right hand, a remote PR2 humanoid robot, and a Vicon motion capture system. Each subject used this teleoperation system to move either a flexible plastic cup or a rigid plastic block to a target location ten times under each of the eight haptic conditions obtained by turning on and off grip-force feedback, contact feedback, and acceleration feedback. The results indicate that the addition of grip-force feedback with gain switching enables subjects to handle objects more delicately, hold objects more stably, and better control the motion of the remote robot's hand. Although certain aspects were improved, such as sensing when the object is in the remote robot's hand, the addition of contact feedback generally led subjects to handle the object more roughly. Finally, adding acceleration feedback slightly improved the subject's performance when setting the object down, as originally hypothesized; interestingly it also allowed subjects to feel vibrations produced by the robot's motion, causing them to be more careful when completing the task. This study supports the utility of grip-force and high-frequency acceleration feedback in teleoperation systems.

6.2 Future Directions

Research presented in this dissertation can be extended through further investigation on alternative data-driven motion mappings and ungrounded haptic feedback in teleoperation. This dissertation can also be extended by studying the interplay between the feedforward and feedback channels. Finally, an important vein of future work lies in creating objective metrics to evaluate the levels of transparency and presence in teleoperation systems.

Data-Driven Motion Mappings

This dissertation showed that variable-similarity motion mappings allow subjects to better complete a targeting task than Cartesian-scaling motion mappings. However, to fully substantiate this claim, we need to validate it using more complicated tasks in which subjects not only move the robot's arm through space, but also interact with objects in the robot's environment to perform a meaningful task. In order to allow subjects to complete such a task, we first need to extend our motion mappings to three dimensions. Both extending our calibration routine to three-dimensional motions and performing the two-dimensional calibration routine in several different horizontal planes are promising approaches for deducing three-dimensional data-driven motion mappings.

I would also like to extend our methods to allow a robot to complete two-handed tasks. While simply replicating our methods for the left hand could work, we need to better understand how humans perform two-handed tasks. The mappings currently consider only the position of the hand in a body-centered coordinate frame. However, in two-handed tasks, the left hand would need to coordinate its position with that of the right hand, and vice versa. Therefore, more research may be required to extend our mappings to two-handed teleoperators.

I also hope to find other motion mappings that improve operator performance in teleoperation. We recommend starting this investigation by further considering theories proposed in the neuroscience literature regarding the cause of systematic errors made by humans completing targeting tasks. For example, Gordon et al. propose that systematic errors are made when a human fails to fully account for the inertia of his or her arm [29]. Another theory states that subjects systematically underestimate the distance of their hand from their body, causing them to produce systematic directional errors [22]. New motion mappings can be created based on these theories and others proposed in the literature.

Finally, I would like to extend my work in modeling human motion errors and creating data-driven motion mappings to the field of physical therapy. The motion mimicking task could be repurposed as a diagnostic tool because errors made during this task generalize across a population. Therefore, a metric could be developed that could inform a therapist how close his or her patient is to having normal motor function. I envision a therapeutic setup that measures human motion as patients mimic the motion of a human-like agent. The resulting patient motion would then be analyzed by custom software and produce a score about the patient's motions. The software could also help direct the physical therapist by providing information about the areas in the subject's workspace in which errors were most abnormal.

I also believe that implementing corrective motion mapping in a virtual physical therapy task could make physical therapy more enjoyable, which could result in greater patient compliance. A task could be developed in which the patient would control the motion of a virtual agent. Corrective motion mapping would be developed for the patient using methods similar to those developed in this dissertation. These motion mappings would enable the motion of the agent to match the patient's intent, rather than his or her produced motion. Implementing such data-driven motion mapping would likely result in higher levels of task performance. Higher levels of task performance could encourage patients, which could lead them to be more energized and to work harder during therapy sessions. There is the obvious risk that subjects could become satisfied with their performance, which would reduce effort and limit the benefits of the therapeutic intervention. To prevent this I propose investigating methods to blend corrective motion mappings with mappings that preserve the user's motion. This would allow physical therapists to control the level of assistance delivered by the motion mappings. The therapist could adjust the assistance level according to the needs of each patient, even as these needs change from session to session.

Ungrounded Haptic Feedback in Teleoperation

This dissertation showed that ungrounded haptic feedback improves operator performance in a teleoperated pick-and-place task. Grip-force feedback with gain switching allowed subjects to hold the object more stably and with lower forces, and it gave subjects better control over the robot's hand position. Early testing showed that the device worked better with a position-position controller, rather than a position-force controller. However, the position-position controller works best when the robot is manipulating a rigid object. When the robotic hand grasps a rigid object, the force applied to the robot's fingertips increases according to Hooke's law. Very little force is applied to the robot's fingertips if it is grasping the object with a commanded grip opening that it close to the width of the object. High forces are applied to the robot's fingertips if it grips the object with a commanded grasp opening that is smaller than the width of the object. On the other hand, in the case of a deformable object, the difference between the device's opening and the robot's opening can be negligible and the operator would feel very little force, even when the robot's hand is applying enough force to deform the object. It is thus not surprising that the results of this study revealed that our implementation of grip-force feedback had more positive effects for subjects manipulating the rigid block. Therefore, we propose that a new control system should be developed that closely links the human's hand to the robot's while accurately reflecting the force applied to the user's hand. This goal could probably be achieved using a position-position controller with gain scheduling [11, 86], so that the value of the proportional gain is continually updated so that the force applied to the user's hand matches the measured force at the robot's fingertips, even when the position control error is small.

Fingertip-contact tactile feedback both positively and negatively affected task performance. Consistent with the hypothesis, contact feedback better allowed the subject to determine when the object was grasped in the robot's hand. However, contact feedback also caused subjects to handle the object more roughly. I believe that the current implementation of contact feedback startled some users, thereby increasing the roughness with which they handled the object. Therefore, alternative methods of delivering contact feedback should be explored with the goal of increasing the positive effects of contact feedback, while lessening its negative effects. One small improvement would be to reduce the moving mass of the platform by switching the magnet and the coil. In this configuration, the heavier magnet (33 grams) would be rigidly attached to the body of the haptic device and the lighter coil (7 grams) would be attached to the moving platform.

High-frequency acceleration of transient vibrations caused by collisions in the robot's environment improved task performance amongst subjects who completed the task with the rigid object. High-frequency acceleration feedback of egovibrations caused by the robot's motion unexpectedly proved more beneficial to user performance. It is worth noting that I purposely eliminated as much egovibration feedback as possible when designing the device's controller because I falsely assumed these vibrations would only serve to annoy the operator, without improving his or her task performance. I was not alone in this misguided assumption, as evidenced by that fact that nearly all research on robot egovibrations treats such vibrations as noise and aims to eliminate them from sensor readings, e.g. [43, 44, 65]. To my knowledge, the sole exception is the research of Kurihara et al., which showed that haptic and auditory feedback of vibrations caused by robot motion increased subjective ownership and the sense of resistance caused by moving a virtual robot arm [55]. This relatively unexplored area of egovibration feedback certainly merits further exploration. However, I note that care must be used when designing such egovibration feedback because it is known that continuously applying strong vibrations to the skin reduces tactile sensitivity [39].

The modalities of haptic feedback were designed to deliver accurate representations of what the robot felt. However, limits in sensor and actuator technology preclude the haptic feedback provided by the device from being indistinguishable from what the operator would feel if her or she were to directly interact with the object. This dissertation showed that the haptic feedback provided by the device was useful to the subjects in this experiment, even if the haptic feedback paled in comparison to the rich sensations encountered in direct manipulation tasks. However, understanding exactly how subjects were able to utilize the haptic feedback was beyond the scope of this work. In the future, I hope to conduct a study investigating the learning curve associated with each modality of haptic feedback to elucidate the naturalness of each feedback modality. If a modality of haptic feedback leads a subject to perform a task well, but doesn't improve his or her performance over time, we can conclude that that modality of feedback had high levels of intuitiveness. However, if a modality causes a subject's performance to improve over time, we can conclude that this modality is useful, but not necessarily intuitive. I hope to conduct such a learning curve study not only using the modalities of feedback discussed in this dissertation, but also using a variety of other haptic, visual, and auditory feedback modalities.

Another interesting research extension for this project would be to consider how to best provide haptic feedback to an operator to controlling a multi-fingered robotic hand. Extending the tactile feedback to a multi fingered design would be a reasonably straightforward extension of the device's current design. One would simply need to place a voice coil actuator at the tip of any finger involved in controlling the robotic hand. These additional voice coils could then be driven using the same control methods developed in this dissertation. Extending grip force feedback to a multi-fingered controller would require more extensive mechanical modifications because the DC motor is positioned to directly actuate the rotational degree-of-freedom of the device. The direct-drive design prohibits a simple extension to a multi-fingered device because it is impossible to fit multiple motors between adjacent metacarpophalangeal joints. A possible alternative design would be to position the motors near the back of the hand and use linkages to transmit forces from the motors to the fingers. This design would be similar to that of the CyberGrasp [13], but would allow the device to both push and pull on the operator's fingers.

Effects of Haptic Feedback on Reach Accuracy in Teleoperation

This dissertation investigated two separate methods of improving the usability of teleoperation systems that measure natural arm movement to control the motion of a remote robot. The first half of this dissertation improved the forward channel of a teleoperation system by introducing data-driven motion mappings. The second half of this dissertation improved the feedback channel by providing the operator with multiple modalities of ungrounded haptic feedback. The effects of data-driven motion mappings and haptic feedback were each independently analyzed, largely treating the feedforward and feedback channels as separate entities.

However, Chapter 5 provides showing that haptic feedback better allowed the subject to control the motion of the remote robot. Unfortunately, the unconstrained design of this study prohibited extensive analysis of the subject's performance in the reach action phase of the teleoperated pick-and-place task. It is reasonable to expect haptic feedback to positively affect an operator's ability to control the motion of a remote robot because the sense of touch plays an important role in allowing one to accurately and consistently move his or her own arm. For example, touch allows subjects completing a typing task to reach more accurately toward the keys and to recognize when a finger movement was executed inaccurately [28]. Furthermore, typing movements are executed with higher trajectory variability when anesthesia is administered to block the sense of touch [81]. The human sense of touch also improves the accuracy of pointing tasks that require full arm movement [83]. Blocking the sense of touch with anesthesia also affects both the spatial movements of the hand and the trajectory of the hand opening in a reach-to-grasp task [19]. The improvements in motion accuracy and consistency are due to the fact that touch allows one to update his or her internal body representation by providing accurate spatial information when the hand makes contact with an object at a known location [56]. The sense of touch also allows one to recognize when a reaching motion was executed inaccurately, when the experienced touch is inconsistent with the expected touch, which allows a person to alter his or her internal motion controller following an inaccurately executed reach.

Therefore, we hypothesize that haptic feedback will improve reach accuracy in teleoperation. We plan to conduct a user study in the near future in which subjects will complete a teleoperated reach-to-grasp task with a virtual robot. A crossover experimental design will be implemented. Subjects will reach and grasp three sets of virtual targets, either with or without haptic feedback. The targets will be presented in a randomly generated order. Subjects will then complete three more sets of trials under the other haptic feedback condition. We will compare each subject's task performance with haptic feedback against his or her performance without haptic feedback to understand whether haptic feedback affects reach accuracy in teleoperation.

We plan to use this study as an opportunity to investigate the interaction between the data-driven motion mappings and haptic feedback. Half of the subjects will complete the task under a population-fit-data driven motion mapping and the other half will complete the task under a Cartesian-scaling motion mapping. This proposed study will show the relative importance and possible synergy of the two techniques pioneered by this dissertation.

Bibliography

[1] Christopher G Atkeson and John M Hollerbach, *Kinematic features of unrestrained vertical arm movements*, The Journal of Neuroscience **5** (1985), no. 9, 2318–2330.

[2] Federico Barbagli, K Salisbury Jr, and Roman Devengenzo, *Enabling multi-finger, multi-hand virtualized grasping*, Proc. IEEE International Conference on Robotics and Automation, vol. 1, 2003, pp. 809–815.

[3] Mohamed Benali-Khoudja, Moustapha Hafez, Jean-Marc Alexandre, and Abderrahmane Kheddar, *Tactile interfaces: a state-of-the-art survey*, Proc. International Symposium on Robotics, vol. 31, 2004.

[4] Massimo Bergamasco, Benedetto Allotta, L. Bosio, L. Ferretti, G. Parrini, G.M. Prisco, Fabio Salsedo, and G. Sartini, *An arm exoskeleton system for teleoperation and virtual environments applications*, Proc. IEEE International Conference on Robotics and Automation, 1994, pp. 1449–1454.

[5] Frank Biocca and Ben Delaney, *Immersive virtual reality technology*, Communication in the Age of Virtual Reality (1995), 57–124.

[6] Luc Boutina, Antoine Eona, Said Zeghloula, and Patrick Lacouture, *From human motion capture to humanoid locomotion imitation application to the robots HRP-2 and HOAP-3*, Robotica, vol. 29, 2010, pp. 325–334.

[7] Liana E. Brown, David A. Rosenbaum, and Robert L. Sainburg, *Limb position drift: Implications for control of posture and movement*, Journal of Neurophysiology **90** (2003), no. 5, 3105–3118.

[8] Jennifer Casper and Robin R. Murphy, *Human-robot interactions during the robot-assisted urban search and rescue response at the world trade center*, IEEE Transactions on Systems, Man, and Cybernetics, Part B: Cybernetics **33** (2003), no. 3, 367–385.

[9] Jessie Y.C. Chen, Ellen C. Haas, and Michael J. Barnes, *Human performance issues and user interface design for teleoperated robots*, Transactions on Systems, Man, and Cybernetics, Part C: Applications and Reviews **37** (2007), no. 6, 1231–1245.

[10] Francesco Chinello, Monica Malvezzi, Claudio Pacchierotti, and Domenico Prattichizzo, *A three DoFs wearable tactile display for exploration and manipulation of virtual objects*, Proc. IEEE Haptics Symposium, 2012, pp. 71–76.

[11] Jang Ho Cho and Doo Yong Lee, *Gain-scheduling control of a teleoperation system*, IEEE International Conference on Systems, Man and Cybernetics, 2009, pp. 1489–1495.

[12] B. Corteville, E. Aertbelien, H. Bruyninckx, J. De Schutter, and H. Van Brussel, *Human-inspired robot assistant for fast point-to-point movements*, Proc. IEEE International Conference on Robotics and Automation, April 2007, pp. 3639–3644.

[13] CyberGrasp, http://www.cyberglovesystems.com/cybergrasp/ (2015).

[14] B. Dariush, M. Gienger, B. Jian, C. Goerick, and K. Fujimura, *Whole body humanoid control from human motion descriptors*, Robotics and Automation, IEEE International Conference on, May 2008, pp. 2677–2684.

[15] A. Davids, *Urban search and rescue robots: from tragedy to technology*, IEEE Intelligent Systems **17** (2002), no. 2, 81–83.

[16] Michel Desmurget, Michael Jordan, Claude Prablanc, and Marc Jeannerod, *Constrained and unconstrained movements involve different control strategies*, Journal of Neurophysiology **77** (1997), no. 3, 1644–1650.

[17] Tamar Flash and Neville Hogan, *The coordination of arm movements: an experimentally confirmed mathematical model*, The Journal of Neuroscience **5** (1985), no. 7, 1688–1703.

[18] Antonio Frisoli, Massimiliano Solazzi, Miriam Reiner, and Massimo Bergamasco, *The contribution of cutaneous and kinesthetic sensory modalities in haptic perception of orientation*, Brain Research Bulletin **85** (2011), no. 5, 260–266.

[19] M Gentilucci, I. Toni, E. Daprati, and M. Gangitano, *Tactile input of the hand and the control of reaching to grasp movements*, Experimental Brain Research **114** (1997), no. 1, 130–137.

[20] Claude Ghez, James Gordon, and Maria Felice Ghilardi, *Contributions of vision and proprioception to accuracy in limb movements*, The Cognitive Neurosciences (1995), 549–564.

[21] Claude Ghez, J.W. Krakauer, Robert L. Sainburg, and Maria Felice Ghilardi, *Spatial representations and internal models of limb dynamics in motor learning*, The New Cognitive Neurosciences **2** (2000), 501–514.

[22] Maria Felice Ghilardi, James Gordon, and Claude Ghez, *Learning a visuomotor transformation in a local area of work space produces directional biases in other areas*, Journal of Neurophysiology **73** (1995), no. 6, 2535–2539.

[23] Michael Gleicher, *Retargetting motion to new characters*, ACM SIGGRAPH, 1998, pp. 33–42.

[24] Raymond C Goertz, *Fundamentals of general purpose remote manipulators*, Nucleonics **10** (1952), no. 11, 36–42.

[25] R.C. Goertz, *Mechanical master-slave manipulator*, Nucleonics **12** (1954), no. 11, 45–46.

[26] R.C. Goertz and W.M. Thompson, *Electronically controlled manipulator*, Nucleonics **12** (1954), no. 11, 46–47.

[27] Susan J. Goodbody and Daniel M. Wolpert, *The effect of visuomotor displacements on arm movement paths*, Experimental Brain Research **127** (1999), no. 2, 213–223.

[28] Andrew M. Gordon and John F. Soechting, *Use of tactile afferent information in sequential finger movements*, Experimental Brain Research **107** (1995), no. 2, 281–292.

[29] James Gordon, Maria Felice Ghilardi, Scott E Cooper, and Claude Ghez, *Accuracy of planar reaching movements II. systematic extent errors resulting from inertial anisotropy*, Experimental Brain Research **99** (1994), no. 1, 112–130.

[30] James Gordon, Maria Felice Ghilardi, and Claude Ghez, *Accuracy of planar reaching movements I. Independence of direction and extent variability*, Experimental Brain Research **99** (1994), no. 1, 97–111.

[31] P. Gourtzelidis, N. Smyrnis, I. Evdokimidis, and A. Balogh, *Systematic errors of planar arm movements provide evidence for space categorization effects and interaction of multiple frames of reference*, Experimental Brain Research **139** (2001), no. 1, 59–69.

[32] Weston B. Griffin, William R. Provancher, and Mark R. Cutkosky, *Feedback strategies for telemanipulation with shared control of object handling forces*, Presence: Teleoperators and Virtual Environments **14** (2005), no. 6, 720–731.

[33] Gary Guthart and John Kenneth Salisbury Jr, *The Intuitive telesurgery system: Overview and application.*, Proc. IEEE International Conference on Robotics and Automation, IEEE, 2000, pp. 618–621.

[34] Antal Haans and Wijnand A. IJsselsteijn, *Embodiment and telepresence: Toward a comprehensive theoretical framework*, Interacting with Computers **24** (2012), no. 4, 211–218.

[35] Blake Hannaford and Allison M. Okamura, *Haptics*, Handbook of Robotics, Springer, 2008, pp. 719–739.

[36] Blake Hannaford, Laurie Wood, Douglas A. McAffee, and Haya Zak, *Performance evaluation of a six-axis generalized force-reflecting teleoperator*, IEEE Transactions on Systems, Man and Cybernetics **21** (1991), no. 3, 620–633.

[37] Sandra G. Hart and Lowell E. Staveland, *Development of NASA-TLX (Task Load Index): Results of empirical and theoretical research*, Advances in Psychology **52** (1988), 139–183.

[38] Dave Hershberger, David Gossow, and Josh Faust, *RViz*.

[39] Nancy W. Hochreiter, Martha J. Jewell, Lois Barber, and Phyllis Browne, *Effect of vibration on tactile sensitivity*, Physical Therapy **63** (1983), no. 6, 934–937.

[40] Peter F. Hokayem and Mark W. Spong, *Bilateral teleoperation: An historical survey*, Automatica **42** (2006), no. 12, 2035–2057.

[41] James Houk and William Simon, *Responses of golgi tendon organs to forces applied to muscle tendon.*, Journal of Neurophysiology **30** (1967), no. 6, 1466–1481.

[42] Wijnand A. IJsselsteijn, Huib de Ridder, Jonathan Freeman, and Steve E. Avons, *Presence: concept, determinants, and measurement*, Human Vision and Electronic Imaging, International Society for Optics and Photonics, 2000, pp. 520–529.

[43] Gökhan Ince, Kazuhiro Nakadai, Tobias Rodemann, Yuji Hasegawa, Hiroshi Tsujino, and Jun-ichi Imura, *Ego noise suppression of a robot using template subtraction*, Proc. International Conference on Intelligent Robots and Systems, IEEE, 2009, pp. 199–204.

[44] Gökhan Ince, Kazuhiro Nakadai, Tobias Rodemann, Hiroshi Tsujino, and Jun-Ichi Imura, *Robust ego noise suppression of a robot*, Trends in Applied Intelligent Systems, Springer, 2010, pp. 62–71.

[45] Leif Jentoft, Yaroslav Tenzer, Daniel Vogt, Ignacio Galiana, and Ian Daniher, *TakkTile*, URL http://www.takktile.com/ (2013).

[46] Roland S. Johansson and J. Randall Flanagan, *Coding and use of tactile signals from the fingertips in object manipulation tasks*, Nature Reviews Neuroscience **10** (2009), no. 5, 345–359.

[47] Rebecca P. Khurshid, Naomi T. Fitter, Elizabeth A. Fedalei, and Katherine J. Kuchenbecker, *Effects of grip-force, contact, and acceleration feedback on a teleoperated pick-and-place task*, Submitted to IEEE Transactions on Haptics.

[48] Rebecca P. Khurshid and Katherine J. Kuchenbecker, *Data-driven motion mappings improve transparency in teleoperation*, Presence: Teleoperators and Virtual Environments **24** (2015), no. 2, 132–154.

[49] C.H. King, Martin O. Culjat, Miguel L. Franco, Catherine E. Lewis, Erik P. Dutson, Warren S. Grundfest, and James W. Bisley, *Tactile feedback induces reduced grasping force in robot-assisted surgery*, IEEE Transactions on Haptics **2** (2009), no. 2, 103–110.

[50] Nathan Koenig and Andrew Howard, *Design and use paradigms for Gazebo, an open-source multi-robot simulator*, Proc. IEEE/RSJ International Conference on Intelligent Robots and Systems, September 2004, pp. 2149–2154.

[51] Dimitrios A. Kontarinis and Robert D. Howe, *Tactile display of vibratory information in teleoperation and virtual environments*, Presence: Teleoperators and Virtual Environments **4** (1995), no. 4, 387–402.

[52] Tatsuya Koyama, Ikuo Yamano, Kenjiro Takemura, and Takashi Maeno, *Multi-fingered exoskeleton haptic device using passive force feedback for dexterous tele-operation*, Proc. IEEE/RSJ International Conference on Intelligent Robots and Systems, vol. 3, 2002, pp. 2905–2910.

[53] Katherine J. Kuchenbecker, Jonathan Fiene, and Günter Niemeyer, *Improving contact realism through event-based haptic feedback*, IEEE Transactions on Visualization and Computer Graphics **12** (2006), no. 2, 219–230.

[54] Katherine J. Kuchenbecker, William R. Provancher, Günter Niemeyer, and Mark R. Cutkosky, *Haptic display of contact location*, Proc. International Symposium on Haptic Interfaces for Virtual Environment and Teleoperator Systems, 2004, pp. 40–47.

[55] Yosuke Kurihara, Taku Hachisu, Katherine J. Kuchenbecker, and Hiroyuki Kajimoto, *Virtual robotization of the human body via data-driven vibrotactile feedback*, Advances in Computer Entertainment, vol. 5, Springer, 2013, pp. 109–122.

[56] James R. Lackner and Paul A. DiZio, *Aspects of body self-calibration*, Trends in Cognitive Sciences **4** (2000), no. 7, 279–288.

[57] Nils Landin, Joseph M. Romano, William McMahan, and Katherine J. Kuchenbecker, *Dimensional reduction of high-frequency accelerations for haptic rendering*, Haptics: Generating and Perceiving Tangible Sensations, Proc. EuroHap-

tics, Part II, Lecture Notes in Computer Science, vol. 6192, Springer, July 2010, pp. 79–86.

[58] Dale A. Lawrence, *Stability and transparency in bilateral teleoperation*, IEEE Transactions on Robotics and Automation **9** (1993), no. 5, 624–637.

[59] P. Letier, E. Motard, and J.P. Verschueren, *Exostation : Haptic exoskeleton based control station*, International Conference on Robotics and Automation, May 2010, pp. 1840 –1845.

[60] Y. Maeda, T. Hara, and T. Arai, *Human-robot cooperative manipulation with motion estimation*, Proc. IEEE/RSJ International Conference on Intelligent Robots and Systems, vol. 4, 2001, pp. 2240–2245.

[61] George E. Martin, *Transformation geometry: An introduction to symmetry*, Springer-Verlag, 1982.

[62] Thomas H. Massie and Kenneth Salisbury Jr., *The PHANToM haptic interface: A device for probing virtual objects*, Proceedings of the ASME Winter Annual Meeting, Symposium on Haptic Interfaces for Virtual Environment and Teleoperator Systems, vol. 55, Chicago, IL, 1994, pp. 295–300.

[63] Michael McKenna and David Zeltzer, *Three dimensional visual display systems for virtual environments*, Presence: Teleoperators and Virtual Environments **1** (1992), no. 4, 421–458.

[64] William McMahan, Jamie Gewirtz, Dorsey Standish, Paul Martin, Jacquelyn A. Kunkel, Magalie Lilavois, Alexei Wedmid, David I. Lee, and Katherine J. Kuchenbecker, *Tool contact acceleration feedback for telerobotic surgery*, IEEE Transactions on Haptics **4** (2011), no. 3, 210–220.

[65] William McMahan and Katherine J. Kuchenbecker, *Spectral subtraction of robot motion noise for improved vibrotactile event detection*, Haptics: Perception, Devices, Mobility, and Communication: Proc. EuroHaptics, Part I (Tampere, Finland) (P. Isakoski and J. Springare, eds.), Lecture Notes in Computer Science, vol. 7282, Springer, June 2012, pp. 326–337.

[66] William McMahan, Joseph M. Romano, Amal M. Abdul Rahuman, and Katherine J. Kuchenbecker, *High frequency acceleration feedback significantly increases the realism of haptically rendered textured surfaces*, Proc. IEEE Haptics Symposium, 2010, pp. 141–148.

[67] Shuhei Nakagawara, Hiroyuki Kajimoto, Naoki Kawakami, Susumu Tachi, and Ichiro Kawabuchi, *An encounter-type multi-fingered master hand using circuitous joints*, Proc. IEEE International Conference on Robotics and Automation, IEEE, 2005, pp. 2667–2672.

[68] Liya Ni and David W.L. Wang, *A gain-switching control scheme for position-error-based force-reflecting teleoperation*, Proc. IEEE Symposium on Haptic Interfaces for Virtual Environment and Teleoperator Systems, 2002, pp. 239–246.

[69] Günter Niemeyer, Carsten Preusche, and Gerd Hirzinger, *Telerobotics*, Handbook of Robotics, Springer, 2008, pp. 741–757.

[70] Ilana Nisky, Sangram Patil, Michael H. Hsieh, and Allison M. Okamura, *Kinematic analysis of motor performance in robot-assisted surgery: A preliminary study*, Studies in Health Technology and Information **184** (2013), 302–308.

[71] Charles R. Noback, Norman L. Strominger, Robert J. Demarest, and David A. Ruggiero, *Discriminative general senses, crude touch, and proprioception*, The Human Nervous System: Structure and Function (2005), 177–192.

[72] Claudio Pacchierotti, Francesco Chinello, Monica Malvezzi, Leonardo Meli, and Domenico Prattichizzo, *Two finger grasping simulation with cutaneous and kinesthetic force feedback, proc. eurohaptics*, Haptics: Perception, Devices, Mobility, and Communication: Proc. EuroHaptics, Lecture Notes in Computer Science, Springer, 2012, pp. 373–382.

[73] Carolina Passenberg, Angelika Peer, and Martin Buss, *A survey of environment-, operator-, and task-adapted controllers for teleoperation systems*, Mechatronics **20** (2010), no. 7, 787–801.

[74] Joel C. Perry, Jacob Rosen, and Stephen Burns, *Upper-limb powered exoskeleton design*, IEEE/ASME Transactions on Mechatronics **12** (2007), no. 4, 408–417.

[75] Rebecca M. Pierce, Elizabeth A. Fedalei, and Katherine J. Kuchenbecker, *A wearable device for controlling a robot gripper with fingertip contact, pressure, vibrotactile, and grip force feedback*, Proc. IEEE Haptics Symposium, 2014.

[76] Rebecca M. Pierce and Katherine J. Kuchenbecker, *A data-driven method for determining natural human-robot motion mappings in teleoperation*, Proc. International Conference on Biomedical Robotics and Biomechatronics, 2012, pp. 169–176.

[77] N.S. Pollard, J.K. Hodgins, M.J. Riley, and C.G. Atkeson, *Adapting human motion for the control of a humanoid robot*, Robotics and Automation, IEEE International Conference on, vol. 2, 2002, pp. 1390–1397.

[78] D. Powell, G. Gilbreath, and M. Bruch, *Multi-robot operator control unit*, SPIE Proc 6230: Unmanned systems technology VIII, Defense Security Symposium, April 2006.

[79] William R. Provancher, Katherine J. Kuchenbecker, Günter Niemeyer, and Mark R. Cutkosky, *Perception of curvature and object motion via contact location feedback*, Robotics Research: the Eleventh International Symposium (ISRR 2003), Springer Tracts in Advanced Robotics, vol. 15, Springer, Siena, Italy, 2005, pp. 456–465.

[80] Morgan Quigley, Ken Conley, Brian Gerkey, Josh Faust, Tully Foote, Jeremy Leibs, Rob Wheeler, and Andrew Y. Ng, *ROS: an open-source robot operating*

system, ICRA Workshop on Open Source Software, no. 3.2, 2009.

[81] Ely Rabin and Andrew M. Gordon, *Tactile feedback contributes to consistency of finger movements during typing*, Experimental Brain Research **155** (2004), no. 3, 362–369.

[82] G. Jagannath Raju, George C. Verghese, and Thomas B. Sheridan, *Design issues in 2-port network models of bilateral remote manipulation*, Proc. IEEE International Conference on Robotics and Automation, IEEE, 1989, pp. 1316–1321.

[83] Ashwini K. Rao and Andrew M. Gordon, *Contribution of tactile information to accuracy in pointing movements*, Experimental Brain Research **138** (2001), no. 4, 438–445.

[84] Joseph M. Romano, Kaijen Hsiao, Günter Niemeyer, Sachin Chitta, and Katherine J. Kuchenbecker, *Human-inspired robotic grasp control with tactile sensing*, IEEE Transactions on Robotics **27** (2011), no. 6, 1067–1079.

[85] Joseph M. Romano, R.J. Webster, and Allison M. Okamura, *Teleoperation of steerable needles*, Proc. International Conference on Robotics and Automation, IEEE, 2007, pp. 934–939.

[86] Wilson J. Rugh and Jeff S. Shamma, *Research on gain scheduling*, Automatica **36** (2000), no. 10, 1401–1425.

[87] R.L. Sainburg, C. Ghez, and D. Kalakanis, *Intersegmental dynamics are controlled by sequential anticipatory, error correction, and postural mechanisms*, Journal of Neurophysiology **81** (1999), no. 3, 1045–1056.

[88] Peter H. Schonemann and Robert M. Carroll, *Fitting one matrix to another under choice of a central dialation and a rigid motion*, Psychometrika **35** (1970), no. 2, 245–255.

[89] Reza Shadmehr and Ferdinando A. Mussa-Ivaldi, *Adaptive representation of dynamics during learning of a motor task*, The Journal of Neuroscience **14** (1994), no. 5, 3208–3224.

[90] Thomas B. Sheridan, *Musings on telepresence and virtual presence*, Presence: Teleoperators and Virtual Environments **1** (1992), no. 1, 120–126.

[91] ______, *Further musings on the psychophysics of presence*, Presence: Teleoperators and Virtual Environments **1** (1996), no. 5, 241–246.

[92] Massimiliano Solazzi, Antonio Frisoli, and Massimo Bergamasco, *Design of a novel finger haptic interface for contact and orientation display*, Proc. IEEE Haptics Symposium, 2010, pp. 129–132.

[93] Mandayam A. Srinivasan and Cagatay Basdogan, *Haptics in virtual environments: Taxonomy, research status, and challenges*, Computers and Graphics **21** (1997), no. 4, 393–404.

[94] Kay M. Stanney, Ronald R. Mourant, and Robert S. Kennedy, *Human factors issues in virtual environments: A review of the literature*, Presence: Teleoperators and Virtual Environments **7** (1998), no. 4, 327–351.

[95] Hong Z. Tan, Mandayam A. Srinivasan, Brian Eberman, and Belinda Cheng, *Human factors for the design of force-reflecting haptic interfaces*, Dynamic Systems and Control **55** (1994), no. 1, 353–359.

[96] Teleop PR2 arm in simulation, URL http://wiki.ros.org/pr2_simulator/ Tutorials/Teleop%20PR2%20arm%20in%20simulation (2013).

[97] Yaroslav Tenzer, Leif P. Jentoft, and Robert D. Howe, *The feel of MEMS barometers*, IEEE Robotics & Automation Magazine (2014).

[98] Yue Peng Toh, Shan Huang, Joy Lin, Maria Bajzek, Garth Zeglin, and Nancy S. Pollard, *Dexterous telemanipulation with a multi-touch interface*, Proc. IEEE-RAS International Conference on Humanoid Robots, IEEE, 2012, pp. 270–277.

[99] A. Trujillo-Ortiz, R. Hernandez-Walls, and F.A. Trujillo-Perez, *RMAOV33: Analysis of variance with repeated measures on three factors test. a Matlab file.*, 2006.

[100] Å.B. Vallbo and R.S. Johansson, *Properties of cutaneous mechanoreceptors in the human hand related to touch sensation*, Human Neurobiology **3** (1984), no. 1, 3–14.

[101] Lawton N. Verner, Kristin A. Jeung, and Allison M. Okamura, *Effects of gripping and translational forces on teleoperation*, Springer Tracks in Advanced Robotics: Multi-point Interaction with Real and Virtual Objects, Springer, 2005, pp. 231–241.

[102] S.M.P. Verschueren, Stephan P. Swinnen, Paul J. Cordo, and Natalia V. Dounskaia, *Proprioceptive control of multijoint movement: unimanual circle drawing*, Experimental Brain Research **127** (1999), 171–181.

[103] Philippe Vindras, Michel Desmurget, Claude Prablanc, and Paolo Viviani, *Pointing errors reflect biases in the perception of the initial hand position*, Journal of Neurophysiology **79** (1998), 3290–3294.

[104] John P. Wann and Sam F. Ibrahim, *Does limb proprioception drift?*, Experimental Brain Research **91** (1992), 162–166.

[105] Jeroen G.W. Wildenbeest, David A. Abbink, Cock J.M. Heemskerk, Frans C.T. van der Helm, and Henri Boessenkool, *The impact of haptic feedback quality on the performance of teleoperated assembly tasks*, IEEE Transactions on Haptics **6** (2013), no. 2, 242–252.

[106] Kimberly J. Wisneski and Michelle J. Johnson, *Quantifying kinematics of purposeful movements to real, imagined, or absent functional object: Implications for modeling trajectories for robot-assisted ADL tasks*, Journal of NeuroEngineering and Rehabilitation **4** (2007), 7.

[107] Bob G. Witmer and Michael J. Singer, *Measuring presence in virtual environments: A presence questionnaire*, Presence: Teleoperators and Virtual Environments **7** (1998), no. 3, 225–240.

[108] Daniel M. Wolpert, Zoubin Ghahramani, and Michael I. Jordan, *Perceptual distortion contributes to the curvature of human reaching movements*, Experimental Brain Research **98** (1994), no. 1, 153–156.

[109] Brian M. Yamauchi, *Packbot: a versatile platform for military robotics*, Defense and Security, International Society for Optics and Photonics, 2004, pp. 228–237.

[110] Pavel Zahorik and Rick L. Jenison, *Presence as being-in-the-world*, Presence: Teleoperators and Virtual Environments **7** (1998), no. 1, 78–89.

[111] Howard N. Zelaznik and Dawn Lantero, *The role of vision in repetive circle drawing*, Acta Psychologica **92** (1996), no. 1, 105–118.